

Study on the Charge Transport Properties of Organic and Herbal Dye based Photovoltaic Cell in Presence of Different Nano Particles

**A thesis submitted for the Degree of Doctor of Philosophy
(Science) of**

Jadavpur University

2024

by

SWAPAN BHUNIA



Condensed Matter Physics Research Centre

Department of Physics

Jadavpur University

Kolkata 700 032

*Dedicated
to
my loving family*

Declaration by the Author

I do hereby declare that the work embodied in this thesis entitled “Study on the charge transport properties of organic and herbal dye based photovoltaic cell in presence of different nanoparticles”, which is being submitted for the degree of Doctor of Philosophy (Science), is my own work and that, to the best of my knowledge and belief, neither the thesis nor any part thereof has been accepted for the award of any other degree or diploma of the university or other institute of higher learning, except where due acknowledgment has been made in the text.

(Swapan Bhunia)

Date:



JADAVPUR UNIVERSITY

KOLKATA - 700 032

INDIA

CONDENSED MATTER PHYSICS RESEARCH CENTRE
DEPARTMENT OF PHYSICS

Prof. N. B. MANIK
BOYSCAST FELLOW, DST, GOVT. INDIA

Professor

Department of Physics

Jadavpur University

Kolkata 700 032

Ph : 033 24138917 (O)

033 24831914 (R)

E-mail : nb_manik@yahoo.co.in

Certificate from Supervisor

*This is to certify that the thesis entitled “Study on the Charge Transport Properties of Organic and Herbal Dye based Photovoltaic Cell in Presence of Different Nano Particles”, submitted by **Swapan Bhunia** who had got his name registered on 9th February 2018 for the award of Ph. D (Science) of Jadavpur University, is absolutely based upon his own work under the supervision of Prof. Dr. Nabin Baran Manik and that neither this thesis nor any part of it has been submitted for either any degree/diploma or any other academic award anywhere before.*

Date: 30.01.2024

Prof. Nabin Baran Manik

Supervisor

Condensed Matter Physics Research Centre

Department of Physics

Jadavpur University

Kolkata - 700032



Dr. NABIN BARAN MANIK

Professor

Department of Physics

Jadavpur University

Kolkata - 700 032

Acknowledgment

First and foremost, I would like to convey my earnest gratitude to my supervisor Prof. Nabin Baran Manik for giving me an opportunity to do my Ph.D. at the Department of Physics, Jadavpur University. I have ever indebted to him for his constant guidance, support, and patience during my six years of research. Without his mentorship, it would not have been possible for me to reach where I stand today. At first, I joined his laboratory as a FDP Fellow under UGC rule and guidance taking a no-objection certificate from my college authority. His profound knowledge of the equipment and rigorous attitude toward research is highly exceptional. Dr. Manik's proper instructions and insightful knowledge allowed me to be on the right track throughout my research endeavor. I am also thankful to him for sharing his insightful knowledge beyond academics which helped me shape my attitude and personality in the research field.

I am also thankful to Prof. A. N. Basu for his valuable suggestions during my work which have helped me to shape the view of my thesis in a better way.

I am also thankful to the seniors and colleagues of my laboratory who have helped me a lot during my work. I would particularly like to thank Dr. A. Halдар, Dr. S. Maity, Dr. Md. R. Islam, Dr. S. Saha, Dr. P. Dalapati, Mr. P. K. Das, Mr. S. Sen. Mr. A.K Karan, Miss S. Rakshit, and Mr. D. Sahoo for their valuable cooperation and encouragement in my work. Further, I would like to convey my gratefulness to all the members of the CMPRC group, Department of Physics, Jadavpur University, for their help and cooperation.

Most of the measurements were done in our laboratory from the instruments that have been procured from the funds of the research projects funded by UGC and CSIR. I would like to acknowledge UGC, and CSIR, India for their financial assistance without which it would not have been possible to procure the instruments.

Last but not least, I would like to express my gratitude and thankfulness to my loving parents because of whom I stand here today. They have been very encouraging and supportive throughout my life. I would thank my wife and child for their cooperation and support during my work. Without their support, successful completion of the work would not have been possible. They have been my strength all through.

List of Tables

Chapter 3

Table 3.1 Extracted value of Hall Coefficient (R_H) of Turmeric dye-based device

Table 3.2 Extracted values of n , ϕ_b , and R_s of the Turmeric dye-based herbal diode

Table 3.3 Extracted values of m and E_c of the Turmeric dye-based herbal diode

Chapter 4

Table 4.1 Values of η and E_g for different cell

Table 4.2 Values of Barrier height (ϕ_b) and Series Resistance (R_s)

Table 4.3 Values of Trap Energy (E_c) of different Cells

Chapter 5

Table 5.1 Values of U (dissociation energy) of Turmeric dye with and without TiO_2 nanoparticles

Table 5.2 Values of Barrier height (ϕ_b), Series Resistance (R_s) and Trap Energy (E_c) of different Cells

Chapter 6

Table 6.1 The extracted value of η from $\ln I$ vs V plot for three different cells without and with TiO_2 and ZnO nanoparticles

Table 6.2 The extracted value of η and R_s for the different cells without and with TiO_2 and ZnO nanoparticles

Table 6.3 Extracted values of trap energy for three different system without and with TiO₂ and ZnO nanoparticles

Table 6.4 Estimated reduction percentage (%) of R_{ss} and E_{ct} in presence of TiO₂ and ZnO nanoparticles

List of Figures

Chapter 1

Fig. 1.1 Flexible Green Electronics: materials, fabrication, devices

Chapter 2

Fig. 2.1 Chemical structure of different natural and organic dyes

Fig. 2.2 Chemical structure of (i) ZnO, (ii) TiO₂

Fig. 2.3 Schematic representation of orbital hybridization structures- sp (linear), sp^2 (trigonal planar) and sp^3 (tetrahedral)-and polymer examples for the sp^2 and sp^3 hybrid orbitals

Fig. 2.4 SP^2 hybridization of C atom

Fig. 2.5 Conductivity of conductive polymers compared to those of other materials, from insulator to conductor. The conductivity of Turmeric dye is shown by an arrow mark which lies in between to insulator and conductor

Fig. 2.6 Metal and dye contact (a) before contact (b) after contact. A potential barrier is formed at the interface

Fig. 2.7 Hopping transport within exponential traps

Fig. 2.8 Random walk between the different sites

Fig. 2.9 Gaussian type distribution of traps

Fig. 2.10 Trapping and de-trapping of carriers at different energy levels distributed exponentially

Fig. 2.11 (a) Distribution of HOMO and LUMO levels in amorphous organic semiconductors (b) Trap states between the LUMO and HOMO

Chapter 3

Fig. 3.1 Curcumin and its chemical structure

Fig. 3.2 Special type of cell used for Hall experiment

Fig. 3.3 Hall probe connection setup

Fig. 3.4 (a) Digital image of special type of cell used for Hall experiment and (b) digital image of Hall probe

Fig. 3.5 (a) Hall probe connection setup symbolic (b) Image of Hall Setup

Fig. 3.6 Schematic diagram of Turmeric dye-based organic device

Fig 3.7 I-V curve for fixed magnetic field

Fig. 3.8 I-B curve for fixed Hall current

Fig. 3.9 Dark I – V characteristic of ITO/Turmeric/Al herbal diode

Fig. 3.10 Schematic energy band diagram of ITO/Turmeric/Al interface where ITO/Turmeric form Schottky contact and Al/Turmeric form Ohmic contact

Fig. 3.11 $\ln I$ versus $1/T$ plot of Turmeric dye-based herbal diode

Fig. 3.12 $\ln I$ versus V plot of Turmeric dye-based herbal diode

Fig. 3.13 (a) $dV/d\ln I$ - Current (I) and (b) $H(I)$ – Current (I) plot of Turmeric dye-based herbal diode

Fig. 3.14 $\ln I$ - $\ln V$ plot of Turmeric dye-based herbal device

Chapter 4

Fig. 4.1 Structure of Turmeric molecule

Fig. 4.2 Cu/Turmeric dye/Al cell. A thin layer of Turmeric dye is sandwiched in between Cu and Al electrode which are used as front and back electrode respectively

Fig. 4.3 Circuit diagram of the reverse bias connection of the diode to the Keithley 2400

Fig. 4.4 Forward and reverse bias I-V curve of three Turmeric diodes

Fig. 4.5 Rectification ratio curves of three Cu/Turmeric/Al diodes

Fig. 4.6 $\ln I$ vs V curve for estimating ideality factor with different dye concentration

Fig. 4.7 $\ln I$ vs. T curves of diodes. (a), (b), (c) are for 20%, 10% and 5% concentration respectively

Fig. 4.8 $\ln I_0$ vs. $1/KT$ curves. (a), (b), and (c) are for 20%, 10%, and 5% concentration respectively. Curves are linear in nature. Data are fitted to estimate E_g

Fig. 4.9 (a), (b), (c) are Curves for estimation of series resistance, barrier height of 5%, 10% and 20% Turmeric dye concentration cells respectively

Fig. 4.10 (a), (b), (c) are Curves for estimation of trap energy (E_c) of 5%, 10% and 20% Turmeric dye concentration cells respectively

Chapter 5

Fig. 5.1 (a) Molecular structure of ZnO, (b) Molecular structure of TiO_2 (c) Molecular structure of Curcumin (d) Basic structure of Turmeric dye-based diode

Fig. 5.2 (a) SEM image of TiO_2 (b) SEM image of Turmeric (c) SEM image of ZnO (d) SEM image of Turmeric+ TiO_2 (e) SEM image of Turmeric+ ZnO

Fig. 5.3 (a) Structure of PVA (b) The circuit diagram of the reverse bias connection of the diode to the Keithley 2400

Fig. 5.4 Forward and reverse bias I-V curve of Turmeric diode

Fig. 5.5 Forward and reverse bias I-V curve Turmeric with TiO_2 diode

Fig. 5.6 Comparison curve of Turmeric diode with and without TiO_2

Fig. 5.7 $\log I-1/T$ curve of ITO/ Turmeric /Cu cell

Fig. 5.8 $\log I-1/T$ curve of ITO/ TiO_2 +Turmeric /Cu

Fig. 5.9 (a), (b) and (c) Curves for estimation of series resistance, barrier height and ideality factor of Turmeric dye-based diode, with TiO_2 , and ZnO nanoparticles respectively

Fig. 5.10 (a), (b), and (c) Curves for estimation of trap energy of Turmeric dye-based diode, Turmeric diode with TiO_2 , and ZnO nanoparticles respectively

Chapter 6

Fig. 6.1 Chemical structure of sunset yellow dye

Fig. 6.2 Structure of (a) PSF dye, (b) TiO_2 nanoparticle, and (c) ZnO nanoparticle

Fig. 6.3 Schematic diagram of the cell

Fig. 6.4 (a) Absorption spectroscopy of SY dye, (b) Tauc plot of SY dye

Fig. 6.5 The x-ray pattern of the SY dye in powder form

Fig. 6.6 (a) DC conductivity plot of SY natural organic dye with temperature. (b) A semi-logarithmic plot of the temperature dependence of the DC electrical conductivity of SY natural organic compound. The solid lines represent the best linear fits to the data

Fig. 6.7 SEM images of (a), (b) PSF + TiO_2 cell and (c), (d) of PSF + ZnO Cell with higher and lower magnifications respectively

Fig. 6.8 Forward dark I-V characteristics of ITO/PSF/Al, ITO/PSF+ TiO_2 /Al, ITO/PSF+ ZnO /Al

Fig. 6.9 $\ln I$ vs V characteristics of ITO/PSF/Al diode (a) for without nanoparticle, (b) for ZnO , (c) for TiO_2 nanoparticle

Fig. 6.10 $dV/d\ln I$ - Current (I) and $H(I)$ - Current (I) plot; (a) & (b): for without nanoparticle, (c) & (d): for ZnO , (e) & (f): for TiO_2 nanoparticles

Fig. 6.11 $\ln I$ - $\ln V$ plot (a) for without nanoparticle, (b) for TiO_2 , (c) for ZnO nanoparticle

List of Abbreviations

Ag	Silver
Al	Aluminium
Al-M	Aluminium coated Mylar
CB	Conduction Band
C ₆₀	Fullerene
CNT	Carbon nanotubes
AC	Alternating Current
Cu	Copper
CV	Crystal Violet
DOS	Density of states
DSSC	Dye-sensitized solar cell
EC	Ethylene carbonate
E _c	Trap energy
FF	Fill Factor
HOMO	Highest occupied molecular orbital
H _n	Trap density
HPV	Herbal dye-based photovoltaics
I-V	Current-Voltage
I-t	Current-Time

I_{ph}	Photocurrent
ITO	Indium tin oxide
J_{sc}	Short-circuit current density
LUMO	Lowest unoccupied molecular orbital
MG	Malachite Green
MR	Methyl Red
MWCNT	Multi-walled carbon nanotubes
NP	Nanoparticle
N_c	Effective density of states
OD	Optical diameter
OPV	Organic photovoltaics
PC	Propylene carbonate
PSF	Phenosafranine
PEC	Photoelectrochemical cell
PEO	Polyethylene oxide
PMMA	Poly (methyl methacrylate)
PVA	Polyvinyl alcohol
PV	Photovoltaics
RR	Rectification Ratio
SCLC	Space charge limited current
SEM	Scanning electron microscope

SWCNT	Single-walled carbon nanotube
T_c	Characteristic temperature
VB	Valence Band
V_{oc}	Open circuit voltage
V_{th}	Transition voltage
TE	Thermionic

Contents

Page No.

Chapter 1

Motivation and Outline

1.1	Introduction	2
1.2	Nonconventional electronic materials and green electronics	2
1.3	Organic and herbal dye as non-conventional electronic materials	3
1.4	Limitation of herbal dye-based device	4
1.5	Objective of our work	6
1.6	Outline of the work	6
1.7	References	9

Chapter 2

Theory of conductivity and charge transport mechanism of herbal dye base device

2.1	Introduction	13
2.1.1	Recent work on nonconventional electronic materials	13
2.1.2	Conductivity of nonconventional electronic material	15
2.1.3	Conductivity of organic materials	18
2.1.4	Hall Experiment to estimate carrier concentrations	20
2.2	Charge Transport mechanism in Organic device	21
2.2.1	Barrier potential of metal-dye contact and charge injection limited current flow at below threshold voltage	22
2.2.2	Bulk limited current flow above the threshold voltage	23
2.3	Different types of charge transport model	24
2.3.1	Transport models with the extended band and double exponential trap states	24
2.3.2	Visenberg and Matters with exponential trap distribution	26
2.3.3	Dispersive transport model	27
2.3.4	Trap assisted Transport model	30
2.4	Space charge limited bulk transport in presence of traps	33
2.5	Estimation of trap energy from steady state dc I-V characteristic	34

2.6	Methods to determine series resistance (R_s) from dark I-V Characteristic	38
2.6.1	$\frac{dV}{dI}$ vs. I method	38
2.6.2	Cheung Cheung method to estimate series resistance ($\frac{dv}{dI}$ vs. I method and H(I) vs I method)	39
2.7	Conclusion	40
2.8	References	41

Chapter 3

Estimation of charge carrier density of solid state thin film of Turmeric dye

3.1	Introduction	47
3.2	Selection of the dye	47
3.3	Brief review on Turmeric dye	48
3.4	Experimental details	49
3.4.1	Sample preparation	49
3.4.2	Measurements	50
3.4.3	Results and Discussions	55
3.5	Conclusion	63
3.5	References	64

Chapter 4

Effect of dye concentration on the band gap of Poly Vinyl Alcohol Turmeric composite thin film

4.1	Introduction	68
4.2	Turmeric dye active materials of non conventional electronic device	68
4.3	Experimental details	69
4.3.1	Sample preparation	69
4.3.2	Measurements	70
4.3.3	Results and Discussions	71
4.4	Conclusion	83
4.5	References	84

Chapter 5

Effect of ZnO, TiO₂ nanoparticles on solid state Turmeric dye thin film

5.1	Introduction	87
5.2	Experimental details	87
5.2.1	Sample preparation	87
5.2.2	Measurements	90
5.2.3	Results and Discussions	91
5.3	Conclusion	101
5.4	References	101

Chapter 6

Study on the Conductivity of a Sunset Yellow and Phenosafranine dye- - Based Diode in Presence of TiO₂ and ZnO nanoparticles

6.1	Introduction	104
6.2	Selection of dyes	104
6.3	Experimental details	106
6.3.1	Sample preparation	106
6.3.1.1	Sunset Yellow Diode	106
6.3.1.2	Measurement on SY natural dye-based diode	107
6.3.1.3	Material Characterization	107
6.3.1.4	Results and Discussion	108
6.3.2	PSF Diode	111
6.3.2.1	Measurements on PSF diode	111
6.3.3.2	Results and Discussions of PSF diode	112
6.4	Conclusion	120
6.5	Reference	120

Chapter 7

Conclusion and Future Scope of the work

7.1	Summary	125
7.2	Findings of the work	127
7.3	Overall conclusion	133
7.4	Future Scope of the work	133

Preface

The work embodied in the thesis entitled “Study on the charge transport properties of organic and herbal dye based photovoltaic cell in presence of different NP” is mainly concerned with studying conductivity and charge transport parameters of Turmeric, SY and PSF dye-based devices in the presence of NP. Our society is updated with electronic goods. We are purchasing new electronic goods, and the old ones go to the white dustbin. So white dustbin fills up with old electronic goods. This is called electronic waste. To meet the enormous electronic waste, the use of nonconventional electronic material has become essential. Most electronic goods are generally made of inorganic materials. They are not biodegradable. People are looking for non-conventional biodegradable electronic materials. Different organic, polymer, and natural dyes are becoming an attractive area for the present research. But they too have their share of difficulties and hurdles, which has motivated us to pursue this research in this field.

The author started research work as an Assistant Professor, at Ramakrishna Mission Residential College, Narendrapur, Kolkata-700103, for the partial fulfillment of the Career Advancement Scheme under the UGC Faculty Development Programme. Thereafter, author enrolled himself as a research scholar under the supervision of Prof. N.B. Manik, Professor, Department of Physics, Jadavpur University, Kolkata-700032.

For studying the electrical characteristics of the organic and natural dye-based diode, dark I-V measurements have been done by changing various parameters such as dye concentration, changing electrodes, incorporating NP, and cell fabrication techniques, etc. Attempts have been made to study the internal features such as charge carrier density, trap energy, series resistance, and also barrier height which gives an idea of the conduction mechanism of the device. Attempts have been made to address some of the problems both experimentally and theoretically so that the vast possibility of using nonconventional electronic materials may be explored.

In this work, we have studied mainly the Turmeric dye. Typical conductivity of this dye is quite low. Different NPs are used to enhance the conductivity. The conductivity of this dye in presence of different NP such as Titanium Oxide (TiO_2), Zinc Oxide (ZnO) has been studied. The effect of the concentration of the dye has also been studied. In this thesis, we have studied the conductivity, charge carrier density, bandgap energy, and Hall mobility of Turmeric dye in solid thin film by using Hall Experiment. We have also studied few other dyes such as Phenosafranin, Sunset Yellow. From the dark I-V characteristics it is observed that Barrier height (Φ_b), Trap Energy (E_c), and Series Resistance (R_s) of Turmeric dye-based cells get

changed in presence of NP. The data are studied by considering the SCLC model in presence of exponentially distributed trap states and the relation between Φ_b , R_s and total trap density H_n is discussed. It is expected that due to the addition of TiO_2 and ZnO , there occurs a change in the distribution of trap states, and the trap energy and total trap charge density gets reduced. This also reduces the Series Resistance (R_s). Lowering of both Series Resistance (R_s) and Trap Energy (E_c) helps in better charge conduction and enhances the overall performance of the devices. The study in the field of organic and herbal dye-based photovoltaic devices is relatively new and although few works are being done, but there is no established theory to explain the charge transport mechanism of these systems. A theory that fits a certain system may deviate a lot in the case of another system. So, further study is required for a better understanding of these problems. The outcome of this work will be extremely helpful to develop and understand the nonconventional electronic device.

Chapter 1

Motivation and Outline

- 1.1 Introduction
- 1.2 Nonconventional electronic materials and green electronics
- 1.3 Organic and herbal dye as non-conventional electronic materials
- 1.4 Limitation of herbal dye-based device
- 1.5 Objective of our work
- 1.6 Outline of the work
- 1.7 References

1.1 Introduction

Use of electronic devices are increasing day by day. Most of these devices are made of inorganic materials which are not biodegradable, environmentally friendly or renewable in nature. Electronic waste coming from these materials will be a major problem in coming days. Due to this, recently researchers all over the world are looking for alternative herbal and organic/polymers as non-conventional electronic materials. Green electronics made with these materials are becoming important day by day. Harvesting energy directly from the sun using natural dye-based photovoltaic (PV) technology is currently being considered as an important component for future global energy generation [1-4]. This chapter provides a brief review of different non-conventional herbal and organic materials that may be used to prepare electronic and optoelectronic devices in future.

1.2 Non-Conventional Electronic Materials and Green Electronics

The transistor's discovery in 1947 by John Bardeen, Walter H. Brattain, and William B. Shockley of the Bell research staff gave us a series of new electronic devices [5-9]. Transistors, along with such subsequent developments as integrated circuits, are made of crystalline solid materials called semiconductors which have electrical properties that can be varied over an extremely wide range by the addition of suitable quantities of other elements. Day by day requirements for electronic applications and devices are increasing. Along with different electronic devices like diode, triode, transistor, FETs, MOSFETs, and electronic switches, different opto-electronic devices like Light Emitting Diode (LED), Photo Detector (PD), and Photovoltaic Cell (PVC) are taking place side by side. Almost a revolution has taken place in electronic materials to develop these devices. Starting from vacuum valves, Silicon, Germanium, GaAs, GaP, GaAlP are used as electronic materials [10-14]. But these materials are not biodegradable and as a consequence, electronics waste is becoming a major problem. Now people are looking for non-conventional biodegradable electronic materials. The green electronics will be very attractive in near future. Different portable, flexible, biodegradable electronic devices with organic and herbal materials are being used. Fig. 1.1 shows different aspects of flexible green electronics. At a glance different devices, materials, and process techniques are highlighted in this figure.



Fig. 1.1 Flexible Green Electronics: materials, fabrication, devices, perspectives

1.3 Organic and Herbal dye as non- conventional electronic materials

As mentioned, the study of different herbal dyes and their applications in electronic devices has opened up a new horizon of science. Earlier, herbal dyes were used for coloring the food substrates, leathers, and fibers like wool, silk, and cotton. Herbal dyes also have a significant impact on Ayurvedic practices. The presence of anti-carcinogenic properties in herbal dyes has also been observed by a few researchers. Now-a-days herbal dyes used as food coloring

substance and also to add flavor of the food. Recently different herbal dyes are being studied to develop different electronic devices. These herbal dye-based devices have many advantages. The herbal dye-based devices are nature-friendly, biodegradable, and cost-effective. There are also varieties of dyes to study. It may be fabricated over a large area on different substrates from its solution by simple processing techniques, such as sol-gel, spin-coating, solvent casting, sublimation, and dip coating. Natural dyes like Turmeric, Hibiscus Rosasinesis, and Sesbania Grandiflora are used as photosensitizers due to their large absorption coefficient in the visible region in the dye-sensitized solar cell. Detailed review on different dyes which has been taken in any study will be discussed in respective chapters.

The optical and electrical properties of several herbal dyes have recently been studied in order to produce various electronic devices. However, many publications have lately been published on the use of derived natural dyes from natural sources [15-19]. Karakuş et al. used *Pelargonium hortorum* and *Pelargonium grandiflorum* as sensitizers in their DSSCs and attained power conversion efficiency (PCE) values of 0.065% and 0.067%, respectively [20-24]. Ramanarayanan et al. extracted the dye from the leaves of red amaranth and tested the effect of several solvents, such as water and ethanol, achieving PCE of 0.230% and 0.530%, respectively. Hosseinné et al. isolated the dye from *Sambucus ebulus* and reported a PCE of 1.15%. Even though all of these studies demonstrated low PCE compared to other conventional cells, the method of operation and performance are of considerable interest, primarily to seek new insights and understanding for these advanced cells. Various colors were derived from red cabbage, onion peels, and spinach and employed as sensitizers for the DSSCs in these studies. However, we have found very little literatures that describes the conductivity, charge carrier density, and charge transport mechanism of the herbal dye-based devices.

1.4 Limitation of Herbal Dye-based Device

Despite many possibilities, there are still some limitations of herbal dye-based devices. As the herbal materials are disordered amorphous solids and dominated by weak van der Waals forces, the conductivity of these materials are low. One of the reasons is trap distribution in the energy space between HOMO and LUMO in the herbal materials. During the charge transport process, free charges are traveling from one molecule to another and depend on the energy gap between

HOMO and LUMO. Trapping sites in organic semiconductors can be generated by structural flaws (leading to local positional or energy-oriented disorder), dipoles, and expanding contamination (impurities or dopants). Charge carrier trapping often limits the charge carrier transport properties of materials. For these reasons, charge carrier trapping effects should always be considered when analysing the performance of organic photovoltaic devices (OPVs). Traps can be classified into shallow traps and deep traps, which result in different anomalous properties in electrical characteristics. These traps decrease the device's performance. So, it will be essential to know about the trap energy. Another limitation of herbal dye-based devices is their high series resistance. The reasons for the high series resistance of herbal dye-based devices are poorly explained. Furthermore, the effect of traps on R_s is also poorly understood. So, observation about the background physics of this high-value resistance and its impact on the overall performance on the device could be exceptionally significant for the advancement of the efficiency of the herbal dye-based device. One of the important reasons for the degradation of performance is the amorphous disorder nature of the herbal dye that influences the charge injection and the flow of charge carriers in the herbal dye-based devices. Though there are some reported literature denotes the performance and electrical characterization of the herbal dye-based devices, but the study on the charge carrier density of the herbal dye-based devices has not been properly discussed. Other challenges with organic photovoltaic devices include charge carrier mobility and recombination [25-29]. The active layer must be kept thin in order to enable charge transmission and minimize recombination losses. The lack of understanding of the charge transport mechanism of the dye-based OPV devices is also a problem to the device's performance. Researchers in this field are trying various techniques in this regard which include different architectures to fabricate the devices, incorporating new guest materials in these devices. We have introduced TiO_2 and ZnO NP in the herbal dye-based devices to enhance the device conductivity. Another important parameter in any electronic device is the amount of charge carrier density, which controls the overall device performance. So, it will be essential to obtain the charge carrier density, ideality factor, and series resistance to better understand and improve the herbal dye-based devices.

To unleash the full potential of using these materials in different electronic and optoelectronic devices, some of the above issues should be addressed and resolved. Considering these aspects we have undertaken this work with the following objective.

1.5 Objectives of our work

The objective of the present work is to investigate the semiconducting properties and charge transport mechanisms of different organic and herbal dye-based electronic devices in presence of different nanoparticles. Generally, the conductivity of herbal dyes is low. We have selected a few herbal and organic dyes namely Turmeric, Phenosafranine, Sunset Yellow, for our study. We have introduced TiO_2 , and ZnO NP to enhance the conductivity. We have measured and compared the conductivity of these dyes. We have also measured and compared the trap energy, barrier height, and series resistance of these dyes. Electrical and transient current measurements of the herbal dye-based devices have been done. All these experimental works have been done to understand the charge transport mechanism of the devices.

In this thesis, we have also reviewed different literatures related to the role of different herbal dye devices. From these literatures, we have followed a few techniques to prepare Herbal photovoltaic HPV cells. By using the spin coating technique, different HPV cells have been prepared with various herbal dyes. Generally, in inorganic PVs vacuum coating or sputtering technique is used which is very costly. Sometimes it becomes quite impossible to prepare large-area devices using these techniques. One of the major advantages of HPV is related to its preparation techniques. There is also no such barrier to fabricate the device or depositing the film over a large area though the efficiency of the devices by using this process is quite low. But considering the advantages to deposit film in a large area, the overall cost will be low as expected in the coming days.

The outcome of this work will be useful to do further work with these dyes. Our initiations shall be encouraging to characterize other new materials in the future. Moreover, the findings of the work will be useful to resolve some issues related to herbal dye-based PV (HPV) devices. This study will be helpful in developing a simple and cost-effective technique that can improve the device's performance. Our work on charge transport may also be applied to other systems.

1.6 Outline of the work

The outline of our work is mentioned in this section. The whole work is organized into seven chapters

In **Chapter 1** we have discussed the problem of electronic waste and discussed the advantages of the natural dye-based device. Recently organic dyes and polymer-based photovoltaic devices have emerged as an alternative to their inorganic counterparts. However, these devices suffer from low conductivity and stability. To overcome this hindrance new guest materials are being introduced. Different herbal dyes are guest materials in this regard. The addition of TiO_2 and ZnO NP increases the conductivity of these devices. It is very important to study the charge conduction process of these devices with or without NP. It will be informative and meaningful if further studies are done in this field. Keeping this in mind we have mentioned the objectives of this work. Our study, and the possible outcomes of this work are also mentioned in this chapter.

In **Chapter 2** we have discussed the review of conductivity and the charge transport mechanism of herbal dye-based devices. Current-voltage (I-V) characteristics and charge-trapping mechanisms in herbal dye-based devices are also discussed. Herbal devices are prone to traps. In order to understand the charge transport process, it is very important to have knowledge about the concept of traps in these devices. Here we have also discussed the origin of traps and the various trap distribution models. We have reviewed the basic current conduction process in natural dye-based devices. We have followed a theoretical model of charge transport mechanisms of Herbal dye-based devices. The flow of current in natural dyes can be attributed to injection-limited current flow and bulk-limited current flow. At voltages below the threshold voltage, the current flow is considered as injection-limited current flow, and at voltages above threshold voltage, the current flow is considered as bulk-limited current flow. In this regard, we have used the space-charge limited current (SCLC) model with exponential trap distribution. We have measured trap energy, barrier height, and series resistance using the SCLC model. In this chapter, we have also briefly discussed thermionic emission theory and the magnetic field effect on moving charges for natural dye-based devices. We have shown the role of different NPs on series resistance, barrier height, and trap energy of herbal dye thin film.

From **Chapter 3** to **Chapter 6** we have mentioned the experimental work of our work

In **Chapter 3** we have studied the conductivity, charge carrier density, and mobility of Turmeric dye-based devices. We have shown the changes of current and voltage of Turmeric dye solid state device with changing magnetic field to measure the hall voltage and estimate the charge concentration. The results are mentioned in this chapter. We have also made a diode

out of Turmeric dye and measured the reverse saturation current, rectification ratio, ideality factor, series resistance, barrier height, and trap energy. The diode has a high ideality factor and series resistance. As a result, we have assessed the trap energy of the device while considering the exponential trap distribution.

In **Chapter 4** by altering the concentration of Turmeric dye, we have investigated its conductivity. The band gap has been measured by investigating the diode characteristic. We have taken three different concentrations of Turmeric dye to prepare three cells with ITO/Turmeric/Al structure. By varying the I-T characteristic we have shown the semiconducting property and measured band gap energy of the cells. We have also studied the change of the trap energy, barrier height, and series resistance of the cells with the dye concentration. The barrier height is a very important parameter that identifies the charge transport across the metal-semiconductor interface. The results are mentioned in this chapter.

In **Chapter 5** we have studied the effect of NP on solid-state Turmeric dye thin film. The steady-state current-voltage characteristics have been studied. We have studied and compared the charge transport parameters such as barrier height, series resistance, and trap energy with or without the presence of NP. It is observed that for the Turmeric dye, the barrier height and series resistance of the Turmeric dye cell decreases by about 30% with the addition of TiO_2 . Results are discussed in this chapter. Here we have also discussed the effect of ZnO NP on Turmeric dye-based solid-state thin film. We have also estimated and compared the barrier height, series resistance, and trap energy of the cells.

In **Chapter 6** we have investigated the DC electrical conductivity of the natural organic component sunset yellow (SY) dye. This dye has strong DC conductivity. The DC electrical conductivity is measured using an impedance spectrometer at temperatures ranging from 303 K (30°C) to 373 K (100°C) with a bias voltage of 4V. In this chapter, we have also investigated Phenosafranine (PSF) dye-based organic diode. We have shown the influence of the trap energy of PSF dye on R_s in the presence of TiO_2 and ZnO NP. We have found that addition of nanoparticles with organic and herbal dye reduces trap energy, which boosts the conductivity and efficiency of the device.

In **Chapter 7** the summary and overall findings of the work are highlighted. This chapter concludes with an overall conclusion of the work and the future prospects of work in this field.

1.7 References

1. A.K.N. Reddy et al, Electric Power Generation System from Speed Breaker by using Rack and Pinion Mechanism, Energy19 561 (1994)
2. M. I. Blair et al, Aspects of Energy Conversion, Proceeding of summer School, Lincoln College, Oxford, England, July 14-25, (1975)
3. J. Singh et al, Biomass conversion to energy in India – A critique. Renewable and Sustainable Energy Reviews, 2010, 14 : 1367-1378
4. L. Ahmad et al, he Effect of greenhouse gases on earth's temperature, International Journal of Environmental Monitoring and Analysis, 2015, 3(2) : 74-79
5. H. Ross A, et al, A multi-wall carbon nanotube-molecular semiconductor composite for bi-layer organic solar cell, Physica E, 2007, 37 : 124-127
6. D. Corzo, et al, Flexible electronics: status, challenges and opportunities, Frontier in electronics (2020), 1:1-13
7. C, W. Tang, et al, Two-layer organic photovoltaic cells, Nature, 2001, 414(6861) : 338
8. N. Pragma, et al, An overview of global climate changing in current scenario and mitigation action. Renewable and Sustainable Energy Reviews, 2012, 16 : 2329-2336
9. N. Nakicenovicand et al, CO₂ Reduction And Removal: Measures For The Next Century, Energy16 1347 (1991)
10. M. Payne et al, Solution-Processable Small-Molecule Semiconductors, (2015), ISBN : 978-3-642-35947-7 : 1-12
11. National Research Council Advancing the Science of Climate Change, The National Academies Press, (2010)
12. O.Ellabban, H.Abu-Rub and F.Blaabjerg, Renewable and Sustainable Energy Reviews 39 749 (2014)

13. REN21, Renewables 2010 Global Status Report (Paris: REN21 Secretariat) 15 (2010)
14. Y. Hubenova et al, Conversion of Solar energy into electricity by using duckweed in direct photosynthetic plant fuel cell, Bioelectrochemistry, (2012), 87 : 185-191
15. A. S. Mahdi et al, Recent advance in organic solar cell: materials, design, and performance, Journal of optics, (2003)
16. Analysis of Wind Energy, European Wind Energy Association, (2007)
17. Solar Energy Perspectives: Executive Summary, International Energy Agency, (2011)
18. F. M. Li et al, “Organic Thin Film Transistor Integration: A Hybrid Approach”, 2011, [1st ed.], Wiley-VCH Verlag GmbH & Co. KGaA, Weinheim, Germany, 1-11
19. W. Schottky, “Halbleitertheorie der Sperrschicht”, Naturwissenschaften, 1938, 26, 843-843
20. V. I. Arkhipov, H. von Seggern and E. V. Emelianova, “Charge injection versus space-charge-limited current inorganic light-emitting diodes”, Applied Physics Letters, 2003, 83, 5074–5076
21. Grid Connected Renewable Energy, Solar Electric Technologies, (2004)
22. E. Omar, et al, Renewable energy resources: Current status, future prospects and their enabling technology, Renewable and Sustainable Energy Reviews, 2014, 39 : 748-764
23. Intergovernmental Panel on Climate Change, Cambridge University Press, 1075 (2011)
24. N. F. Mott, “Electrons in Disordered Structures”, Advances in Physics, 1967, 16, 49-144
25. H. Bässler et al, “Charge transport in disordered organic photoconductors: a Monte carlo simulation study”, Physica Status Solidi. B. Basic research, 1993, 175, 15-56
26. G. Yu et al, Science, Polymer Photovoltaic Cells: Enhanced Efficiencies via a Network of Internal Donor-Acceptor Heterojunctions, 270 1789 (1995)

27. P. Peumans et al, Small molecular weight organic thin-film photodetectors and solar cells, J. Appl. Phys, 93 3693 (2003)
28. H. Hoppe et al, Organic solar cells: An overview, Energy Mater Sol. Cells, 80 105 (2003)
29. C. J. Brabec et al, Origin of the Open Circuit Voltage of Plastic Solar Cells, Adv. Funct. Mater, 11 15 (2001)

Chapter 2

Theory of conductivity and charge transport mechanism of herbal dye-based device

2.1 Introduction

2.1.1 Recent work on nonconventional electronic materials

2.1.2 Conductivity of nonconventional electronic material

2.1.3 Conductivity of organic materials

2.1.4 Hall Experiment to estimate carrier concentration

2.2 Charge Transport mechanism in Organic devices

2.2.1 Barrier potential of metal-dye contact and charge injection-limited current flow at below threshold voltage

2.2.2 Bulk limited current flow above the threshold voltage

2.3. Different types of charge transport models

2.3.1 Transport models with the extended band and double exponential trap states

2.3.2 Visenberg and Matters with exponential trap distribution

2.3.3 Dispersive transport Model

2.3.4 Trap assisted Transport Model

2.4 Space charge limited bulk transport in presence of traps

2.5 Estimation of trap energy from steady state dc I-V characteristic

2.6 Methods to determine series resistance (R_s) from dark I-V characteristics

2.6.1 $\frac{dV}{dI}$ Vs. I Method

2.6.2 Cheung Cheung Method to estimate Series Resistance

$(\frac{dV}{d \ln I})$ Vs. I Method and $H(I)$ Vs. I Method

2.7 Conclusion

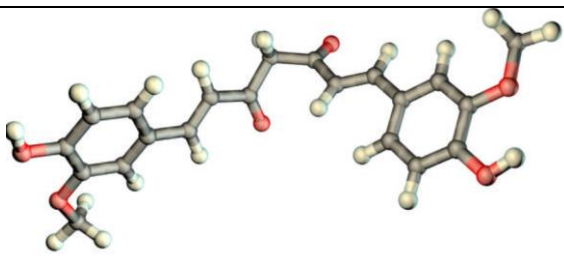
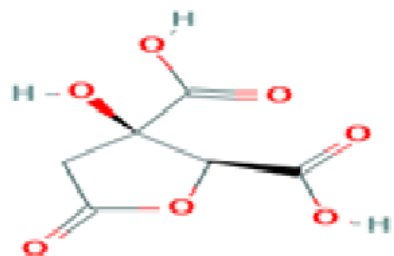
2.8 Reference

2.1 Introduction

Herbal dyes are non-polluted, biodegradable organic dyes. People are trying to search for various electrical properties of these materials to use as active materials of nonconventional electronic (NCE) devices. Several types of electrical and optoelectronic properties have been studied using natural dyes. Natural dyes have received considerable attention due to their manufacturing cost advantages, fabrication methods, material variety, and mechanical flexibility but there are no such charge transport theories on the herbal dye-based device. However, few literatures are available on charge transport theories of amorphous, disorder solids. We assume that natural dyes are amorphous and disordered.

2.1.1 Recent work on nonconventional electronic materials

In the following section of this chapter different charge transport theories of organic devices are discussed. Understanding the current-voltage characteristics of a specific device structure of herbal dyes, its conduction mechanisms, and the influences of the interfaces between herbal dye and electrodes is very important for improving the performance of herbal dye-based devices. Scientists and researchers are working on herbal dye-based non-conventional electronic devices. A few herbal dyes and their chemical structure are shown below in Fig. 2.1

Name	Chemical Structure
Turmeric dye	
Hibiscus Rosasinesis	

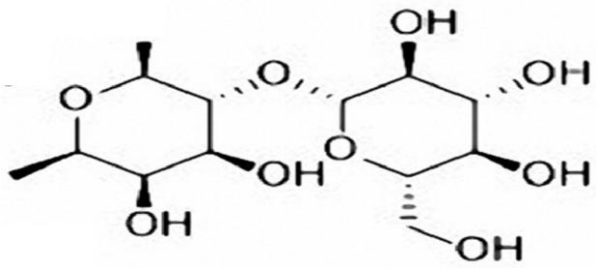
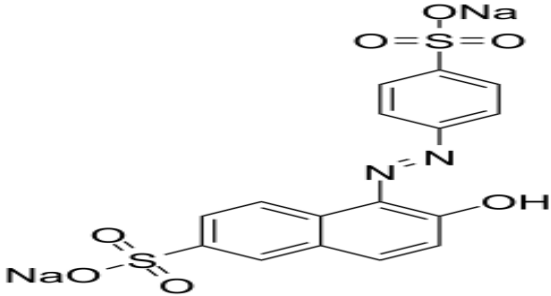
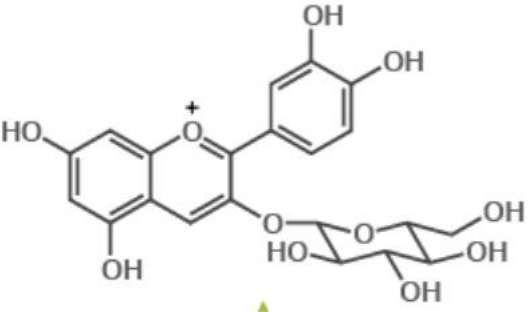
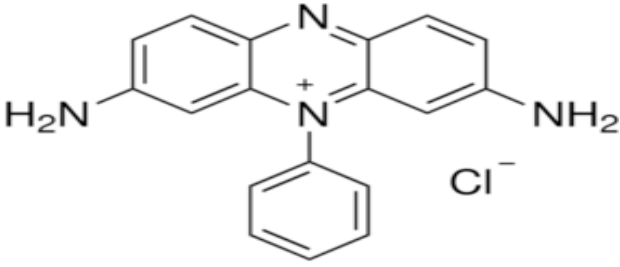
Sesbania grandiflora	
Sunset Yellow	
BlackBerry	
Phenosafranine (PSF)	

Fig 2.1 Chemical structure of different natural and organic dyes

To understand the electronic and optoelectronic properties of nonconventional electronic devices, we have reviewed the principles of the charge transport theorem which one in disorder

amorphous organic solar cells. We have also used a few NP which act as acceptor materials. These are Zinc Oxide (ZnO), and Titanium dioxide (TiO₂). The chemical structures of these NPs are given below in Fig. 2.2.

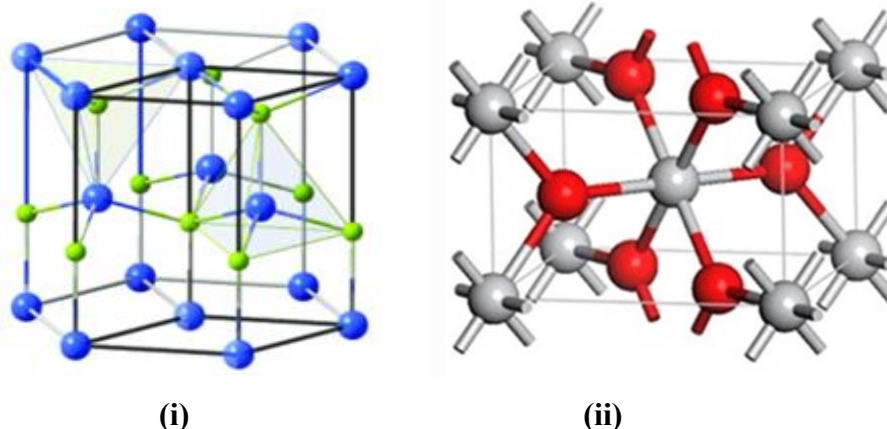


Fig 2.2 Chemical structure of (i) ZnO, (ii) TiO₂

The exact role of NP in the charge transport mechanism of organic and herbal dye-based devices is still unknown. We have assumed that image charge will be higher in the presence of NP in the organic or herbal dye-based cell. So, more charges inject from electrode to dye and as a consequence the current will increase. It can be said that NP places in between two or more molecules of organic and herbal dye. So density of hopping site increases and as a result current also increases.

2.1.2 Conductivity of nonconventional electronic material

Natural dyes are generally insulators with high resistivity and are used as dielectric. The discovery of conductivity in organic solids has opened a new dimension in the field of material science. A. J. Heeger and his co-workers [1-4] pointed out that in conjugated polymers which shows that chemical bonding leads to one unpaired π electron per carbon atom. The π binding is due to sp^2p_z hybridization of the carbon orbital as shown in Fig. 2.3 and 2.5. But the conductivity of natural dyes has never been studied. There is no definite band structure in natural dyes and most of them are amorphous, and disordered in nature. Every natural dye

consists of a polymer. For example, Turmeric dyes consist of curcumin polymer. These polymers are bonded by carbon atoms.

Recently, natural dyes have been synthesized and doped suitably to improve electrical conductivity. Fig. 2.5 shows a comparison of the electrical conductivity of different inorganic material and natural dyes.

Few organic dyes show a semiconducting property. However, the semi-conductivity of these dye depends on the structure of the materials [5-8]. We have scrutinized that different chemical structure comprises different single molecules, short chains of molecules, and long polymer chains. It has been found that the insulating polymers or ‘plastics’ have σ bonds between the constituent carbon atoms whereas the conducting natural dyes have π -conjugated bonds which give rise to delocalized filled and empty π -orbitals.

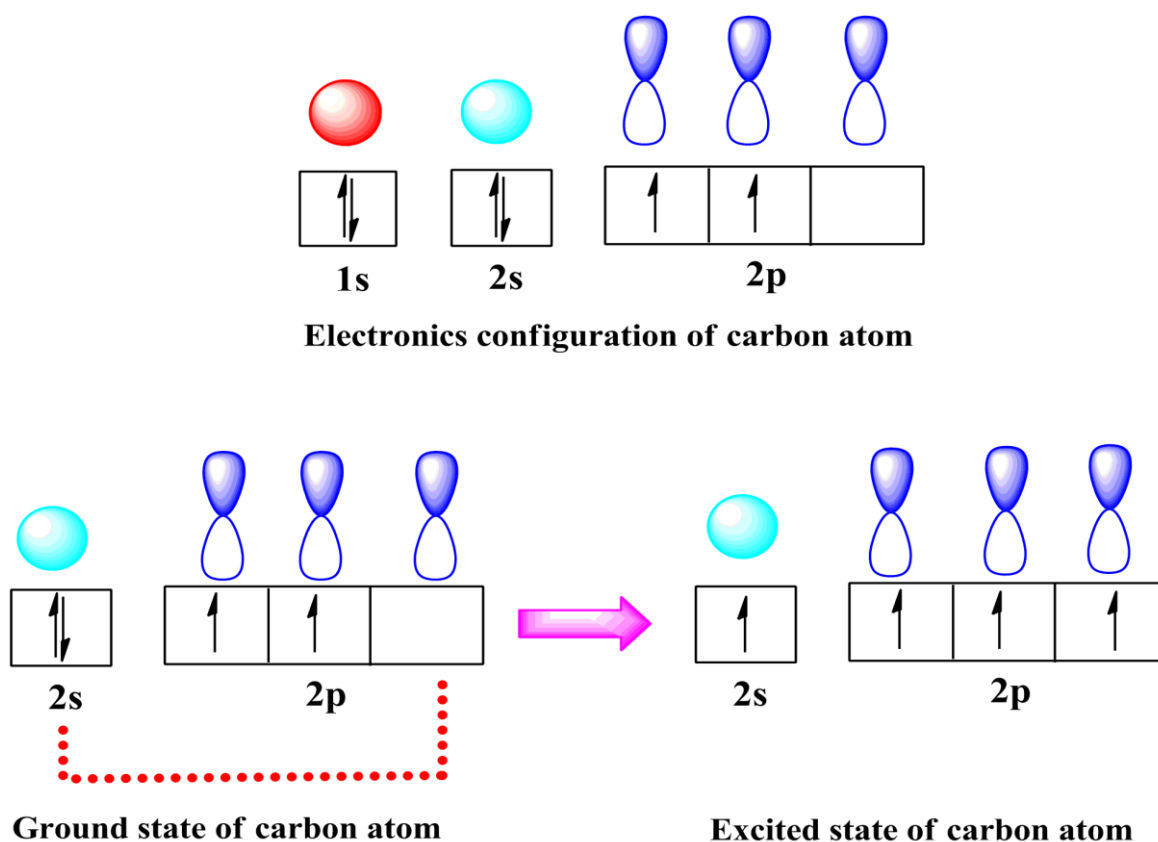
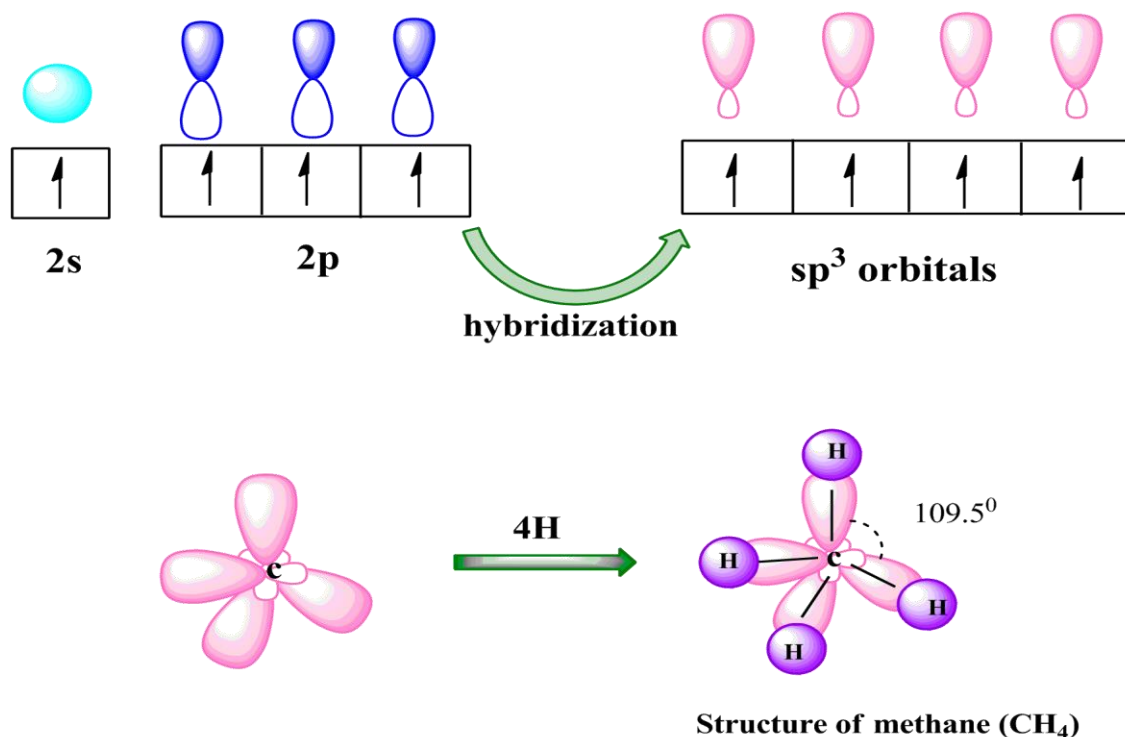


Fig. 2.3 Schematic representation of orbital hybridization structures (linear), sp^2 (trigonal planar), and sp^3 (tetrahedral) and polymer examples for the sp^2 and sp^3 hybrid orbital

Fig. 2.4 SP^2 hybridization of C atom

As a result, the orbitals of successive carbon atoms along the backbone overlap, resulting in electron delocalization along the polymer's backbone. Charge transport along the backbone of the polymer chain is due to this electron delocalization. A few natural and organic dyes are shown in Fig. 2.1.

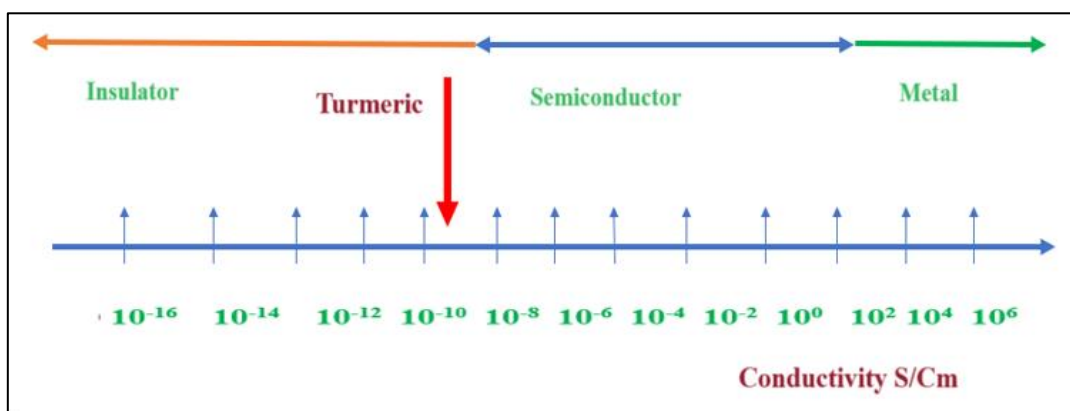


Fig. 2.5 Conductivity of conductive polymers compared to those of other materials, from insulator to conductor. The conductivity of Turmeric dye is shown by an arrow mark which is in between to insulator and conductor

2.1.3 Conductivity of organic materials

Electrical conductivity is one of the physical properties of a material that is determined by its structure and its free charges [9-12]. The existence of free electrons in a substance is responsible for electrical conduction. In the absence of an external electric field, electrons flow at random, resulting in no net velocity for individual electrons and no electric current. When an electric field is applied to a conductor, electrons have a limited resultant velocity termed as (drift velocity) in the specified direction, i.e., in the direction opposite to the electric field, resulting in an electric current.

When an electric field \mathbf{E} is given to a conductor with free electrons n per unit volume, the electrons are accelerated and drifted towards positive ions/lattice sites by the force $e\mathbf{E}$. From Newton's second law, we have

$$m \frac{dv}{dt} = e\mathbf{E} \quad (2.1)$$

Where, m , e , and v are the mass, charge, and velocity respectively of the electron.

The electron moves with a constant velocity when the electric field is removed. Typically, Eqn. 2.1 does not occur due to the presence of resistance induced by the interactions of wandering electrons with lattice atoms, impurities, and defects. Now as to the above consideration, Eqn. 2.1 is modified into

$$m \frac{dv}{dt} + \gamma v = e\mathbf{E} \quad (2.2)$$

Where γ is a resistive/damping constant and γv is the damping/resistive force caused by electron-lattice atom interaction. Electrons accelerate between two subsequent collisions, and electrons also impart energy to the lattice atoms. Finally, the electron acquires a constant drift speed v_d as a result of Eqn. 2.2 reduces into,

$$\gamma v_d = e\mathbf{E}$$

$$\text{Or } \gamma = \frac{e\mathbf{E}}{v_d} \quad (2.3)$$

From the Eqn. 2.2 and 2.3, we have

$$m \frac{dv}{dt} + \frac{eE}{V_d} v = eE \quad (2.4)$$

It is a true differential equation of motion for an electron in the presence of both resistance and electric forces. The solution of this differential equation is given below

$$V = V_d \left(-e^{\frac{eE}{mV_d} t} \right) \quad (2.5)$$

This relationship demonstrates that the electron's velocity, v , is directly proportional to the external electric field and inversely proportional to the resistive constant. The equation $\frac{mV_d}{eE}$ has a time dimension known as relaxation time which is the average duration between two consecutive collisions.

$$\tau = \frac{mV_d}{eE} \quad (2.6)$$

Rearranging the above relation, we have

$$V_d = \frac{eE\tau}{mV_d} \quad (2.7)$$

From the general formula of current density, J , and the microscopic view of Ohm's law, we have

$$J = n e V_d = \sigma E \quad (2.8)$$

Where σ is the electrical conductivity of the material. After rearranging the above relation and using Eqn. 2.7, we have

$$\sigma = \frac{neV_d}{E} = \frac{n \tau e^2}{m}$$

This equation demonstrates that the material's electrical conductivity is proportional to the number of free electrons per unit volume (population density) and relaxation time. In our experiment, we have used

$$J = \frac{I}{A} \quad \text{where } I = \text{current, and } A = \text{area of the thin film.}$$

$$E = \frac{V}{d} \quad \text{where } V = \text{applied voltage, and } d = \text{thickness of the film}$$

$I = \sigma A \frac{V}{d}$ Keeping A , and d fixed we can plot I vs V . From this graph we can estimate the conductivity of nonconventional materials. The thickness of the thin film have not been measured. So, we have used the Four Probe method to estimate the conductivity and bandgap of the materials.

$$\text{The resistivity of a semiconductor is } \rho = A e^{\frac{E_g}{2Tk}} \quad (2.9)$$

Where E_g is Band Gap in eV, k is Boltzmann constant $= 8.617 \times 10^{-5} \text{ eVK}^{-1}$ and T is the absolute temperature.

2.1.4 Hall Experiment to Estimate Carrier Concentrations

In this thesis, we have discussed the magnetic field effect and estimated the charge carrier density of the herbal dye-based device. We have taken Turmeric dye [$C_{21}H_{20}O_8$] as the active ingredient for this study. Turmeric is the most widely available and least expensive natural dye. It is simply the powdered rhizome of a natural plant called *Curcuma Longa* L [13-17]. We have assumed the current carriers present in the device as a result of the breaking of the π^* bond in this case. The magnetic force on the carrier is

$$E_m = e (\mathbf{v} \times \mathbf{H}) \quad (2.10)$$

And it is compensated by Hall field (\mathbf{F}_h). So we can write,

$$F_h = e E_h \quad (2.11)$$

Where \mathbf{v} is the drift velocity of the carrier.

$$\text{So, } E_h = R J \times H \quad (2.12)$$

Where (y) is the current density = $qn v$

From Eqn. 2.10, Eqn. 2.11, and Eqn. 2.12 we can write

$$R = \frac{V_h Z}{J H}$$

Where V_h is Hall voltage, as J is along the X direction, H is along the Z direction, so E_h will be along the Y direction. For one type of carrier, we can write

$$\text{Hall coefficient (R)} = \frac{E_h}{J H} = \frac{v H}{q n v H} = \frac{1}{n q} \quad (2.13)$$

From experiments in modern physics by Adrian C. we can say for two types of carrier Hall Co-efficient is

$$R = \frac{\mu_p^2 p - \mu_e^2 n}{2(\mu_p - \mu_e)^2} \quad (2.14)$$

Where mobility of holes and electrons are defined by μ_p and μ_e , and the carrier densities of holes and electrons are represented by p and e . Here we assume the carrier is an electron arises due to the breaking π^* bond. We choose μ_p is zero. So, Eqn. 2.13 becomes Eqn 2.14. Hall voltage is proportional to $1/n$ or its resistivity when the magnetic field and input current are fixed. In this system, one carrier dominates

So, conductivity $\sigma = n q \mu$ where μ is the mobility of charge carriers.

Thus $\mu = R \sigma$ here $\sigma = 1.5 \times 10^{-10} \text{ } \Omega \text{ m}^{-1}$

2.2 Charge transport mechanism in organic devices

The flow of current in an organic or natural dye may be considered as (i) injection-limited current and (ii) bulk-limited flow of current. The injection limited current mainly occurs at low voltage or below the threshold voltage and above threshold voltage, the transport may be considered as bulk transport current [18-22].

2.2.1 Barrier potential of metal–dye contact and charge injection- limited current flow at below threshold voltage

The metal-organic semiconductor interface has a major impact of any organic dye-based device's performance [23-28]. In a metal dye interface, band bending occurs due to differences in the work functions of the metal and the organic dye. When the metal and the organic dye come in contact, charge transfer and equilibration take place. This leads to the alignment of energy levels and the creation of potential gradient, forming a barrier at the interface. The barrier potential serves as an energy barrier that aids in the separation and movement of charge carriers. There are two types of contact formation at the interface that can be formed as a result of band bending effect. These contacts are Ohmic contact and Schottky contact. The energy band diagram before and after contact is shown in Fig. 2.6 below.

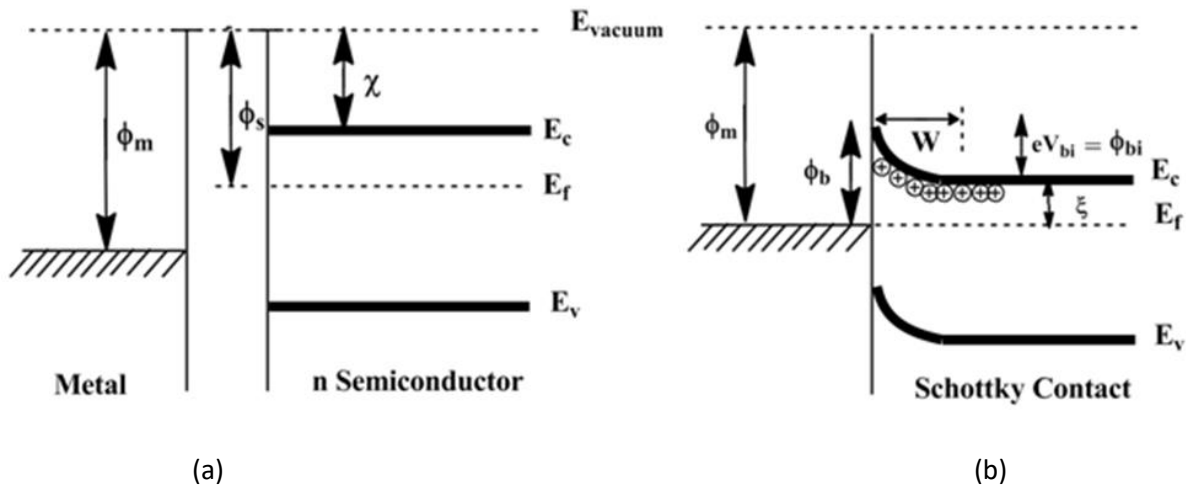


Fig 2.6 Metal and dye contact (a) before contact (b) after contact. A potential barrier is formed at the interface

where ϕ_m denotes the metal work function and ϕ_s denotes the semiconductor work function. If $\phi_m > \phi_s$, electrons will go from the n type semiconductor to the metal in the case of a n type semiconductor. This transfer of electrons will happen until the alignment of the fermi levels of metal and semiconductor reaches to same energy level. As a result of transfer of electrons to the metal, a depletion layer of positive charges with a thickness (W) will be formed near this interface. For an ideal contact between a metal and an n-type semiconductor, the barrier height is expressed as,

$$\phi_b = \phi_m - \chi \quad (2.15)$$

Where ϕ_b can also be expressed as,

$$\phi_b = eV_{bi} + \xi \quad (2.16)$$

$$= \phi_{bi} + \xi \quad (2.17)$$

Where χ is the electron affinity of the semiconductor, e is the electronic charge, ξ is the energy difference between the conduction band and the fermi energy level of the semiconductor and eV_{bi} is the band bending at zero bias which can also be defined as built in potential ϕ_{bi} formed between metal and semiconductor [29-37].

The built in potential can be expressed as,

$$\phi_{bi} = eV_{bi} = \frac{eN_D W^2}{2\epsilon} \quad (2.18)$$

Where W is the thickness of the depletion layer, ϵ is the permittivity of the semiconductor materials and N_d is the ionized donor density.

Therefore, a Schottky barrier will form at equilibrium for an n-type semiconductor when $\phi_m > \phi_s$ because of the effects of electron transport from semiconductor to metal, shown in Fig. 2.5. Reverse bias refers to the application of a positive voltage across the semiconductor, which increases the band bending. Forward bias refers to the application of a negative voltage across the semiconductor, which lowers the band bending and increases the passage of electrons from the semiconductor to metal.

2.2.2 Bulk-limited current flow at above threshold voltage

The bulk limited current flow occurs on above the threshold voltage. The bulk-limited depends mainly on the structural properties of the natural dye instead of the metal-natural dye contact. If a natural dye is sandwiched between two electrodes, and if either electrode has a low barrier height (ohmic response) to the natural dye metal interface, then the injected carriers form the electrode which has a space charge region. They reach equilibrium by free carriers inside

natural dyes. Because the mobility of carriers is very low, therefore, before traversing injected carriers from one electrode to the other electrode, more and more charges are added. When an external electric field is provided, additional charges are injected from the low barrier electrode to the natural dye, and an equilibrium stage is attained. When the injected carriers are comparable to or higher than the free carrier concentration at this point, the current flow is known as space charge-limited current [38,39].

2.3 Different types of charge transport models

In the following section, we will briefly discuss different transport models which has been developed by different workers by using different types of trap distribution. We will also describe the space charge limited current (SCLC) transport model which we have used in our present work.

2.3.1 Transport models with the extended band and double exponential trap states

Hack and Shur [40-44] presented a model in 1984 to explain the charge transport process in amorphous silicon transistors. From this theory we have assumed that amorphous natural dyes follow the conduction process of amorphous silicon and there are trap states in between valence band (LUMO) and conduction bands (HOMO) and these trap states may be divided into deep states and tail states as shown in Fig. 2.6. Free charge carriers are available for conduction as a result of the contribution from these two states along with the carrier from band states.

In this model, we consider that there are localized acceptors like exponential trap states in the energy gap, illustrated in Fig. 2.6. When the Fermi level in the accumulation zone switches from deep to tail localized states in the energy gap, the transition from below to above threshold voltage happens. Considering the contribution of charge carriers from both these states we have estimated the expression of current. The density of acceptor-like states $g_A(E)$ (exponential states with deep and tail states) is approximately exponential with the energy of the form,

$$g_A(E) = g_1 \exp\left(\frac{E}{E_1}\right) + g_2 \exp\left(\frac{E}{E_2}\right) \quad (2.19)$$

Here g_1 and g_2 are the concentration of tail and deep localized trap states respectively. E_1 and E_2 are equal to kT_1 and kT_2 respectively where k is the Boltzmann constant. For the tail states T_1 is the characteristic temperature which is of the order of 300K and for deep states T_2 is the characteristic temperature which is of the order of 1000K.

To estimate the expression of the current for the diode, Poisson's equation is solved with the total charge which is equal to $(N + n_{free})$.

Where N is the density of charge induced into both the deep and tail localized states given by

$$qN = \int_{E_{F0}}^{E_C} \frac{g_A(E) dE}{1 + \exp\left(\frac{E - E_F}{kT}\right)} \quad (2.20)$$

where q is the electronic charge, g_A is the density of localized acceptor states, E is the energy, E_{F0} the bulk Fermi level, E_F , E_C represents the electron Fermi level and bottom of the conduction band respectively. Again, the free charge carrier n_{free} coming from the band states is given by,

$$n_{free} = N_C \exp\left(\frac{E_F - E_C}{kT}\right) \quad (2.21)$$

So, the total charge will be $(N + n_{free})$. Taking this charge and solving Poisson's equation becomes the expression of current for the organic or natural dye-based devices which is of the form,

$$I_{ds} = \frac{q\mu_0 w}{L} N_c \exp\left(\frac{-E_{FO}}{KT}\right)^{\frac{KT_e}{q}} \left[\frac{\sin\left(\frac{\pi T}{T_2}\right)}{2\pi\epsilon KT_2 KT g_{FO}} \right]^{T_2/T} [Cox V_g]^{\frac{2T_2 - T}{T}} V_{ds} \quad (2.22)$$

C_{ox} is the insulator capacitance per unit area.

But this model has limitations and cannot explain the experimental data in most organic and natural dye-based systems.

2.3.2 Vissenberg and Matters with exponential tarp distribution

Vissenberg and Matters have studied the field effect in an organic thin-film transistor [44]. Here we have seen the transport model based on variable range hopping in an exponential DOS, as illustrated in Fig. 2.7. In this model conductivity in the organic dye is described as the transport of carriers through a resistor network. The percolation criterion is associated with temperature, the Fermi level, and the width of the DOS's exponential tail. Charge transport in this concept is accomplished through variable-range hopping. The model is based on the following exponential DOS

$$g(E) = \frac{N_t}{kT_0} \text{Exp}\left(\frac{E_F}{kT_0}\right) \quad (-\infty < E \leq 0) \quad (2.23)$$

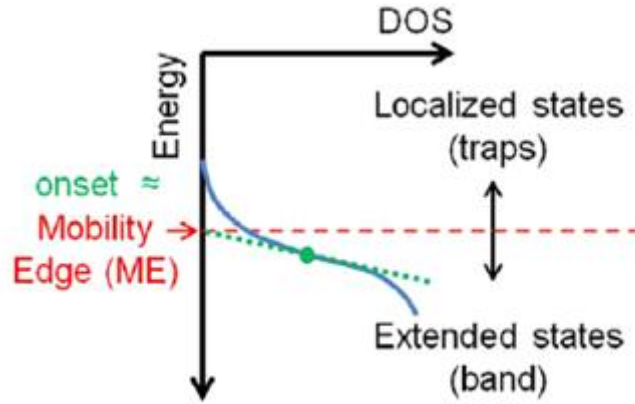


Fig.2.7 Hopping transport within exponential traps

where N_t is the number of states per unit volume, k is Boltzmann's constant, and T_0 is the parameter that indicates the width of the exponential distribution.

In equilibrium, the energy distribution of the carriers is given by the Fermi - Dirac distribution, $f(E, E_F)$, where E_F is the Fermi energy.

The carrier occupation δ can be written as,

$$\begin{aligned}\delta &= \frac{1}{N_t} \int g(E) f(E, E_F) dE \\ &= \text{Exp}\left(\frac{E_F}{k_B T_0}\right) \Gamma(1 - T/T_0) \Gamma(1 + T/T_0)\end{aligned}\quad (2.24)$$

Where $\Gamma(Z) = \int_0^{\infty} dy \exp(-y) y^{Z-1}$

Using the percolation theory, they have calculated the expression for conductivity as a function of occupation δ and the temperature T in the following form,

$$\sigma(\delta, T) = \sigma_0 \left[\frac{\pi N_t \delta (T_0/T)^3}{(2\alpha)^3 B_c \Gamma(1 - T/T_0) \Gamma(1 + T/T_0)} \right]^{T_0/T} \quad (2.25)$$

where σ_0 is the conductivity pre factor, α is the wave-function overlap parameter, kT_0 is the width of the exponential tail of the DOS, and B_c is a constant (~ 3.8). The fitting parameters are σ_0 , α , and T_0 . The width of the DOS and the overlap parameter primarily determine mobility in this model. This expression of conductivity is used to describe the field effect mobility, μ_{FE} in OFET. But this model is quite unable to explain the experimental data of many systems including our data also

2.3.3 Dispersive transport model

i) Scher-Montrol model

Dispersive transport has been described by Scher-Montrol. This model was originally derived for the positional disorder [47,48]. To describe the effects of disorder it can be said that a distribution function $\psi(t) \sim t^{-(1+\alpha)}$ of transition rates between hopping sites will be same as Fig 2.8.

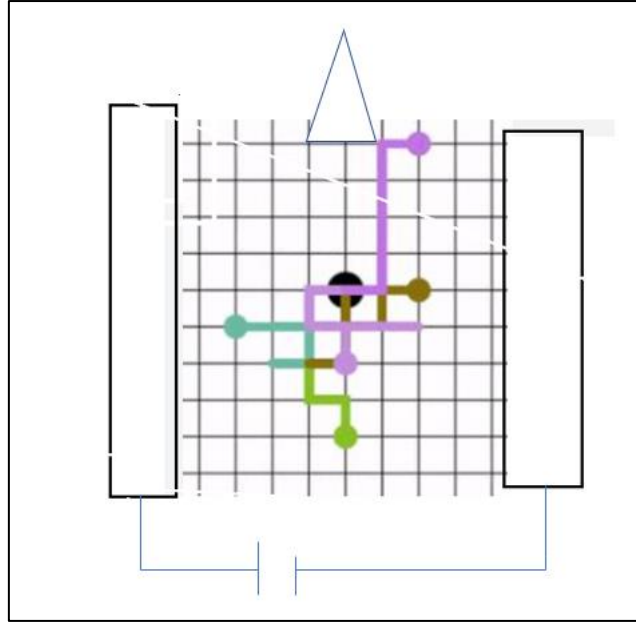


Fig. 2.8 Random walk between the different sites

The model predicts that as time goes on, a growing percentage of carriers will experience at least one prolonged waiting period at some location, causing a dispersion in transit time. Hence this model is termed as dispersive transport model.

From Scher-Montrol model photocurrent transient will decay as

$$j(t) \sim t^{-(1-\alpha)} \quad \text{for } t < t_T \quad (2.26)$$

$$j(t) \sim t^{-(1+\alpha)} \quad \text{for } t > t_T \quad (2.27)$$

At low fields it may be assumed that $l(E) \propto E$. the transit time thus varies with thickness and field as $(L/E)^{1/\alpha}$. Mobility can be written as

$$\mu \sim \frac{W_0 L^{(1-1/\alpha)}}{E} L^{-1/\alpha} \sinh\left(\frac{e\rho E}{2kT}\right)^{1/\alpha} \exp\left(-\frac{\Delta_0}{kT}\right) \quad (2.28)$$

ii) Bassler formalism

Organic dye hopping sites are found in statistically distinct contexts since there is no long-range order. Thus, distribution can affect both site energies and intersite distances. The formalism is built primarily using Monte Carlo techniques and is based on fluctuations in site energy and intersite distances. The temperature dependence of the low field mobility can be written as [49,50]

$$\mu(T) = \mu_0 \exp\left[-\left(\frac{T_0}{T}\right)^2\right] \quad (2.29)$$

At high fields a carrier will gain energy $eE\rho$ upon jumping from one site to another separated by a distance ρ . Then at high fields the mobility can be written as

$$\mu(T, E) = \mu_0 \exp\left[-\left(\frac{T_0}{T}\right)^2\right] \exp\left(\frac{E}{E_0}\right) \quad (2.30)$$

In this model the traps follow a Gaussian type distribution shown in Fig. 2.9

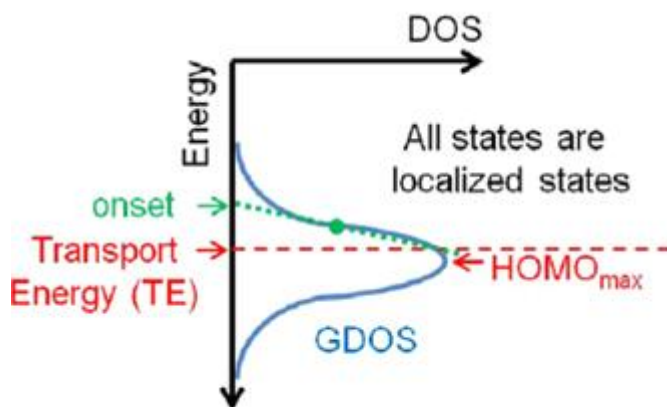


Fig. 2.9 Gaussian type distribution of traps

2.3.4 Trap assisted transport models

i) Poole – Frenkel model

The Poole-Frenkel effect shows how an applied field reduces the carrier's ionization energy in a Coulomb Potential. The effect is based on Coulomb centers, or traps, which are charged when empty. For the 1D case, this leads to field-dependent mobility (μ) and can be written as

$$\mu = \exp\left(\frac{\beta_{PF} E^{1/2}}{kT}\right) \quad (2.31)$$

$$\text{where } \beta_{PF} = \left(\frac{e^3}{\pi\epsilon\epsilon_0}\right)^{1/2}$$

Here E is the electric field, e is the electronic charge, ϵ is the dielectric constant at high frequency, and ϵ_0 is the permittivity of free space; kT has its usual meaning.

The Poole-Frenkel effect cannot account for mobilities of charges because mobility decreases with increasing field. Though several attempts have been made to modify 1D Poole-Frenkel effect to make it more realistic. Here the field dependencies are like the 1D Poole-Frenkel effect. But in our study, the experimental data contradicts this theory.

ii) Kinetic rate model

Bagley (1970) proposed a model assuming transport occurs by hopping over multiple barriers separated by a distance ρ with an average height ΔG . Bagley's expression for mobility is [45]

$$\mu = \frac{2\rho v}{E} \exp\left(-\frac{\Delta G}{2kT}\right) \sinh \frac{\rho e E}{2kT} \quad (2.32)$$

Where v is an attempt to escape frequency. Bagley's model leads to mobility that is strongly field dependent at high fields but field independent at low fields.

Seki (1974) proposed a barrier model based on tunneling of carriers between neutral molecules to adjacent charged molecules. This model is 1D and assumes that forward and reverse jumps are symmetrical. We assumed that energy levels can be described by an average fluctuation amplitude U_0 and distance λ_0 . Seki's expression for mobility is

$$\mu = \frac{\lambda_0}{\tau_0 E} \exp\left(-\frac{\rho}{\rho_0}\right) \exp\left(-\frac{U_0}{kT}\right) 2 \sinh \frac{e\lambda_0 E}{kT} \quad (2.33)$$

τ_0 and λ_0 are constants with dimensions of time and distance, ρ_0 a wave function decay constant and ρ is the intersite distance. The Seki and Bagley models lead to mobilities with similar field and temperature dependence.

iii) Multiple trapping and de-trapping model

In this model, the traps are considered as exponential and carriers are being trapped and released i.e. de trapped which is shown in Fig. 2.10

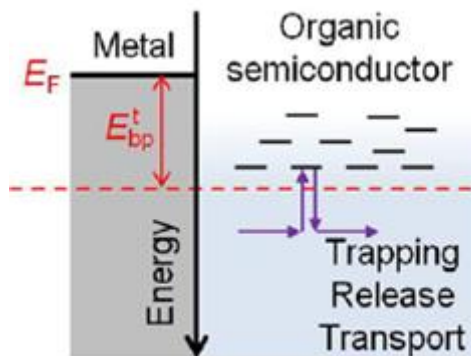


Fig. 2.10 Trapping and de-trapping of carriers at different energy levels distributed exponentially

The basic limitation of the kinetic rate model is that it does not agree with experimental results. Because the predicted field and temperature dependence of the mobility does not agree with the experimental results. In most of the natural or organic dyes, mobility decreases over an extended range of fields and mobility increases with the temperature. Field-independent mobilities at low fields are seldom observed. The models cannot account for mobilities that decrease with increasing field.

Apart from these models, there are also some other models available in the literatures. These models are not uniquely applicable to all organic or natural dye systems. Basically, the disorder materials are considered as insulators and space charge formation during transport. There is a Space Charge transport model which we have used in our present work and it will be discussed in the following section.

2.3 Space Charge limited bulk transport model in the presence of traps

We have started to work in this field by reviewing different literature and got interested to study on organic and natural dye-based devices that will be used as nonconventional electronic material. In this thesis, we have investigated a small part of the charge transport mechanism of nonconventional electronic materials.

Because of the weak molecular links and structural disarray of organic and natural dyes, they are more likely to include electrical traps. According to Fig. 2.11(b), these traps introduce energy levels into the space between the organic or natural dye. Devices built of organic and NCE materials can function and perform better when these trap levels are charged and discharged. While the trap's origin is currently unclear, theoretical models have been created in the past to investigate their effects on various system aspects. A significant portion of the conduction carriers injected from the electrodes become caught due to the trap levels, and the charges are typically crowded close to the electrodes.

Steady-state dark 'Current-Voltage' (I-V) characteristics can reveal a lot of information regarding the charge transport process. Measurement of series resistance (R_s) and barrier height (Φ_b) from non-linear I-V relation is important for device application. The effect of traps and their distribution shows the power law I-V relation. Estimation of characteristic temperature ' T_t ' and trap energy ' E_t ' is also important for the trap charge limited conduction process.

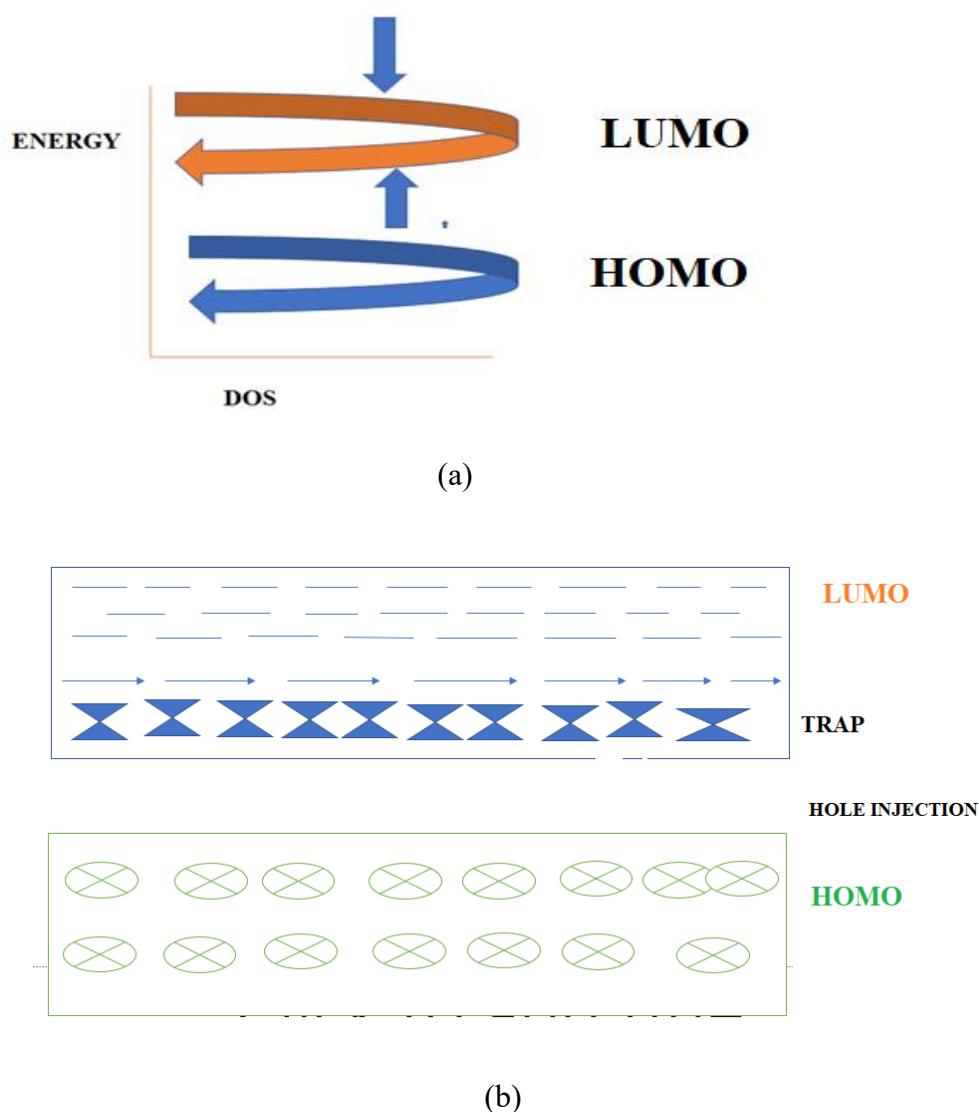


Fig. 2.11 (a) Distribution of HOMO and LUMO levels in amorphous organic semiconductors (b) Trap states between the LUMO and HOMO

2.5 Estimation of trap energy from the steady state dc I-V characteristics

The dark I-V characteristics, as discovered in the literature, can be fitted with the notion that the carriers during conduction through the device may be trapped at distinct trap levels between the LUMO and HOMO states. A hypothesis based on trap charges is used to explain the change in the conduction process. The starting equations are for one-dimensional single or double (e.g., for electron or holes or both) carrier drift current and Poisson equations

$$J_d = nq\mu E$$

$$\frac{dE}{dx} = \frac{q}{\varepsilon}(n + n_t) \quad (2.34)$$

where J_d is the drift current density, μ is the carrier mobility, E is the electric field strength, n and n_t are the free and trapped charge concentrations, respectively, q is the unit charge, and ε is equal to $\varepsilon_0\varepsilon_r$ with ε_0 being the permittivity of vacuum and ε_r the relative dielectric constant. The above equations can be solved for two cases as follows

Case I: When trap charge density is much less than free carrier density ($n_t \ll n$)

Then the above Eqn. 2.30 may be written as

$$\frac{dE}{dx} = \frac{q}{\varepsilon} n \quad (2.35)$$

Free charge carriers consist of both injected and thermally generated.

There are always some thermally generated free carriers present in the material. Let it be denoted by n_0 . For metals, this number is very high so that injected space charge density n is negligible compared to n_0 . For insulators, n_0 is negligible for high injection levels. But for the very small external field, the injection of carriers into the insulator is very low. Therefore, for low external voltages considering the presence of free charge carriers the above equation can be written in the form

$$J_d = \{n(x) + n_0\}q\mu E$$

$$\frac{dE}{dx} = \frac{q}{\varepsilon} n(x) \quad (2.36)$$

at the low injection level $n(x)$ may be approximated as $n(x) \sim 0$, then the above equation takes the form

$$(2.37)$$

$$J_d = n_0 q \mu E$$

$$E = \text{cons} \tan t$$

which is ohms law

And for high injection levels when injected carriers are over-numbered thermally generated free carriers may be written as Eqn. 2.31.

To solve Eqn. 2.31 we replace $n(x)$ from the first equation with the second and

realizing that $E = - \frac{dV}{dx}$ where V is the potential we have

$$\begin{aligned} \frac{dE}{dx} &= \frac{1}{\mu \epsilon E} J_d \\ \frac{d^2V}{dx^2} \frac{dV}{dx} &= \frac{J_d}{\mu \epsilon} \\ \frac{d}{dx} \left\{ \left(\frac{dV}{dx} \right)^2 \right\} &= \frac{2J_d}{\mu \epsilon} \end{aligned} \tag{2.38}$$

Integrating ... w.r.t. ... x

$$\Rightarrow \frac{dV}{dx} = \sqrt{\frac{2J_d}{\mu \epsilon}} x + \text{cons} \tan t$$

If we take field E to be zero at $x=0$ then the above constant is zero. Taking the sample

thickness to be L we have by integrating the above equation w. r. t. x between $x=0$

to $x=L$

$$\begin{aligned}
\therefore \int_0^V dV &= \sqrt{\frac{2J_d}{\mu\epsilon}} \int_0^L x^{1/2} dx \\
\therefore V &= \sqrt{\frac{2J_d}{\mu\epsilon}} \frac{L^{3/2}}{3/2} \\
\therefore V^2 &= \left(\frac{2J_d}{\mu\epsilon}\right) \frac{4}{9} L^3 \\
\Rightarrow J_d &= \frac{9}{8} \mu\epsilon \frac{V^2}{L^3}
\end{aligned} \tag{2.39}$$

This is a space-charge limited current equation.

Case II. When trap charge density is much greater than the free carrier density ($n_t \gg n$)

Eqn. 2.31 takes the form

$$\frac{dE}{dx} = \frac{q}{\epsilon} n_t \tag{2.40}$$

The above equation along with Eqn. 2.32 cannot be solved if we do not know the relation between n and n_t . We consider two types of trap distribution, in case ‘a’ we assume single trap energy and in case ‘b’ traps have exponential energy distribution.

- a) For traps having a single discrete energy E_s trap charge carrier density can be written as

$$\begin{aligned}
n_t = n_s &= \frac{N_c}{1 + \exp\{(E_s - F_n)/kT\}} \\
n_s &= N_c \exp\{(F_n - E_s)/kT\} \\
&= n / \theta
\end{aligned} \tag{2.41}$$

Where $\theta = \exp(E_s / kT)$

Then the solution of Eqn. 2.36 and Eqn. 2.35 with this form of n_t can be done exactly in the same way as mentioned before and the result will be the form

$$J_d = \frac{9}{8} \mu\epsilon \frac{V^2}{L^3} \frac{1}{1 + \frac{1}{\theta}} \tag{2.42}$$

This is the Discrete Trap Charge Limited conduction process

- b) When traps have an exponential energy distribution the trap charge concentration (n_t) is given as

$$n_t = H_n \exp\left(\frac{F_n}{kT_t}\right) \quad (2.43)$$

where H_n is the trap density, F_n is the electron fermi energy, k is Boltzmann's constant and T_t is the characteristic temperature of the exponential trap distribution (i. e. $T_t = E_t/k$, where E_t is the characteristic trap energy). The relation between n_t and n can be found as

$$\begin{aligned} n_t &= H_n \exp\left(\frac{F_n}{kT_t}\right) \\ n_t &= C_n \exp\left(\frac{F_n}{kT_t}\right) \\ n_t &= H_n \exp\left(\frac{F_n}{kT_t} * \frac{T}{T_t}\right) \\ &= H_n \left(\frac{n}{N_c}\right)^{1/m} \quad \text{where } m = \frac{T}{T_t} \end{aligned}$$

Therefore, from Eqn. 2.34 we have

$$\begin{aligned} \frac{dE}{dx} &= \frac{q}{\epsilon} C n^{1/m} \\ &= \frac{q}{\epsilon} C \left(\frac{J}{qE\mu}\right)^{1/m} \\ \therefore \frac{d^2V}{dx^2} * \left(\frac{dV}{dx}\right)^{1/m} &= \frac{q}{\epsilon} C \left(\frac{J}{q\mu}\right)^{1/m} \\ \therefore \frac{d}{dx} \left\{ \left(\frac{dV}{dx}\right)^{(1+m)/m} * \frac{m}{1+m} \right\} &= \frac{q}{\epsilon} C \left(\frac{J}{q\mu}\right)^{1/m} \end{aligned}$$

Integrating w.r.t x

$$\left\{ \left(\frac{dV}{dx}\right)^{(1+m)/m} * \frac{m}{1+m} \right\} = \frac{q}{\epsilon} C \left(\frac{J}{q\mu}\right)^{1/m} x + \text{constant}$$

Therefore, from Eqn. 2.31 we have

The value of this constant is zero because at $x=0$, $dV/dx=0$. Therefore

$$\frac{dV}{dx} = \left(\frac{1+m}{m}\right)^{m/(m+1)} \times \left(\frac{C}{\epsilon}\right)^{m/(m+1)} \times q^{(m-1)/(m+1)} \times \left(\frac{J}{\mu}\right)^{1/(m+1)} \times x^{m/(m+1)}$$

Integrating again w. r. t. x between $x=0$ to $x=L$, the sample thickness we have

$$\int_0^V dV = \left(\frac{1+m}{m}\right)^{m/(m+1)} \times \left(\frac{C}{\epsilon}\right)^{m/(m+1)} \times q^{(m-1)/(m+1)} \times \left(\frac{J}{\mu}\right)^{1/(m+1)} \int_0^L x^{\frac{m}{(m+1)}} dx$$

$$\begin{aligned}
V &= \left(\frac{1+m}{m}\right)^{m/(m+1)} \times \left(\frac{C}{\epsilon}\right)^{m/(m+1)} \times q^{(m-1)/(m+1)} \times \left(\frac{J}{\mu}\right)^{1/(m+1)} \times \frac{m+1}{2m+1} \times L^{\frac{2m+1}{m+1}} \\
V^{m+1} &= \left(\frac{1+m}{m}\right)^m \times \left(\frac{C}{\epsilon}\right)^m \times q^{(m-1)} \times \left(\frac{J}{\mu}\right) \times \frac{m+1}{2m+1}^{m+1} \times L^{2m+1} \\
J &= N_c \mu \frac{m+1}{2m+1}^{m+1} \left(\frac{\epsilon m}{(m+1)H_n}\right)^m q^{(m-1)} \frac{V^{m+1}}{L^{2m+1}} \quad (2.44)
\end{aligned}$$

$$[\therefore C = \frac{H_n}{N_c^{1/m}}]$$

This is the Space Charge Limited Conduction process.

The most notable feature in the above equation is the power law dependence $J \sim V^{m+1}$. This type of I-V relation arises due to traps that are exponentially distributed between the LUMO and HOMO. Our experimental findings of the Current-Voltage (I-V) relation is best fitted with this model.

2.6 Methods to determine series resistance (R_s) from dark I-V characteristics

From the Current Voltage characteristics and $\ln I$ Vs. V characteristics of organic solar cell in dark mode. It is observed that the $\ln I$ Vs. V plot is linear at low bias voltage and deviates from linearity at high bias voltage [46-51].

2.6.1 $\frac{dV}{dI}$ Vs. I Method

This deviation of the I-V characteristics is due to the presence of series resistance. To measure the series resistance, we have followed few equations, shown below,

$$I = I_0 \left[\exp \left(\frac{q(V - IR_s)}{nkT} \right) - 1 \right] \quad (2.45)$$

$$\frac{dI}{dI} = \frac{d}{dI} \left[I_0 \left[\exp \left(\frac{q(V - IR_s)}{nkT} \right) - 1 \right] \right] \quad (2.46)$$

$$1 = I_0 \frac{q}{nkT} \left(\frac{dV}{dI} - R_s \right) \exp \left(\frac{q(V - IR_s)}{nkT} \right) \quad (2.47)$$

$$1 = \frac{q}{nkT} \left(\frac{dV}{dI} - R_s \right) \times I \quad (2.48)$$

$$\frac{qI}{nkT} \frac{dV}{dI} = 1 + IR_s \frac{q}{nkT} \quad (2.49)$$

$$\frac{dV}{dI} = \frac{nkT}{qI} + R_s \quad (2.50)$$

The first term of the left hand side Eqn. 2.45 can be negligible at the high voltage when the value of the current is high. So, this Equation can be written as

$$\frac{dV}{dI} \approx R_s \quad (2.51)$$

2.6.2 Cheung Cheung Method to estimate Series Resistance ($\frac{dV}{d \ln I}$ Vs. I Method and $H(I)$ Vs. I Method)

Moreover, there are also various methods to determine device R_s from the dark I-V characteristics. One of the important methods is Cheung Cheung method which we have used to extract the device R_s [44]. According to this method we have followed few equations, shown below,

$$I = I_0 \left[\exp \left(\frac{q(V - IR_s)}{nkT} \right) - 1 \right] \quad (2.52)$$

$$\frac{dI}{d \ln I} = \frac{d}{d \ln I} \left[I_0 \left[\exp \left(\frac{q(V - IR_s)}{nkT} \right) - 1 \right] \right] \quad (2.53)$$

$$\frac{dI}{d \ln I} = \left[I_0 \frac{q}{nkT} \exp \left(\frac{q(V - IR_s)}{nkT} \right) \left[\frac{dV}{d \ln I} - \frac{dIR_s}{d \ln I} \right] \right] \quad (2.54)$$

$$I = \left[\frac{q}{nkT} \left[\frac{dV}{d \ln I} - \frac{dIR_s}{d \ln I} \right] I \right] \quad (2.55)$$

$$\frac{nkT}{q} = \frac{dV}{d \ln I} - IR_s \quad (2.56)$$

$$\frac{dV}{d \ln I} = \frac{nkT}{q} + IR_s \quad (2.57)$$

So, from this equation it can be said that the plot of $\frac{dV}{d \ln I}$ Vs. I give the value of ideality factor (η) from the intercept at the Y axis and the slope of the curve gives the value of R_s .

Apart from that we can verify the value of R_s extracted from $\frac{dV}{d \ln I}$ Vs. I plot by simplifying the Eqn. 2.40 in modified form shown below,

$$I = I_0 \left[\exp \left(\frac{q(V - IR_s)}{nkT} \right) \right] \quad (2.58)$$

$$\ln \frac{I}{I_0} = \left(\frac{q(V - IR_s)}{nkT} \right) \quad (2.59)$$

$$\ln I - \ln I_0 = \frac{qV}{nkT} - \frac{qIR_s}{nkT} \quad (2.60)$$

$$V = \frac{nkT}{q} \ln I - \frac{nkT}{q} \ln I_0 + IR_s \quad (2.61)$$

Putting the expression of I_0 then equation will be written as,

$$V = \frac{nkT}{q} \ln I - \frac{nkT}{q} \ln \left[AA^* T^2 \exp \left(-\frac{q\phi_B}{kT} \right) \right] + IR_s \quad (2.62)$$

$$V = \frac{nkT}{q} \left[\ln \frac{I}{AA^* T^2} \right] + n\phi_B + IR_s \quad (2.63)$$

$$V - \frac{nkT}{q} \left[\ln \frac{I}{AA^* T^2} \right] = n\phi_B + IR_s \quad (2.64)$$

Now by considering,

$$H(I) = V - \frac{nkT}{q} \left[\ln \frac{I}{AA^* T^2} \right] \quad (2.65)$$

$$H(I) = n\phi_B + IR_s \quad (2.66)$$

By putting the value of η extracted from equation [45-46] we can extract the value of R_s . The plot of this equation gives a straight-line where the slope gives the value of R_s and the intercept at the y axis gives the value of barrier height (ϕ_B). So according to this Cheung Cheung method we can determine the value of R_s in two ways and show the consistency of two methods with each other.

2.7 Conclusion

In this chapter we have discussed different charge transport model for amorphous, disordered solids. For herbal dyes, there is no such charge transport theory is available. In the above discussed theories are generally used for organic amorphous solids. Since the herbal dyes are also amorphous in nature, it is our idea that it may also be applicable to our systems also.

According to the discussion, nanoparticle composite natural dye materials have been proven to have better mechanical, thermal, and electrical properties than the single natural dye from which they were prepared. ZnO and TiO₂ NP have also been reported to improve conductance due to better excitons dissociation and electron transport to electrodes. However, when compared to its inorganic equivalent, its conductance is still quite low, and further research is needed to improve it. Another challenge in our study is to focus more on the synthesis of nonconventional electronic materials, which will be applicable to a wide range of electronic devices and have greater environmental stability. More research is also needed on the creation of various NP which may improve the conductivity of natural dye. In the following chapters, we will estimate the conductivity, the charge carrier density from the Hall experiment. The bandgap energy from the I-T characteristic, the series resistance, the barrier height, and the trap energy from the steady state dark I-V characteristics of various organic and natural dye-based photovoltaic devices, will also be estimated.

2.8 References

1. S. Iijima, Helical microtubules of graphitic carbon, *Nature* 354 56 (1991)
2. M.J. Kellt, *Low Dimensional Semiconductors*, Oxford University Press, (1995)
3. P. M. Ajayan et al, Nanometre-size tubes of carbon, *Progress of Phys*, 60 1025 (1997)
4. J. W. Mintmire et al, Electronic and structural properties of carbon nanotubes, *Carbon* 33 893 (1995)
5. SP. Somani et al, Improving photovoltaic response of poly(3-hexylthiophene)/ n-Si heterojunction by incorporating double-walled carbon nanotubes, *Applied Physics Letters*, 89 1-2 223505 (2006)

6. A.J. Ferguson et al, Fullerenes and carbon nanotubes as acceptor materials in organic photovoltaics, *Materials Letters*, 115–125 90 (2013)
7. Y.H. Kim et al, Semi-transparent small molecule organic solar cells with laminated free-standing carbon nanotube top electrodes, *Solar Energy Materials and Solar Cells*, 244–250 96 (2012)
8. D.D. Tune et al, Single-walled carbon nanotube network electrodes for dye solar cells, *Solar Energy Materials and Solar Cells*, 1665–1672 94 (2010)
9. F. Xu et al, Single-walled carbon nanotube anodes based high performance organic light-emitting diodes with enhanced contrast ratio, *Organic Electronics*, 302–308 13 (2012)
10. K. Aitola et al, Flexible metal-free counter electrode for dye solar cells based on conductive polymer and carbon nanotubes, *Journal of Electroanalytical Chemistry*, 70–74 683 (2012)
11. K. Aitola et al, Highly catalytic carbon nanotube counter electrode on plastic for dye solar cells utilizing cobalt-based redox mediator, *Electrochimica Acta*, 206–209 111 (2013)
12. A. Arena et al, Photovoltaic properties of multi-walled carbon nanotubes, *Microelectronic Journal*, 1659–1662 39 (2008)
13. G. Keru et al, Nitrogen-doped carbon nanotubes synthesized by pyrolysis of (4-[(pyridine-4-yl) methyldene] amino} phenyl) ferrocene. *Journal of Nanomaterials*, 1–7 2013 (2013)
14. J.M. Lee et al, Exciton dissociation and charge-transport enhancement in organic solar cells with quantum-dot/N-doped CNT hybrid nanomaterials, *Advanced Materials*, 2011–2017 25 (2013)
15. S.P. Somani et al, Carbon nanotube incorporation: a new route to improve the performance of organic-inorganic heterojunction solar cells, *Diamond and Related Materials*, 585–588 17 (2008)

16. S. Cataldo et al, Carbon nanotubes and organic solar cells, *Energy & Environmental Science*, 5919–5940 5 (2012)
17. S. Guenes et al, Conjugated polymer-based organic solar cells, *Chemical Reviews*, 1324–1338 107 (2007)
18. S. Bhattacharyya et al, Photovoltaic properties of dye functionalized singlewall carbon nanotube/conjugated polymer devices, *Chemistry of Materials*, 4819–4823 16 (2004)
19. S.K. Hwang et al, Flexible multilevel resistive memory with controlled charge trap band N-doped carbon nanotubes, *Nano Letters*, 2217–2221 12 (2012)
20. J.M. Lee et al, Selective electron- or hole-transport enhancement in bulk heterojunction organic solar cells with N- or B-doped carbon nanotubes, *Advanced Materials* 629–633 23 (2011)
21. D. Jana et al, Effect of chemical doping of boron and nitrogen on the electronic, optical, and electrochemical properties of carbon nanotubes, *Progress in Materials Science*, 565–635 58 (2013)
22. S. Iijima et al, Single-shell carbon nanotubes of 1-nm diameter, *Nature* 603–605 363 1993
23. T. Guo et al, Catalytic growth of single-walled nanotubes by laser vaporization, *Chemical Physics Letters* 49–54 243 (1995)
24. H. Allouche et al, Chemical vapor deposition of pyrolytic carbon on carbon nanotubes: part 1. Synthesis and morphology, *Carbon*, 2897–2912 41 2003
25. F. Danafar et al, Influence of catalytic particle size on the performance of fluidized-bed chemical vapor deposition synthesis of carbon nanotubes, *Chemical Engineering Research and Design* 214–223 89 (2011)
26. M. Kumar et al, Carbon nanotube synthesis and growth mechanism, 307-497, 9, (2011)
27. S.N. Bondi et al, Laser assisted chemical vapor deposition synthesis of carbon nanotubes and their characterization, *Carbon* 1393–1403 44 (2006)

28. E. Kymakis et al, Single-wall carbon nanotube conjugated polymer photovoltaic devices, *Applied Physics Letters*, 112–114 80 (2002)
29. M. Endo et al, Carbon nanotubes. In *Topics in Applied Physics*, Jorio A, Dresselhaus MS (eds), Springer 13–62 44 (2008)
30. M. Shah et al, Electrical characterization of the ITO/NiPc/PEDOT : PSS junction diode, *J. Appl. Phys*, 104-405 43 (2010)
31. F. Yakuphanoglu, Controlling of silicon–insulator–metal junction by organic semiconductor polymer thin film, *Synth. Met.* 1551-1555 160 (2010).
32. F. Yakuphanoglu et al, Inorganic–organic photodiodes based on polyaniline doped boric acid and polyaniline doped boric acid:nickel(II) phthalocyanine composite, *Sensors & Actuators: A. Physical*, 191-196 153 (2009).
33. S. K. Cheung et al, Extraction of Schottky diode parameters from forward current-voltage characteristics, *Applied Physics Letters*, 85-87 49 (1986)
34. M. Benhaliliba, Extracted electronic parameters of a novel Ag/Sno2: In/Si/Au Schottky diode for Solar cell application, *Journal of Nano- and Electronic Physics*, 02029 1-4 7 (2015)
35. H. Hoppe, Nanoscale Morphology of Conjugated Polymer/Fullerene-Based Bulk-Heterojunction Solar Cells, *Adv. Funct. Mater.* 14 1005 (2004)
36. Q. Pei et al, Polymer Light-Emitting Electrochemical Cells: In Situ Formation of a Light-Emitting p–n Junction, *Chem. Soc.* 118 3922 (1996)
37. M. Law et al, Nanowire dye-sensitized solar cells, *Nature Materials* 4 455 (2005)
38. J. Bisquert et al, Physical Chemical Principles of Photovoltaic Conversion with Nanoparticulate, Mesoporous Dye-Sensitized Solar Cells, *J. Phys. Chem. B* 108 8106 (2004)
39. R. F. Cozzens et al, *Electrical Properties of Polymer*, Academic Press, New York (1982)

40. T.A. Skotheim, Dekker, Handbook of Conducting Polymers, New, York (1986)
41. S. Glenis et al, Influence of the doping on the photovoltaic properties of thin films of poly-3-methylthiophene, Thin Solid Films, 139 221 (1986)
42. H. B. Slimane et al, Advances in Physics Theories and Applications, 22 (2013)
43. A. K. Ghosh et al, Photovoltaic and rectification properties of Al/Mg phthalocyanine/Ag Schottky-barrier cells, J. Appl. Phys. 45 230 (1974)
44. R. N. Marks et al, The photovoltaic response in poly(p-phenylene vinylene) thin-film devices, J. Phys.: Condens. Matter. 6 1379 (1994)
45. J. J. M. Halls et al, Exciton diffusion and dissociation in a poly(p-phenylenevinylene)/C₆₀ heterojunction photovoltaic cell, Appl. Phys. Lett. 68 3120 (1996)
46. G. Li et al, High-efficiency solution processable polymer photovoltaic cells by self-organization of polymer blends, Nature Mater. 4 864 (2005)
47. F. Zhang et al, Soluble Polythiophenes with Pendant Fullerene Groups as Double Cable Materials for Photodiodes, Adv. Mater. 13 1871 (2001)
48. W. J. Yoon et al, Plasmon-enhanced optical absorption and photocurrent in organic bulk heterojunction photovoltaic devices using self-assembled layer of silver nanoparticles, Sol. Energy Mater. Sol. Cells, 94 128 (2010)
49. Y. Kim et al, Device annealing effect in organic solar cells with blends of regioregular poly(3-hexylthiophene) and soluble fullerene, Appl. Phys. Lett. 86 063502 (2005)
50. W. C. Luk et al, Enhanced conversion efficiency of polymeric photovoltaic cell by nanostructured antireflection coating, Organic Electronics, 12 557 (2011)
51. S. Cheylan, Organic light-emitting diode with indium-free metallic bilayer as transparent anode, Organic Electronics, 12 818 (2011)

Chapter 3

Estimation of charge carrier density of solid state thin film Turmeric dye

- 3.1 Introduction
- 3.2 Selection of the dye
- 3.3 Brief review on Turmeric dye
- 3.4 Experimental details
 - 3.4.1 Sample preparation
 - 3.4.2 Measurements
 - 3.4.3 Results and Discussions
- 3.5 Conclusion
- 3.6 References

3.1 Introduction

In the previous chapter, we have described the theory of conductivity, and charge transport mechanism of organic and natural dye-based devices. It will be a major field of study in the coming years. We have estimated the conductivity and Hall coefficient of Turmeric dye in solid thin film form in this present chapter. We have measured the Hall coefficient (H_C) of Turmeric using the Hall Effect's working principle. The curves of Hall voltage (V_H) - Hall current (H_C) and Hall voltage (V_H) - Magnetic field (B_H) are found to be linear. These curves have been used to calculate the Hall coefficient. The average value of the Hall coefficient (R) is $22.4 \times 10^{-4} \text{ m}^3\text{C}^{-1}$. The conductivity (σ) of the film is $1.5 \times 10^{-10} \Omega \text{ m}^{-1}$ [1]. We have estimated charge carrier density from this parameter, and its typical value is $2.8 \times 10^{23} \text{ m}^{-3}$. We have also made a Turmeric dye based diode and measured the reverse saturation current, rectification ratio, ideality factor, series resistance, barrier height, and trap energy. The diode has a high ideality factor and series resistance. One of the primary causes for this high value is the presence of traps. As a result, we assessed the trap energy of the device while considering the exponential trap distribution.

3.2 Selection of the dye

Herbal dyes were once used to color food items, leather, and fibres such as wool, silk, and cotton. It is now used in curries to flavour and colour the diet. It has a high medicinal value used to treat inflammation, skin wounds, and coughs for ages. Few researchers have demonstrated its antitumor effects. Curcumin known as (Pigment of Turmeric) Dye-Sensitized Solar Cell performance has been reported by Khalil Ebrahim Jasim and Seamas Cassidy. Various herbal dyes have recently been investigated in order to produce various electronic devices. These natural dye-based devices offer lot of benefits. Herbal dye-based devices are environmentally benign, biodegradable, and cost-effective. There are also several dyes to investigate. Natural dyes such as Turmeric, Hibiscus Rosasinesis, and Sesbania Grandiflora are utilized as photosensitizers in dye-sensitized solar cells due to their high absorption coefficient in the visible region [1-3]. Graetzel and colleagues first reported non-silicon-based solar cells in 1991. However, there are not many studies on the semiconducting properties of Turmeric dye and also not study on the charge carrier density of Turmeric dye. The conductivity of the herbal dye is likely to bring up a new level in material science.

In this chapter, we have studied the magnetic field effect on Turmeric dye and estimated charge carrier density. The chemical composition of Turmeric dye is shown in Fig. 3.1. The chemical formula is $C_{21}H_{20}O_8$. The melting point is 183°C .

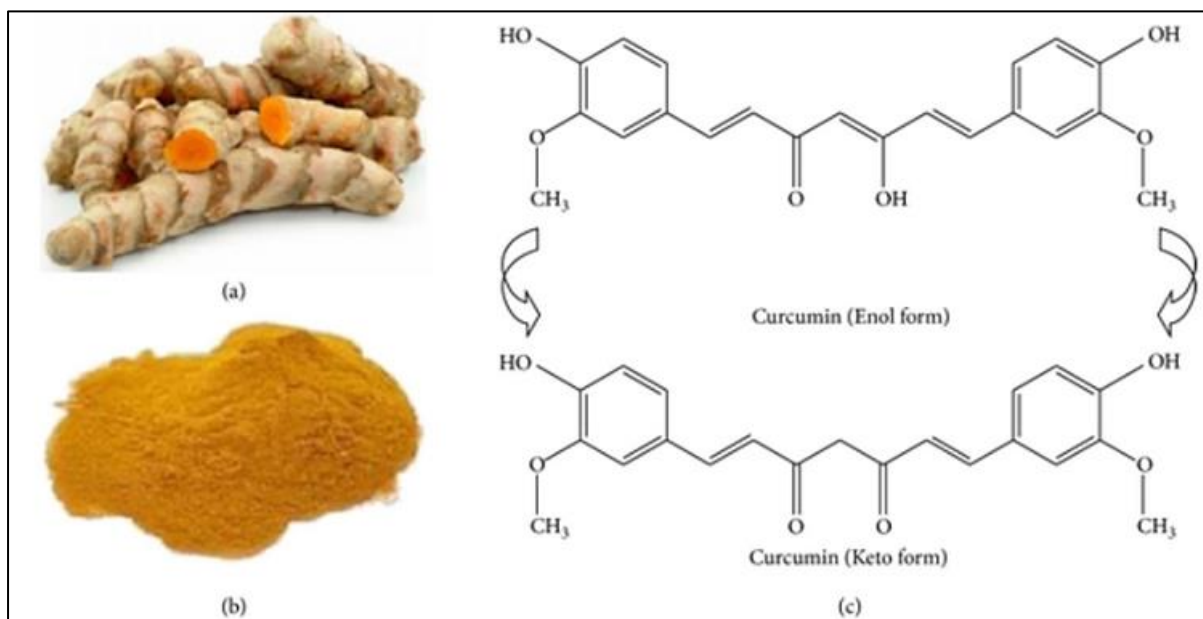


Fig. 3.1 Curcumin and its chemical structure

3.3 Brief review on Turmeric dye

In our previous chapter we have mentioned a brief review on herbal dye. In this present section we will discuss different work carried out with Turmeric dye. Turmeric dyes were once used to color for textile industry. It is now used in curries to flavor and color for the diet. It is also used to treat inflammation, skin wounds, and coughs in medicine. Few researchers have demonstrated its antitumor effects. Curcumin (Pigment of Turmeric) Dye-Sensitized Solar Cell performance has been reported by Khalil Ebrahim Jasim and Seamas Cassidy. Few researchers have recently investigated to produce various electronic devices. Natural dyes such as Turmeric, Hibiscus Rosasinesis, and Sesbania Grandiflora are utilized as photosensitizers in dye-sensitized solar cells due to their high absorption coefficient in the visible region [1-3]. Graetzel and colleagues first reported non-silicon-based solar cells in 1991. However, there are not many studies on the charge carrier density of Turmeric. The conductivity of the Turmeric dye is likely to bring up a new level in material science. Effect of nano particle and dye

concentrations on Turmeric dyes are not reported in literature. We have undertaken this in our study. It can be fabricated over a vast area on various substrates using basic processing techniques such as sol-gel, spin-coating, solvent casting, sublimation, dip coating, and so on. Among the other herbal dye, Turmeric is easily available and one of the cheapest natural dye. It is a powder form of rhizome of a natural plant named *Curcuma Longa* L [4].

3.4 Experimental details

3.4.1 Sample preparation

In order to prepare the sample (PVA), Poly Vinyl Alcohol solution has been prepared. 1gm of (PVA) is dissolved in 15 ml of double distilled water and thoroughly mixed to make a translucent viscous PVA solution. PVA serves as an inert binder in this case. This solution is divided into three 5ml portions. Each component is stored in a pre-cleaned test tube. To prepare a 20% Turmeric solution 1 gm of Turmeric powder is added to one of the test tubes and thoroughly mixed with the help of magnetic stirrer. 2ml of this solution is then spin-coated with an 800 rpm motor speed on a unique sort of glass plate shows in Fig. 3.2. The cell was then dried for 10 hours under a vacuum (10^{-3} mm) before and after the deposition of another glass plate. The cell is now prepared to measure the Hall coefficient. The measured setup is then shown in Fig. 3.3. We have taken 20% Turmeric solution because we have measured the band gap of 20% Turmeric solution as 2.82 eV and 3.36 eV for 5% Turmeric solution in next chapter we have estimated [5].

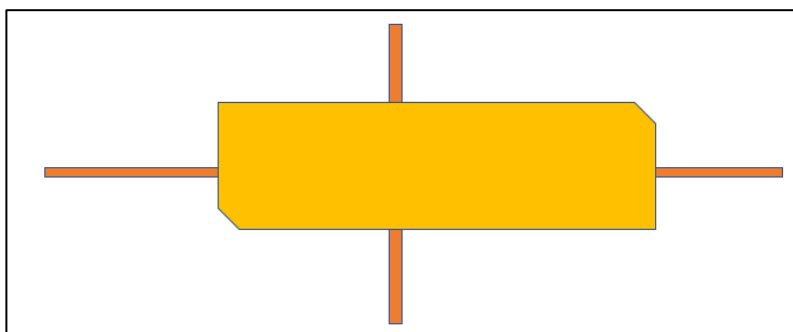


Fig. 3.2 Special type of cell used for Hall experiment

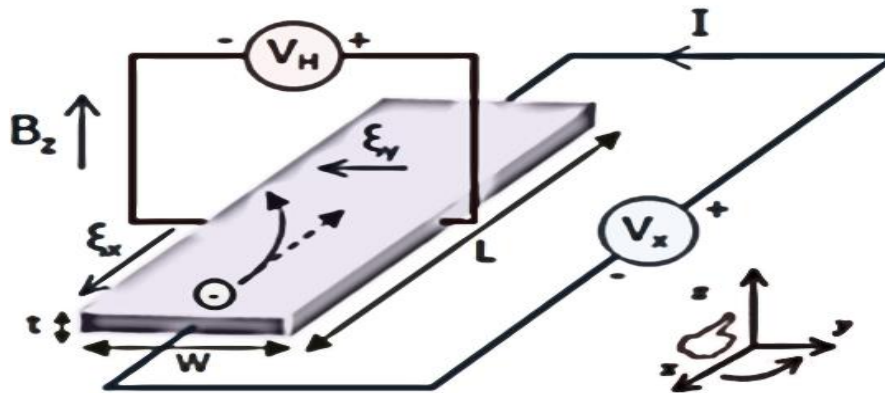


Fig. 3.3 Hall probe connection setup

3.4.2 Measurements

Estimation of charge carrier density

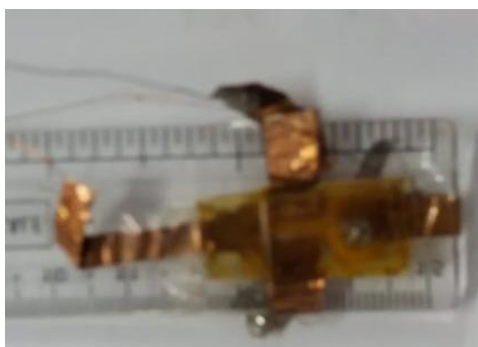
Special Cell Preparation

The Hall experiment method was used in this study to assess the charge carrier density of a Turmeric dye-based thin film. First, we made a Hall sample. Then two clean glass plates of $3 \times 2 \text{ cm}^2$ and four 1.5 cm adhesive Cu tape were taken. These two glass plates were cleaned with distilled water and acetone, then dried for 3 hours under a Hoover (10^{-3} mm). Two Cu tapes were attached along the X-axis with a 1.5 cm gap. Another two are joined along the Y-axis with a 1 cm spacing on a clear glass plate. To make a clear viscous polyvinyl alcohol solution 1 gram of polyvinyl alcohol (PVA) was mixed well with 15 mL of double-distilled water. PVA was used as an inert binder in this case. Turmeric dye was discovered in both the hydrophobic and hydrophilic pockets of PVA; an aqueous PVA solution may be easily cross-linked to form a hydrogel and loaded with Turmeric dye. PVA is widely utilized in a variety of applications due to its remarkable qualities, including as its water-soluble nature, strong optical transmission, and stable thermal properties. Apart from that, PVA is elastic and has oxygen/aroma barrier qualities. When PVA is mixed with another semiconducting dye, the quantity of hydroxyl groups connected to its carbon backbone generates a significant amount of hydrogen bonding, which has a significant impact on its physicochemical bulk properties. As a result of this hydrogen bonding between PVA chains, they have binder qualities. In this study, we used Turmeric dye as the active ingredient of the device. We can improve the charge carriers during the charge transport process by increasing dye concentration, which will

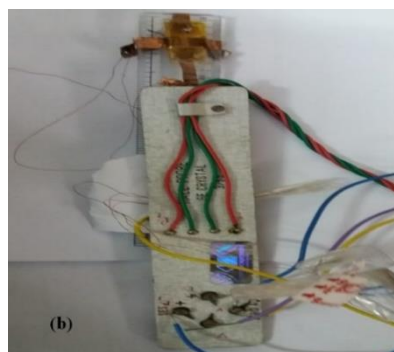
increase the total current of the device. Previously, only a few investigations on the influence of Turmeric color concentration on performance have been conducted [6-13]. We also noticed that the current is greater at increasing dye concentrations. We put 5 mL of PVA solution in a clean test tube and added 1 gram Turmeric powder from the FGO product. A magnetic stirrer was used to thoroughly mix this mixture. 2 mL of this semi-solid was then spin-coated on a unique sort of glass plate at an 800 rpm motor speed. A clear cello tape was used to snugly wrap a clean glass plate around a Turmeric dye-based unique sort of glass plate. Now, the Turmeric thin film was dried for 10 hours under a vacuum (10^{-3} mm). Another glass plate is attached for protection from the environment. The Hall sample was now ready to be measured for the Hall coefficient. Fig. 3.2 show the model and a digital image of the Hall sample, respectively. Fig. 3.3 illustrate the circuit schematic and digital image of the Hall setup, respectively.

Experimental setup

For the Hall experiment, we have developed a Turmeric dye-based Hall sample. The Hall sample is attached to the Hall probe supplied Hall setup (Digital, DHE-21). The Hall probe has four terminals: two for voltage connectors and two for current connectors. The Hall sample has four Cu tapes, two along the X-axis and two along the Y-axis. We have used X-axis Cu tape to connect the voltage connection and Y-axis Cu tape to connect the current connector. We have employed a digital Hall setup (DHE-21) and an electromagnet model EMU -75.



(a)



(b)

Fig. 3.4 (a) Digital image of special type of cell used for Hall experiment and (b) digital image of Hall probe

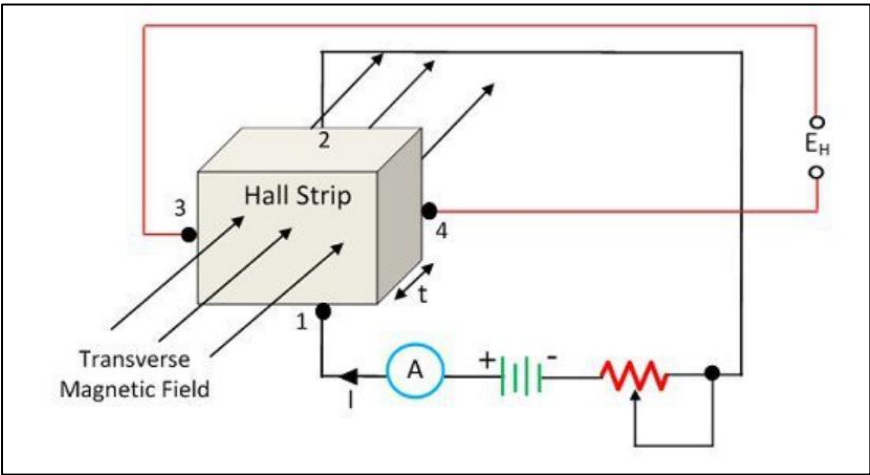
For magnetic field effect measurement, we have used a Digital Gauss-meter (DGM-102) and a constant power supply (DPS-175). Following the "zero field potential" configuration, we have placed the Hall sample in the magnetic field as shown in Fig. 3.4, turned on the electromagnet power supply, and adjusted the current to 2 mA. We have turned the Hall sample so that it is perpendicular to the magnetic field. This change will result in the highest possible Hall voltage. We have measured Hall voltage in both current and magnetic field directions. We have measured the Hall voltage as a function of current while maintaining a steady magnetic field. Similarly, while maintaining the current constant, we have measured Hall voltage as a function of magnetic field.

Theory of Hall Experiment

We have discussed the theory of the Hall experiment in the previous chapter of section 2.1.4

Study of the electrical characteristic of Turmeric dye-based herbal diode

Aside from that, we have prepared one Turmeric dye-based diode after observing the conductivity and charge carrier density. With that we have extracted data like the device's rectification ratio, ideality factor, series resistance, reverse saturation current, etc., among other crucial data. In order to construct the diode, we have sandwiched the Turmeric dye between two electrodes ITO and Al. ITO serves as the front electrode, and Al serves as the back electrode.



(a)



(b)

Fig. 3.5 (a) Hall probe connection setup symbolic (b) Image of Hall Setup

Fig. 3.1 depicts the chemical composition of Turmeric dye. The melting point is 183°C. We have used the Shockley equation, which is shown below, to analyze the dark I-V properties [14-18].

$$I = I_0 \left[\exp \left(\frac{qV}{nKT} \right) - 1 \right] \quad (3.1)$$

Where I_0 is the reverse saturation current which is given by,

$$I_0 = AA^*T^2 \exp \left(-\frac{q\Phi_B}{KT} \right) \quad (3.2)$$

Where I_0 is the reverse saturation current, q is the electronic charge, K is the Boltzmann constant, T is the temperature, V is the applied voltage, and n is the ideality factor.

To prepare the cell, we have prepared a PVA solution by combining 1 mg of PVA (bought from S. D. Fine Chem. Ltd., Boisar, India) with 10 mL of distilled water in a clean beaker. The PVA solution is then agitated using a magnetic stirrer for 30 minutes. The PVA solution is then mixed with 20 mg of Turmeric dye, and the mixture is well agitated for further 30 minutes to create the Turmeric dye solution. The solution is then spin-coated on ITO-coated glass at a speed of 1500 rpm, dried, and then repeated at a speed of 2500 rpm. The aluminum electrode

is similarly spin-coated with this solution, and it is then dried. We have then sandwiched these two electrodes to create the herbal diode based on Turmeric dye [19,20]. Before being characterized, this synthesized Turmeric dye-based herbal diode is then held in a vacuum for 12 hours [21]. Fig. 3.6 shows the schematic structure of the Turmeric dye-based herbal diode.

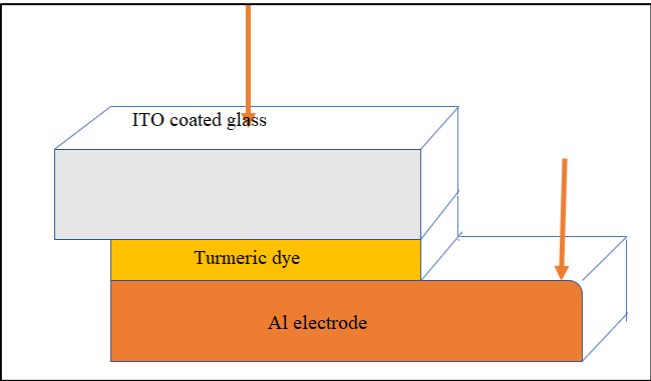


Fig. 3.6 Schematic diagram of Turmeric dye-based organic device

The Keithley 2400 source measure unit is used to measure the steady-state I-V characteristics of the Turmeric dye-based herbal diode. The positive battery terminal is linked to the ITO, and the negative battery terminal connected with the Al electrode for the measurement. Steps of 0.5 V have been used to change the voltage across the device from 0 to 8 V. The experiment is conducted at 26°C, which is the average room temperature [18].

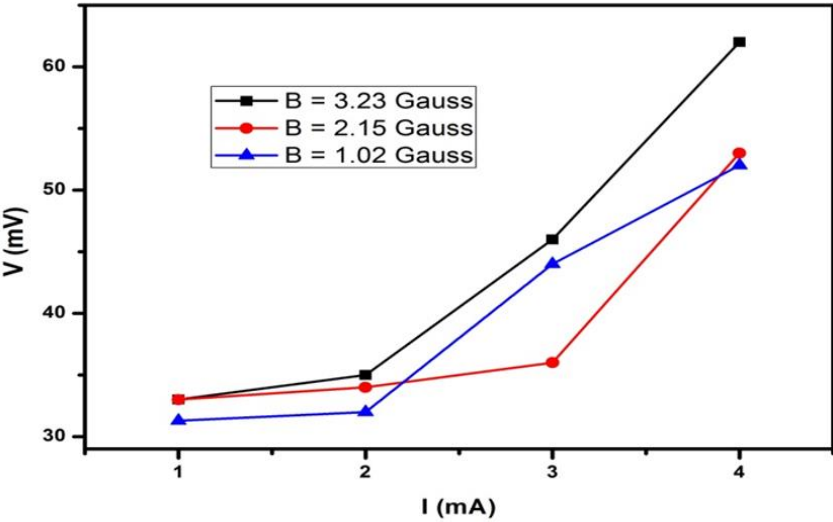


Fig. 3.7 I-V curve for fixed magnetic field

3.4.3 Results and Discussion

While maintaining a constant magnetic field, we have measured Hall voltage and displayed the curve in Fig. 3.7. Then, while maintaining a constant Hall current, we have measured Hall Voltage and displayed the curve in Fig. 3.8. We presume curves to be linear. From these curves, we have estimated the Hall coefficient.

Calculation of mobility and charge carrier density

Average Hall coefficient $R = 0.0022 \text{ m}^3 \text{ Coulomb}^{-1}$

$$\text{Charge carrier density } n = \frac{1}{Rq} = 2.8 \times 10^{23} \text{ m}^{-3}$$

$$\text{Mobility of charge carrier } (\mu) = R \sigma = 3.3 \times 10^{-13} \text{ m}^2 \text{ volt}^{-1} \text{ sec}^{-1}$$

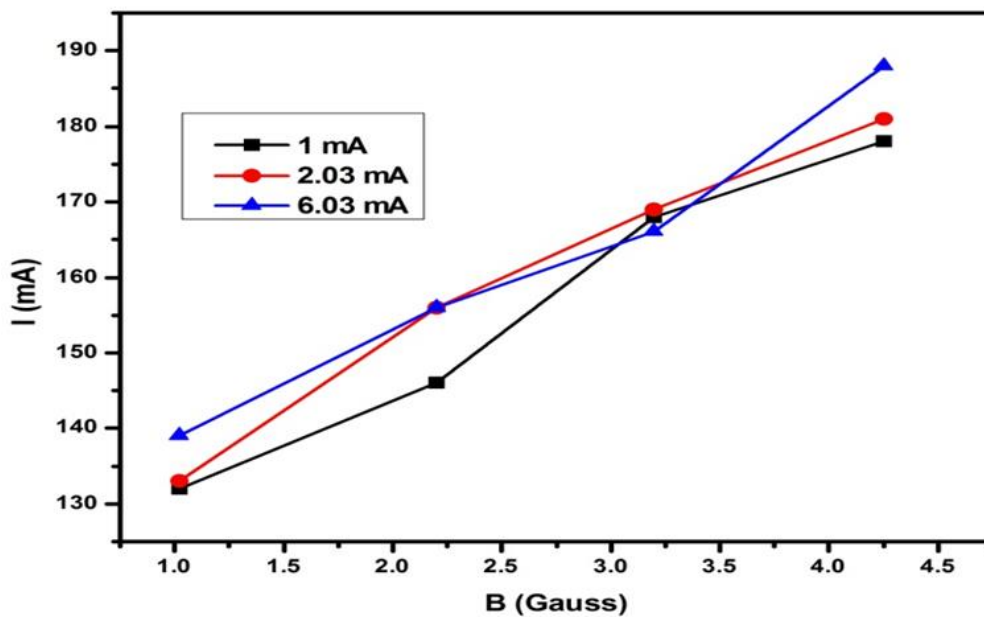


Fig.3.8 I-B curve for fixed Hall current

We have estimated the Hall coefficient of Turmeric dye film for different Hall currents shown in Table 3.1. Its values are different for different Hall currents. So, we have taken the average value of Hall coefficient ($R = 0.0022 \text{ m}^3 \text{ Coulomb}^{-1}$). We have investigated the charge carrier density, and its value is ($n = \frac{1}{Rq} =$) $2.8 \times 10^{23} \text{ m}^{-3}$. We have compared the data with intrinsic Germanium (Ge), Silicon (Si), and Gallium Arsenide (GaAs).

Table 3.1 Extracted value of Hall coefficient (R_H) of Turmeric dye-based device

The thickness of the sample in meter	R_H from the slope of the B vs V_H graph		R_H from the slope of the V_H vs I_H graph	
5×10^{-4}	Hall current I in mA	$R_H = \frac{\Delta V_H Z}{\Delta B I}$ in $\text{m}^3 \cdot \text{Coulomb}^{-1}$	B in Tesla	$R_H = \frac{\Delta V_H Z}{\Delta I B}$ in $\text{m}^3 \cdot \text{Coulomb}^{-1}$
	2	37.24×10^{-4}	0.050	14.41×10^{-4}
	4.03	18.34×10^{-4}	0.215	29.20×10^{-4}
	6.02	12.25×10^{-4}	0.323	27.43×10^{-4}

Using Turmeric dye, we also created one diode in this research, and we looked at a number of different metrics, including the reverse saturation current, rectification ratio, ideality factor, and the diode series resistance. We have looked at the dark I-V characteristic of this Turmeric dye-based diode to investigate these aspects. Fig. 3.9 illustrates this diode's dark I-V characteristic. It is clear from Fig. 3.9 that the device behaves like a diode. Additionally, it has been noted that the device conductivity is extremely low, almost in the microampere range. The device's rectification ratio is 407 at 2.5 V and rise to 543 at 3.5 V. ITO is used as a high-work function electrode, and Al is utilized as a low work function electrode. The band diagram of the ITO/Turmeric dye/Al device is shown in Fig. 3.10. Here Turmeric dye is treated as an n-type semiconductor. This diagram demonstrates how the ITO/Turmeric dye interface forms rectifying contact and Al/Turmeric dye interface creates an ohmic contact.

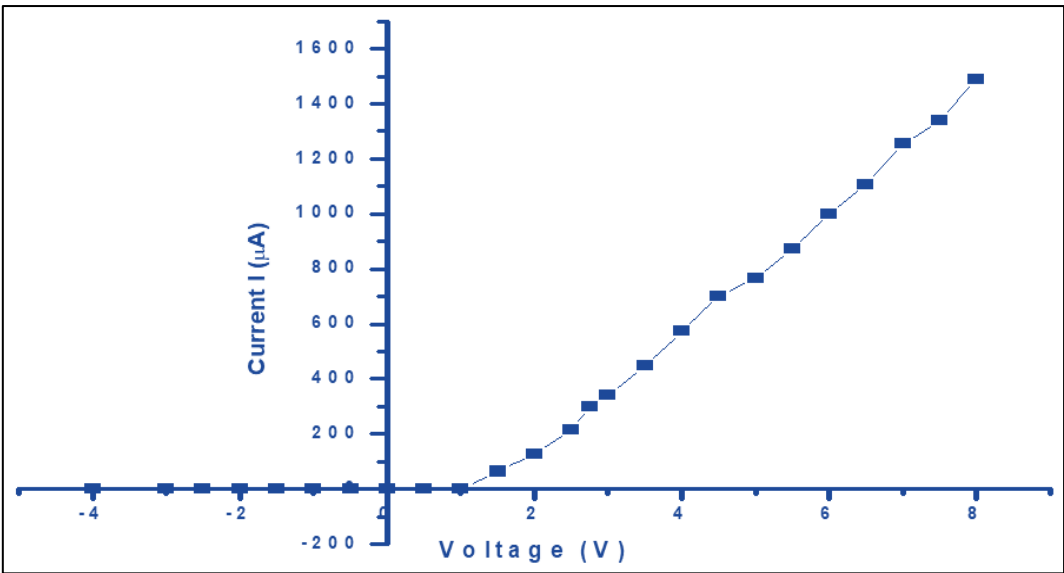


Fig. 3.9 Dark I – V characteristic of ITO/Turmeric/Al herbal diode

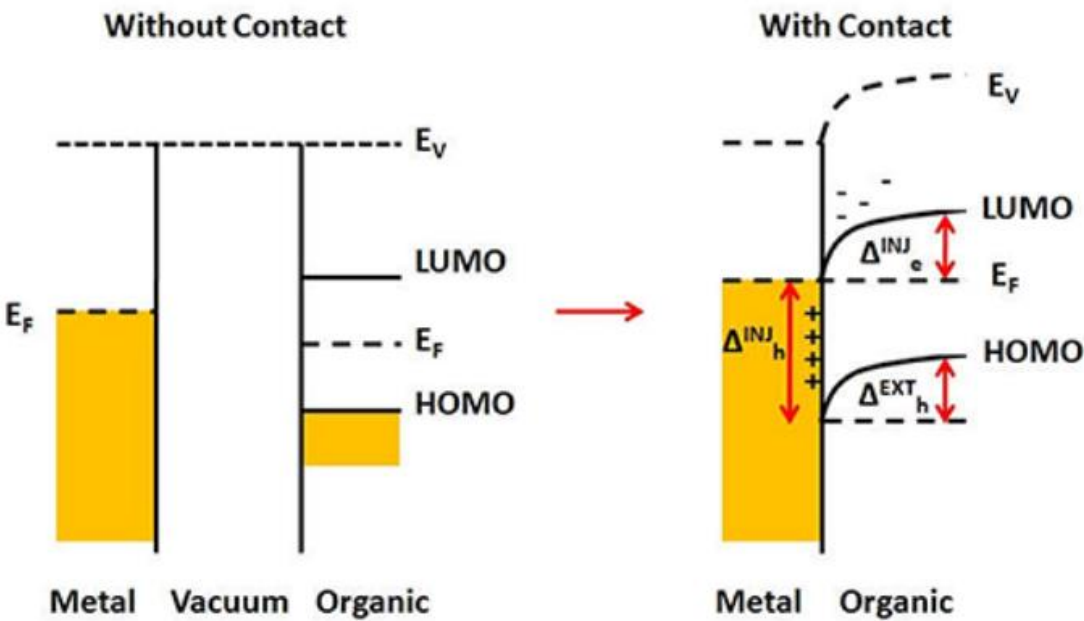


Fig. 3.10 Schematic energy band diagram of ITO/Turmeric/Al interface where ITO/Turmeric form Schottky contact and Al/Turmeric form Ohmic contact

Therefore, because of this rectifying contact, the I-V characteristics of the device produce an asymmetric curve when voltage is placed across it.

Fig. 3.11 displays the $\ln I$ Vs. $1/T$ plot of the Turmeric dye-based herbal diode. We have measured the reverse saturation current from this curve, which is roughly 14.29 A. Additionally, we have estimated the device ideality factor using Eqn. 3.3 from the slope of the curve shown in Fig. 3.11.

$$\eta = \frac{q}{kT} \frac{dV}{d \ln I} \tag{3.3}$$

The diode's $\ln I$ vs. V plot demonstrates linearity at low voltage, but the curve deviates from linearity as the voltage rises. It has been noted from Fig. 3.11 that η has a relatively high value. The diode's ideality factor (n) value is almost exactly 18.84. The diode's high series resistance (R_s) played a major role in the departure of the curve's shape. Therefore, we have also measured the device's R_s in this chapter. We have employed the Cheng Cheung equation [22–26] presented below to calculate R_s .

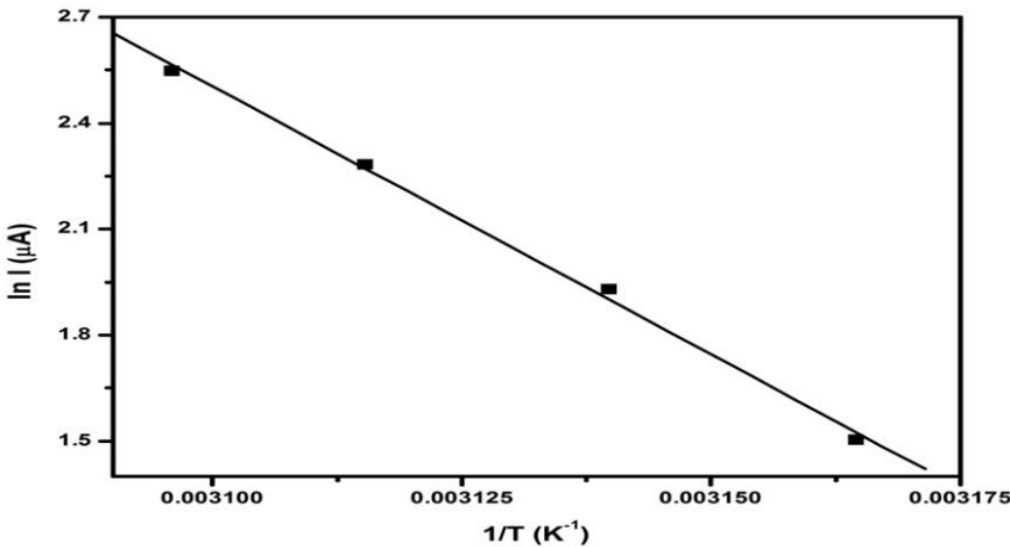


Fig. 3.11 $\ln I$ versus $1/T$ plot of Turmeric dye-based herbal diode

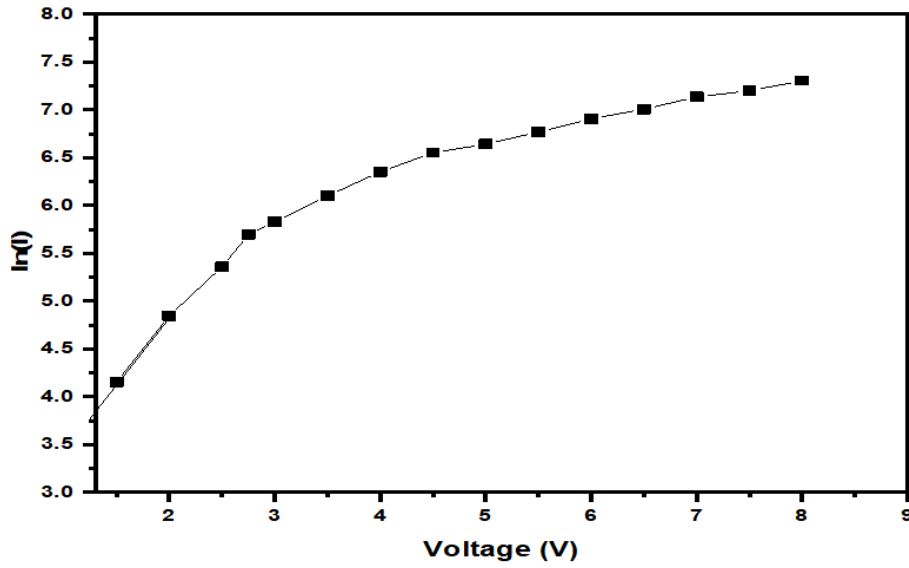


Fig. 3.12 $\ln I$ vs V plot of Turmeric dye-based herbal diode

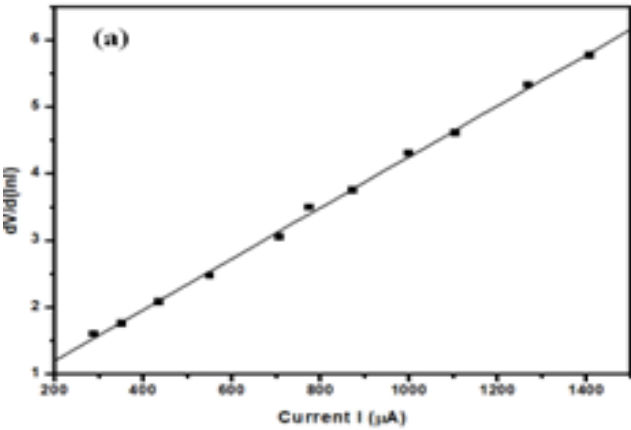
$$\frac{dV}{d\ln I} = \frac{nKT}{q} + IR_s \quad (3.4)$$

$$H(I) = n\phi_b + IR_s \quad (3.5)$$

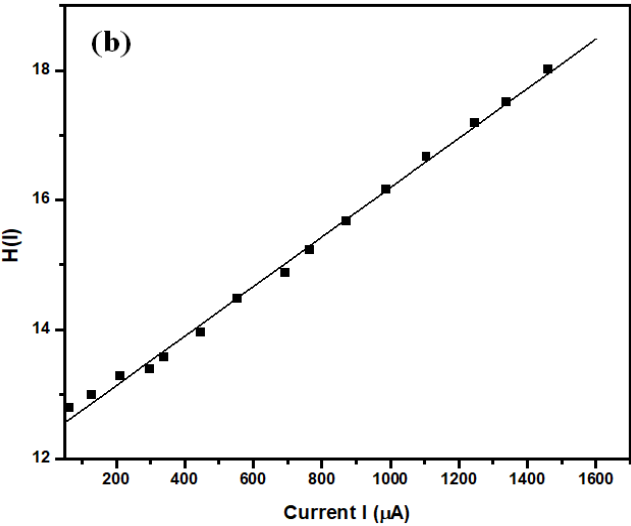
Where,

$$H(I) = V - \left(\frac{nKT}{q} \right) \ln \frac{I}{AA^*T^2} \quad (3.6)$$

From Eqn. 3.4, we have measured the device R_s . To extract the device R_s , we have plotted $\frac{dV}{d\ln I}$ vs. I curve shown in Fig. 3.13. The $\frac{dV}{d\ln I}$ vs. I plot gives a straight line with an intercept of $\frac{nKT}{q}$.



(a)



(b)

Fig. 3.13 (a) $dV/d\ln I$ - current (I) and (b) $H(I)$ – current (I) plot of Turmeric dye-based herbal diode

We have determined the value of η from the intercept, and the slope of the curve yields the value of R_s . We have also investigated the value of R_s using Eqn. 3.5. We have plotted the $H(I)$ vs. I curve displayed in Fig. 3.13(b) using the equation. The slope of this curve yielded the value of R_s , and the intercept yielded the value of barrier height (Φ_b). The extracted values of

R_s of the Turmeric dye-based diode by using $\frac{dV}{d\ln I}$ vs. I and H (I) vs. I plot shows consistency with each other. The extracted values are shown in Table 3.2.

Table 3.2 Extracted values of n , ϕ_b , and R_s of the Turmeric dye-based herbal diode

Sample	Value of η	Value of ϕ_b (eV)	R_s from $dV/d\ln I$ plot ($K\Omega$)	R_s from H(I) vs I plot ($K\Omega$)
ITO/Turmeric/Al	16.73	0.74	3.82	3.81

The results suggest that the Turmeric dye may be used as a natural diode. The Turmeric diode's ideality factor (η) value is almost 16.73, and the value of R_s is 3.81 K. The Cheung Cheng method is used to calculate the value of R_s , which was then validated using the H (I) vs. I plot. The retrieved value of R_s using these two methods is substantially identical, demonstrating the constancy of these two methods. The electronics parameters η and R_s of the Turmeric dye-based diode are found to be high. The presence of series resistance, interfacial features of the metal herbal dye contact, abnormalities in the thickness of herbal dye, charge recombination process, and the presence of series resistance are all explanations for this high value of ideality factors.

It is commonly understood that the contact resistance and the neutral area of the semiconductor contribute to the device R_s in any semiconductor-based electrical and optoelectronic device. Due to structural instability and weak molecular bonding, these herbal dyes are prone to electronic traps that inject additional energy levels inside the energy band between HOMO and LUMO. The trap condition restricted charge carrier flow at the interface throughout the structure, resulting in a reduction in the overall current of the Turmeric dye-based herbal diode. In this chapter, we have measured the trapped energy of the Turmeric dye electronic device in this chapter. To measure the trap energy, we have regarded the trap distribution to be exponential, and the trap energy density can be given by [27-31],

$$n_t = H_n \exp\left(\frac{F_n}{KT_c}\right) \tag{3.7}$$

Where H_n is the trap density, F_n is the electron Fermi level, K is the Boltzmann constant, and T_c is the characteristic temperature which is given by,

$$T_c = \frac{E_c}{K} \quad (3.8)$$

Where E_c is the characteristic trap energy.

Now by considering this exponential trap distribution, we have estimated the E_c using the space charge limited current equation given by,

$$I = AN_c \mu q^{1-m} \left(\frac{m\varepsilon}{H_n(m+1)} \right)^m \left(\frac{2m+1}{m+1} \right)^{m+1} \left(\frac{V^{m+1}}{L^{2m+1}} \right) \quad (3.9)$$

Where N_c is the effective density of states, μ is the mobility, ε is the product of the permittivity of the vacuum (ε_0) and the dielectric constant (ε_r), V is the applied voltage, L is the thickness of the active layer, and m is the ratio of the characteristic temperature T_c with absolute temperature T ($m = \frac{T_c}{T}$).

From Eqn. 3.9, it can be said that the space charge limited current exhibits the power-law dependence in between current voltage,

$$I \approx V^{m+1} \quad (3.10)$$

Using this equation, we have estimated the trapped energy of the Turmeric diode from $\ln I$ vs. $\ln V$ plot. The $\ln I - \ln V$ plot is shown in Fig. 3.14

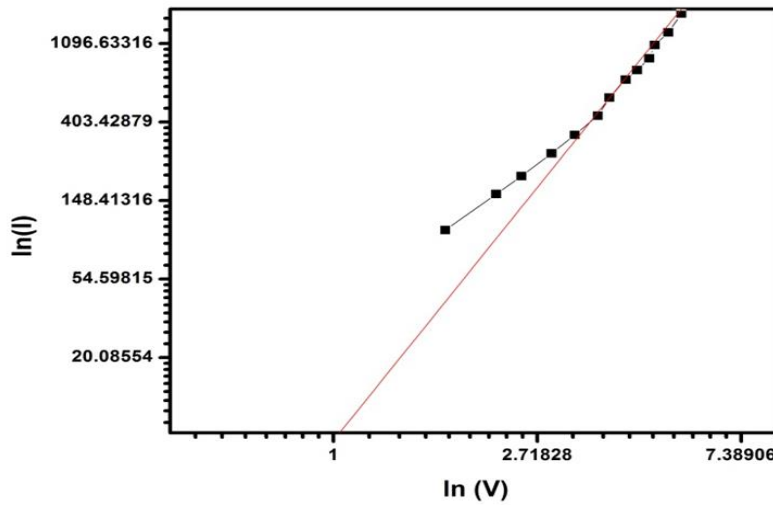


Fig. 3.14 $\ln I - \ln V$ plot of Turmeric dye-based herbal device

From Fig. 3.14 the plot has two zones, one region is below the transition voltage, with m smaller than 1. The conduction process in this region is governed by ohmic conduction. While the others are above transition voltages where SCLC regulates the conduction process. The value of m in this region is bigger than 2. Table 3.3 shows the retrieved values of m and E_c .

Table 3.3 Extracted values of m and E_c of the Turmeric dye-based herbal diode

Sample	Value of m	Value of E_c (eV)
ITO/Turmeric/Al	2.3	0.059

The foregoing results indicate that as the herbal dye becomes more prone to traps, the charge injection and transport mechanisms become restricted by traps. As a result, the overall device current is lowered, and the diode's electrical characteristics η , R_s are high when compared to a semiconductor diode. According to the foregoing results, we may increase the diode current and improve the diode's various electronic properties by minimizing the trap energy of the Turmeric diode.

3.5 Conclusion

In review section we have discussed different works available on Turmeric dye. Turmeric dyes are used as a sensitizer in DSSC device. But its semiconducting property is unknown. We have measured semiconducting property of Turmeric dye in our work. In this present chapter we have investigated the charge carrier density of a PVA Turmeric composite thin film. The extracted value is approximately $2.8 \times 10^{23} \text{ m}^{-3}$. We have also estimated the charge carrier mobility (μ), which is a function of the Hall coefficient and the conductivity of the film. The Hall mobility value is $3.3 \times 10^{-13} \text{ m}^2 \text{ volt}^{-1} \text{ sec}^{-1}$. Even though the mobility and conductivity of the Turmeric dye thin film are low, the charge carrier density is relatively high. This finding suggests that the Turmeric dye will make a good choice for the non-conventional electronic material. Along with that, we have prepared ITO/Turmeric/Al diode and investigated several electronic properties, including reverse saturation current, rectification ratio, ideality factor, series resistance, and barrier height. We have seen that the ideality factor and series resistance extracted values, which are about 16.73 and 3.82 $\text{K}\Omega$, respectively, are quite high. The existence of traps in Turmeric colour is one of the key causes of these high values. The device's

estimated trap energy is around 0.059 eV. It is clear that the presence of traps limited the flow of charges through the device, and we can thus draw the conclusion that by reducing the trap energy, we can enhance the electronic device overall functionality.

3.5 References

1. S. Wang et al, Progress of conjugated polymers as emerging thermoelectric materials, Progress in polymer science, (2022), 129: 101548
2. H. Krizova et al, Natural dyes: Their Past, Present, Future and Sustainability. In Recent Developments in Fibrous Material Science, In Recent Developments in Fibrous Material Science, 59-71 (2015)
3. K. E. Jasim et al, Curcumin Dye-Sensitized Solar Cell, J. Energy Power Eng., 11 409 (2017)
4. S. Shalini et al, Review on natural dye sensitized solar cells: Operation, materials and methods, Renewable and Sustainable Energy, 51 1306 (2015)
5. G. Richhariya et al, Natural dyes for dye sensitized solar cell: A review, Renewable and Sustainable Energy Reviews, 69 705 (2017)
6. K. Feron et al, Organic Solar Cells: Understanding the Role of Förster Resonance Energy Transfer, J. Mol. 13 17019 (2012)
7. S. Sen and et al, Effect of Electrode on Trap Energy and Interfacial Barrier Height of Crystal Violet (CV) Dye Based Organic Device, Bull. Mater. Sci., (2020), 43: 1-4
8. P. K. Das et al, Effect of Trap Energy on Series Resistance of Phenosafranine Dye Based Organic Diode in Presence of TiO₂ and ZnO Nanoparticles, Adv. Mater. Res.1159 112 (2020)
9. T. I. Benanti et al, Organic Solar Cells: An Overview Focusing on Active Layer Morphology, Photosynth. Res. 87 73 (2006)
10. N. A. N. Aziz et al, Electrical and Hall Effect Study of Hybrid Solar Cell, Clean Energy Technol. 2(4) 322 (2014)
11. V. Vohra, Materials, Natural Dyes and Their Derivatives Integrated into Organic Solar Cells, 11 2579 (2018)

12. T. I. Benanti et al, Organic Solar Cells: An Overview Focusing on Active Layer Morphology, Photosynth. Res., 87 73 (2006)
13. A. R. N. Laily et al, Electrical Conductivity and Hall Effect Study of Organic Solar Cell Using Downy Rose Myrtle Berries as Natural Dye: A Heat Treatment, Mater. Sci. Energy, 84 264 (2018)
14. S. Hasiah et al, Electrical Conductivity of Chlorophyll with Polythiophene Thin Film on Indium Tin Oxide as P-N Heterojunction Solar Cell, J. Phys. Sci., 19 77 (2008)
15. S. Ilić et al, Characteristics of curcumin dye used as a sensitizer in dye-sensitized solar cells, Electronics and Energetics, 32 91 (2019)
16. C. Kittel et al, Introduction to Solid State Physics, (J. Wiley and Sons Inc, N. Y., 1971)
17. S. Sen et al, Effects of two different solvents on Schottky barrier of organic device, Int. J. Adv. Sci. Eng. 6 23(2020)
18. A. Gusain et al, Polymer Solar Cells – Interfacial Progress Related to Performance Issues. Frontiers in Chemistry, (2019), 7
19. P. K. Das et al, Study on the series resistance of crystal violet dye-based organic photovoltaic device in presence of single walled carbon nanotubes, Ind. J. Phys., (2021)
20. S. Chakraborty et al, Improvement of electrical and photovoltaic properties of methyl red dye based photoelectrochemical cells in presence of single walled carbon nanotubes, Front. Optoelectronics, 8 289 (2015)
21. P. K. Das et al, Tuning of series resistance by reducing the trap energy of methyl red dye-based organic devices in the presence of ZnO nanoparticles, Int. J. Renewable Energy Technol, 12 118 (2021)
22. M. Shah et al, Electrical characterization of the ITO/NiPc/PEDOT : PSS junction diode, J. Appl. Phys. 43 405104 (2010)
23. F. Yakuphanoglu, Controlling of silicon–insulator–metal junction by organic semiconductor polymer thin film, Synth. Met. 160, 1551 (2010)
24. S. K. Cheung and N. W. Cheung, Extraction of Schottky diode parameters from forward current-voltage characteristics, Appl. Phys. Lett. 49, 85 (1986)
25. M. Benhaliliba, Extracted electronic parameters of a novel Ag/SnO₂: In/Si/Au Schottky diode for Solar cell application, J. Nano-Electron. Phys. 7 02029 (2015)

26. G. Kunakova et al, Space charge limited current mechanism in Bi₂S₃ nanowires, J. Appl. Phys. 119, 114308 (2016).
27. K J Lakshmi et al, Excessive usage of non renewable energy resources-Its impact on global warming, J. Chem. Bio. Phy. Sci., 6(4) 1261-1266 (2016)
28. M. Kamran et al, Fundamentals of renewable energy systems, Renewable Energy Conversion Systems, 6 1-19 (2021)
29. P. A. Owusu et al, A review of renewable energy sources, sustainability issues and climate change mitigation, Cogent Engineering, 3(1) 1167990 (2016)
30. P. Latake et al, The greenhouse effect and its impacts on environment, Internal Journal of Innovative Research and Creative Technology, 1(3) 333-337 (2016)
31. A. L. El Zein, The effect of greenhouse gases on earth's temperature, International Journal of Environmental Monitoring and Analysis, 3(2) 74-79 (2015)

Chapter 4

Effect of dye concentration on the band gap of Poly Vinyl Alcohol Turmeric composite thin film

4.1 Introduction

4.2 Turmeric dye active materials of nonconventional electronic device

4.3 Experimental details

4.3.1 Sample preparation

4.3.2 Measurements

4.3.3 Results and Discussions

4.4 Conclusion

4.5 References

4.1 Introduction

In the previous chapter, we have discussed the conductivity, charge carrier density and series resistance of the Turmeric dye-based diode. In this chapter we have measured band gap energy, ideality factor, and rectification ratio of the Turmeric dye-based devices. We have prepared and compared the performance of Turmeric dye-based herbal diodes at various dye concentrations. The diodes are made up of sandwiching a layer of Turmeric dye in-between the Cu and Al electrodes. Cu and Al electrodes are used as anode and cathode terminals respectively. With the help of these forward and reverse-biased I-V characteristics are measured. The asymmetric form of the current-voltage (I-V) relationship validates the diode property of the device. We have also investigated how current changes with the temperature (I-T) to test the semiconducting property as well. After examining the I-T curve, we have observed that current rises with temperature. To determine the diode's band gap energy, we have analyzed the data suitably. The concentration of dye affects the value of the band gap such as the band gap reduces when the dye concentration rises. For 5% and 20% concentrations of the dye solution in our experiment, the band gap's highest and minimum values are 3.36 eV and 2.82 eV, respectively. Additionally, we have also investigated the ideality factor (η), trap energy (E_c), barrier height (Φ_b), and series resistance (R_s).

4.2 Selection of the dye

In the review section (section 3.2) we have reviewed briefly on Turmeric dye. However, there are least available publications on the Turmeric dye-based herbal diode's semiconducting properties and how its band gap varies with dye concentration. The semiconductivity of Turmeric dye has been investigated in this chapter by altering its concentration. A diode made of Turmeric dye has been prepared. It is possible to measure the band gap by examining the diode characteristic. Fig. 4.1 displays the Turmeric dye's chemical composition. Its chemical formula is $C_{21}H_{20}O_8$. The melting point is 183°C .

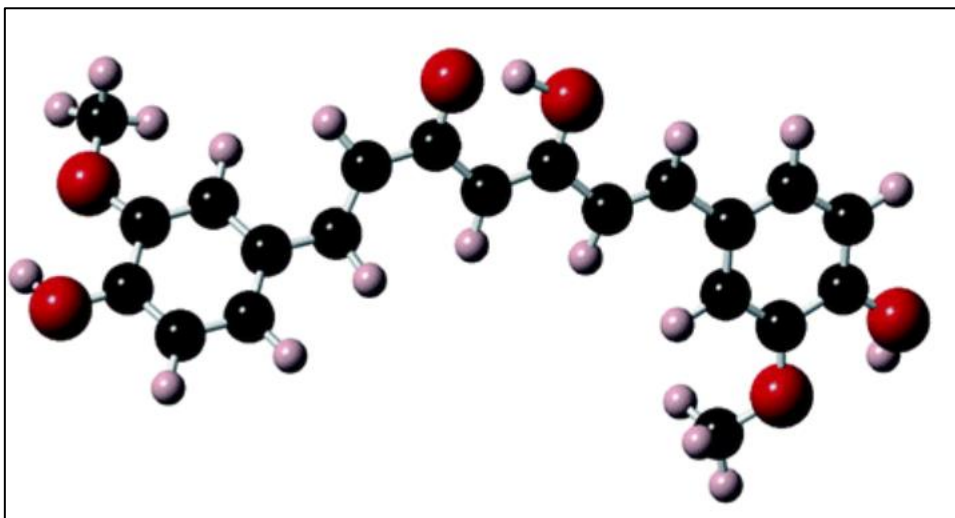


Fig. 4.1 Structure of Turmeric molecule

The Turmeric dye is an amorphous, disorganized fundamental structure. Weak vander waals forces and dipole-dipole interactions hold molecules together. The highest occupied orbital (HOMO) is the band with the highest energy, and the lowest unoccupied molecular orbital (LUMO) is the band with the lowest energy. In this example, CB and VB in the case of inorganic semiconductors are assumed to be equivalent to LUMO and HOMO. When the material is in wafer form, the band gap can be estimated by employing a four-probe approach to analyze the conductivity fluctuation with temperature [7-8].

4.3 Experimental details

4.3.1 Sample preparation

Three distinct cell concentrations have been prepared. To create a clear, viscous PVA solution, 1 gm of Poly Vinyl Alcohol (PVA) is mixed with 15 ml of double-distilled water. PVA serves here as an inert binder. Three 5ml portions, each equal in size, are taken from this solution. Each component is stored in a pre-cleaned test tube. 250 mg of Turmeric powder is added into one of the test tubes and well mixed with a magnetic stirrer to create the 5% turmeric solution. Then, with the motor running at 800 rpm, 2ml of this semi-solid is spin-coated onto a Cu electrode that has been cleaned and prepped. The cell was dried under a vacuum (10^{-3} mm) for

10 hours before and after the Al electrode deposition. Cell 1 (Cu/5% Turmeric dye/Al) is now ready to measure I-V and I-T characteristics. We have constructed Cells 2 and 3 in a similar manner, using 500 mg and 1gm Turmeric powder for 10% and 20% Turmeric solutions, respectively. The cell diagram is illustrated in Fig. 4.2.

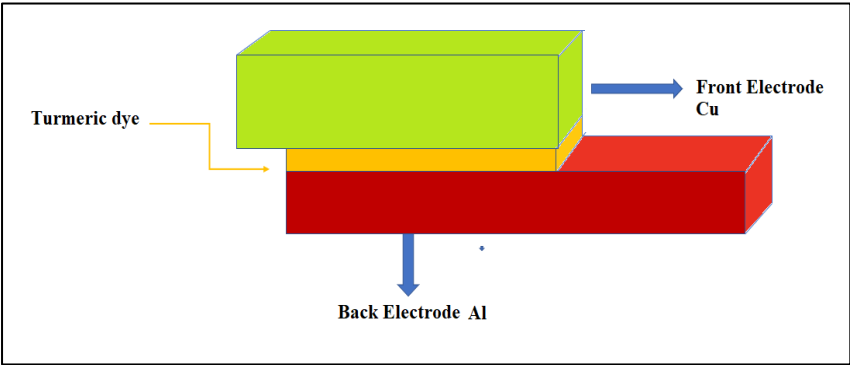


Fig.4.2 Cu/Turmeric dye/Al cell. A thin layer of Turmeric dye is sandwiched in between Cu and Al electrode which are used as front and back electrode respectively

4.3.2 Measurement

Keithley 2400 source measuring unit is used to do I-V measurements. The same measurement can also be made with a dc supply and a digital voltmeter, as shown in Fig. 4.3.

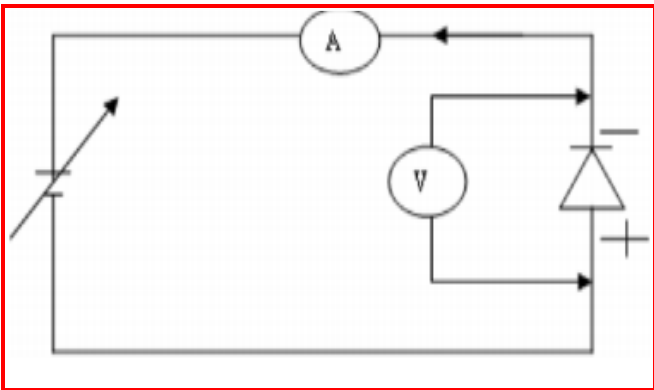


Fig. 4.3 Circuit diagram of the reverse bias connection of the diode to the Keithley 2400

In our lab, a heater with a temperature control circuit is designed. Along with that, Keithley 2400 source measure unit is also used to test the I-T characteristic. The experiment is conducted between 306-348 K in temperature. A K-type thermocouple (Cromel-Allamel) was used to measure temperature with an accuracy of 0.15 K.

4.3.3 Result and Discussions

The positive and negative terminals of the cell are connected to Cu and Al, respectively. We have measured a I-V data graph. The Turmeric diode's I-V curve has a non-linear shape shown in Fig. 4.4. For a Turmeric dye with a 20% concentration, the observable current is high. We have derived the ideality factor (η) from the forward bias curve. The ideality factor (η) evaluates the conformism of the diode to pure thermo-ionic emission. The logarithmic values of current vs voltage are displayed in Fig. 4.6. The ideality factor for three cells is investigated using Eqn. 4.3. For concentrations of 20%, 10%, and 5%, values of η are 32.00, 38.78, and 42.19, respectively.

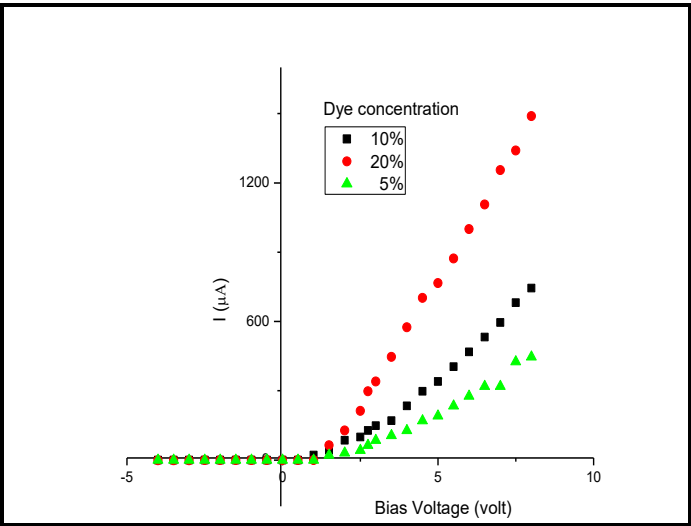


Fig. 4.4 Forward and reverse bias I-V curve of three Turmeric diode

We have also estimated the rectification ratio (RR) shown in Fig 4.5. It exhibits that RR is much for a 20% Turmeric dye-based diode. Here we have observed that the values of the ideality factor are lower for higher concentrations of Turmeric dye.

It is possible to say that the thermionic emission (TE) hypothesis can fit the I-V data of a diode curve. The forward bias I-V characteristics of a diode can be stated as follows in accordance with the TE theory [9–10].

$$I = I_0 \left[\exp \left(\frac{qV}{nkT} \right) - 1 \right] \tag{4.1}$$

Where I_0 is the reverse saturation current which is given by,

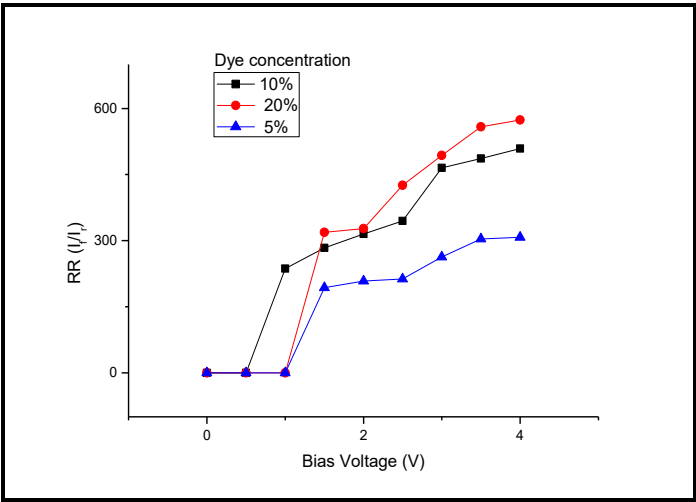


Fig. 4.5 Rectification ratio curves of three Cu/Turmeric/Al diodes

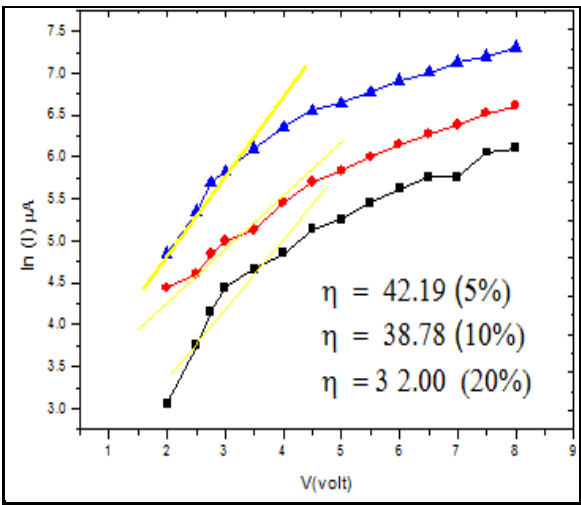


Fig. 4.6 ln I vs V curve for estimating ideality factor with different dye concentration

$$I_0 = AA^*T^2 \exp\left(-\frac{q\phi}{KT}\right) \quad (4.2)$$

Where I_0 is the reverse saturation current, q is the electronic charge, K is the Boltzmann constant, T is the temperature, V is the applied voltage, and η is the ideality factor.

The ideality factor can be calculated from the I-V characteristic by using the following relation.

$$\eta = \frac{q}{kT} \frac{dV}{d \ln I} \quad (4.3)$$

The ideality factor for the three diodes are estimated and values are given in Table 4.1. Covalent bond breakdown, which requires an energy input comparable to E_g , is presumably what produces carriers for the Turmeric dye. E_g can therefore be determined by looking at the carrier's temperature fluctuation. The variation of carriers can be ascertained by analyzing the temperature variation of reverse saturation current, which is the current flowing through the diode under reverse bias conditions and is given by [11].

$$I_0 = C e^{\frac{-E_g}{KT}} \quad (4.4)$$

Where I_0 is reverse saturation current, C is constant, E_g is band gap, and T is Temperature in K. It is seen from Eqn. 4.4 that the saturation current depends on E_g/kT exponentially. Taking logarithms on both sides of Eqn. 4.4 we get

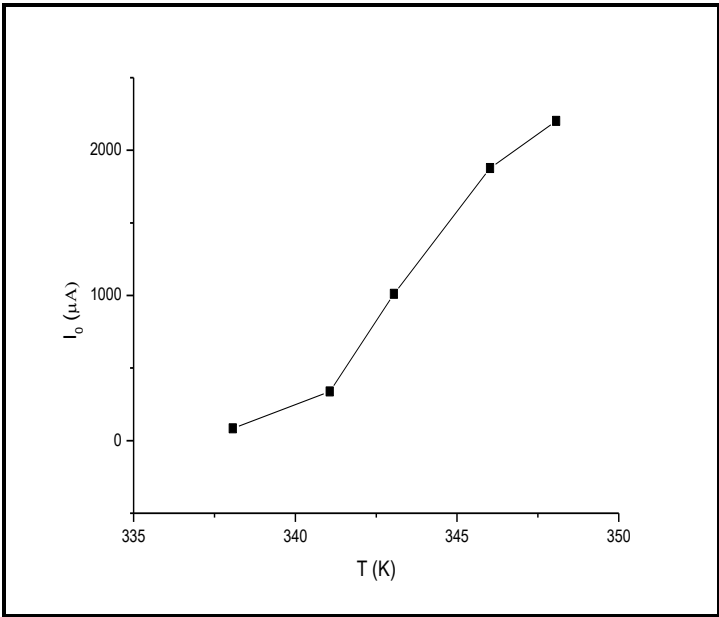
$$\ln I_0 = \ln C - \frac{E_g}{KT} \quad (4.5)$$

According to Eqn. 4.5, the junction temperature is the single factor affecting the reverse saturation current I_0 in semiconductor diodes. It is inversely proportional to the temperature. A straight line with a negative slope having a value of E_g/k is produced by plotting $\ln I_0$ vs $1/T$. We have estimated the value of E_g and the slope (m) of the straight line.

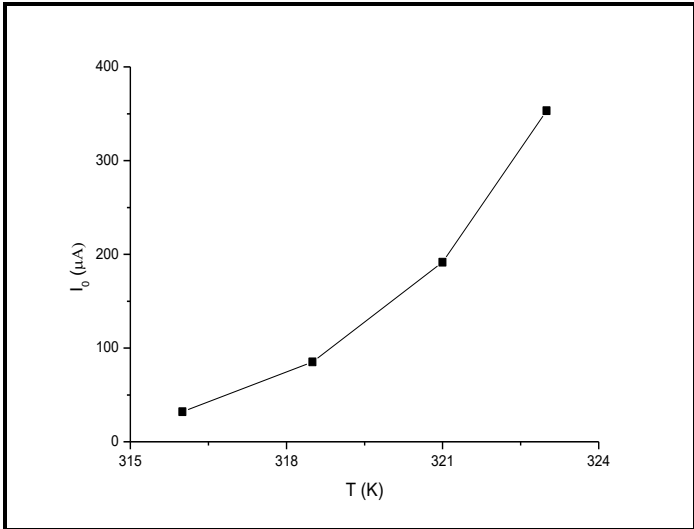
Thus

$$E_g = m k \quad (4.6)$$

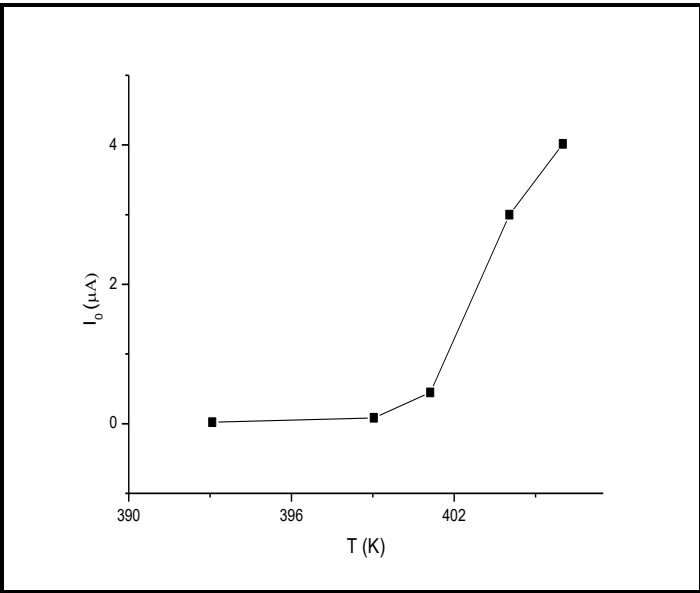
I-T data is also collected while maintaining a fixed reverse bias voltage across the diode in a thermal bath. Here, we have presented I-T statistics for three diodes with 5%, 10%, and 20% weight ratios of Turmeric dye at various concentrations. Plotted I-T values are displayed in Fig. 4.7.



(a)



(b)



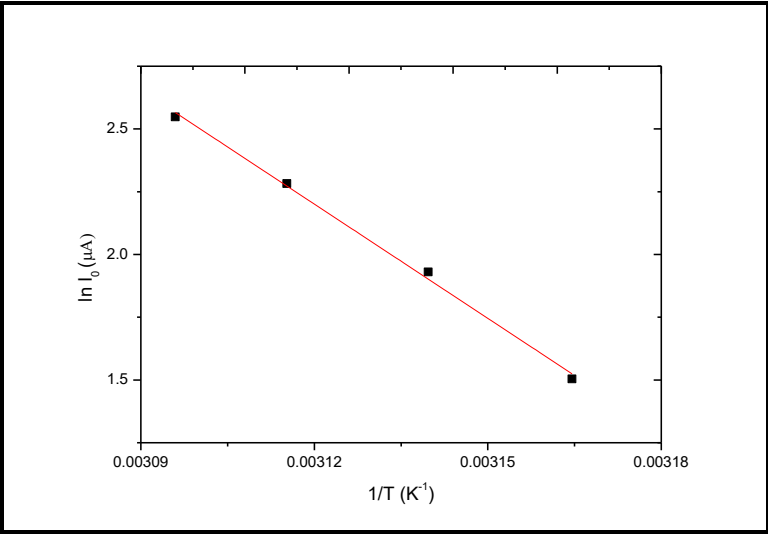
(c)

Fig. 4.7 $\ln I$ vs. T curves of diodes. (a), (b), (c) are for 20%, 10% and 5% concentration respectively

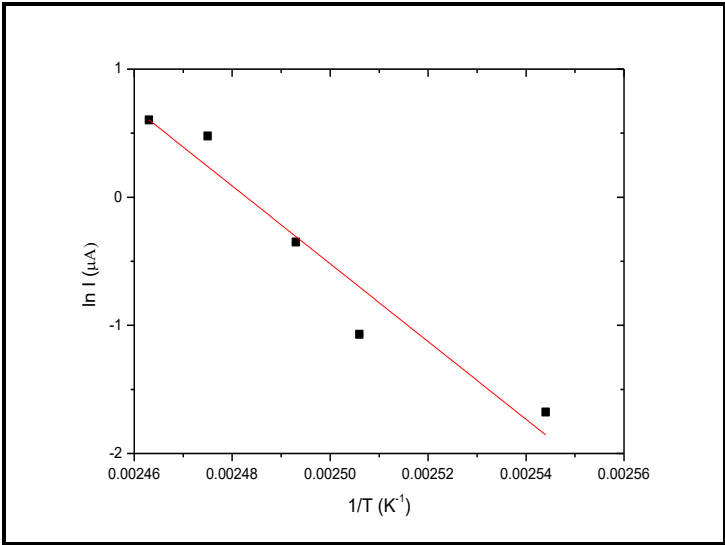
We observed previously that the curves are not linear in nature. The current changes with temperature and also the slope of the curve changes with temperature. We also displayed the data for $\ln I$ vs $1/T$. Curves can be compared to the straight lines in Fig. 4.8. With the help of Eqn. 4.5, we have inspected the band gap energy. It is well known that the ideality factor (η) assesses how well a diode conforms to pure thermo-ionic emission. Our Cu/Turmeric/Al system has a very high ideality factor.

Table 4.1 Values of η and E_g for different cell

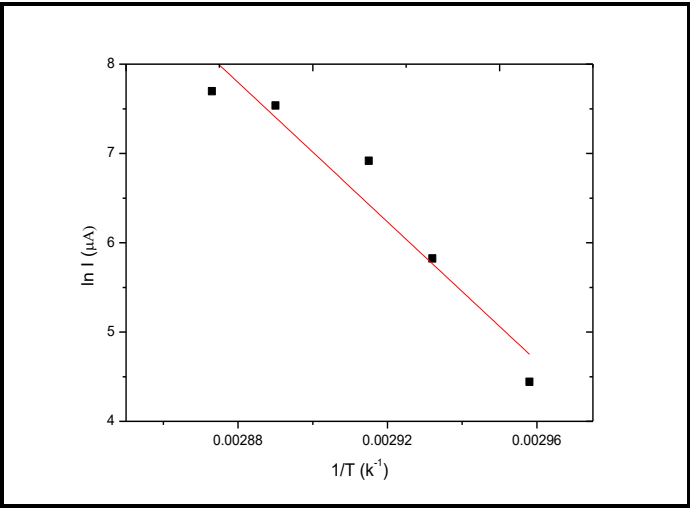
The concentration of Turmeric solution wt (%)	Value of Ideality factor (η)	Value of band gap (eV)
5	42.19	3.36
10	38.78	2.91
20	32.00	2.82



(a)



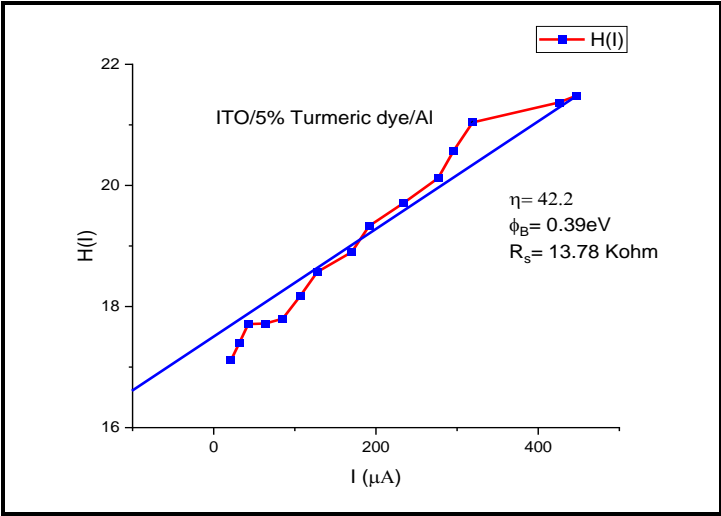
(b)



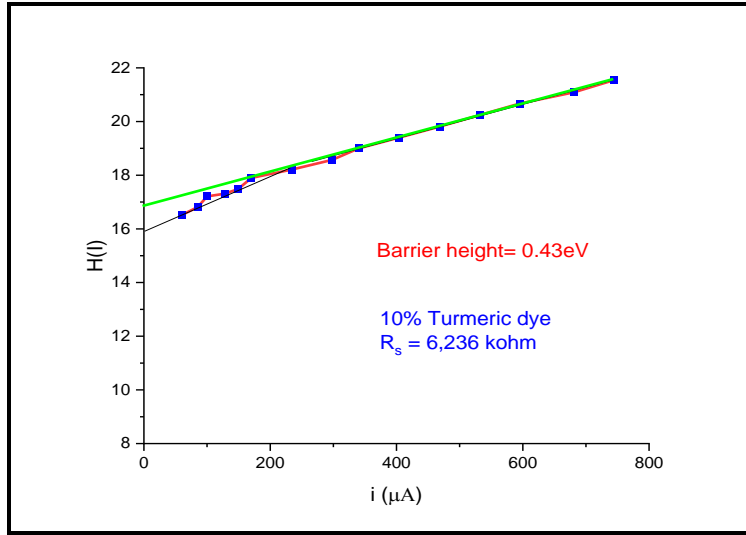
(c)

Fig. 4.8 $\ln I_0$ vs. $1/KT$ curves. (a), (b), and (c) are for 20%, 10%, and 5% concentration respectively. Curves are linear in nature. Data are fitted to estimate E_g .

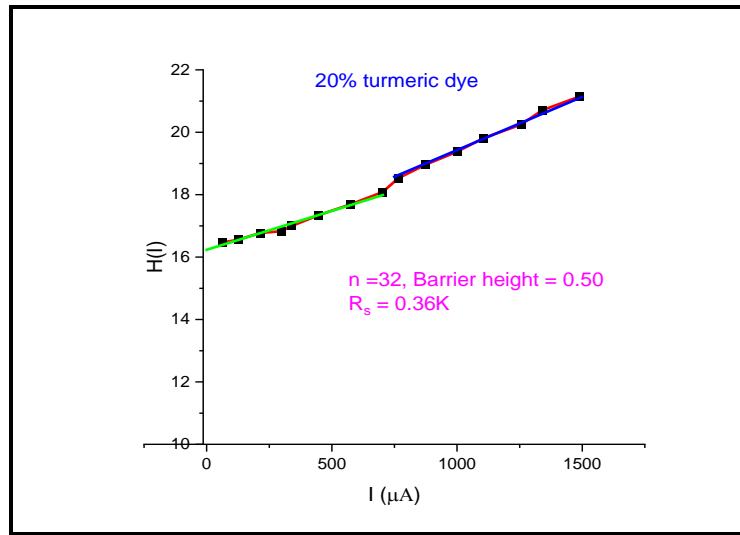
We have used the Shockley equations provided in, Eqn. 4.1 and Eqn. 4.2, to analyze the dark I-V features in order to evaluate the series resistance, barrier height, and trap energy of the three cells [12]. In Fig. 4.9, curves are displayed.



(a)



(b)



(c)

Fig. 4.9 (a), (b), (c) are curves for estimation of series resistance, barrier height of 5%, 10% and 20% Turmeric dye concentration cells respectively

The existence of high series resistance (R_s) in the thin film is shown from the curve's divergence. We have also estimated the device's R_s and Φ_b using the Cheng Cheung equation [13, 14] which is shown below,

$$\frac{dV}{d \ln I} = \frac{nKT}{q} + IR_s \quad (4.7)$$

$$H(I) = n\phi_b + IR_s \quad (4.8)$$

Where,

$$H(I) = V - \left(\frac{nKT}{q}\right) \ln \frac{I}{AA^*T^2} \quad (4.9)$$

From Eqn. 4.7, we have measured the R_s . To extract the R_s , we have plotted $\frac{dV}{d\ln I}$ Vs. I curve. The $\frac{dV}{d\ln I}$ vs. I plot gives a straight line with an intercept of $\frac{nKT}{q}$. The slope of the curve yields the value of R_s . From the intercept we have retrieved the value of the ideality factor (η). Using Eqn. 4.8, we have also calculated the value of R_s . After that we have plotted the $H(I)$ vs. I curve displayed in Fig. 4.9 in accordance with the equation. From this curve's slope, we have estimated the value of R_s , and the intercept yields the barrier height (Φ_b) value. The extracted values of R_s of the Turmeric dye-based diode by using $\frac{dV}{d\ln I}$ vs. I and $H(I)$ vs. I plot shows consistency with each other. We have measured the trap energy. We regarded the distribution of traps to be exponential in order to quantify the trap energy, and using this distribution, the trap energy concentration can be obtained by [27],

$$n_t = H_n \exp\left(\frac{F_n}{KT_c}\right) \quad (4.10)$$

Where H_n is the trap density, F_n is the electron Fermi level, K is the Boltzmann constant, and T_c is the characteristic temperature which is given by,

$$T_c = \frac{E_c}{K} \quad (4.11)$$

Where E_c is the characteristic trap energy.

Now by this exponential trap distribution, we have estimated the E_c from the space charge limited current given by,

$$I = AN_c \mu q^{1-m} \left(\frac{m\varepsilon}{H_n(m+1)}\right)^m \left(\frac{2m+1}{m+1}\right)^{m+1} \left(\frac{V^{m+1}}{L^{2m+1}}\right) \quad (4.12)$$

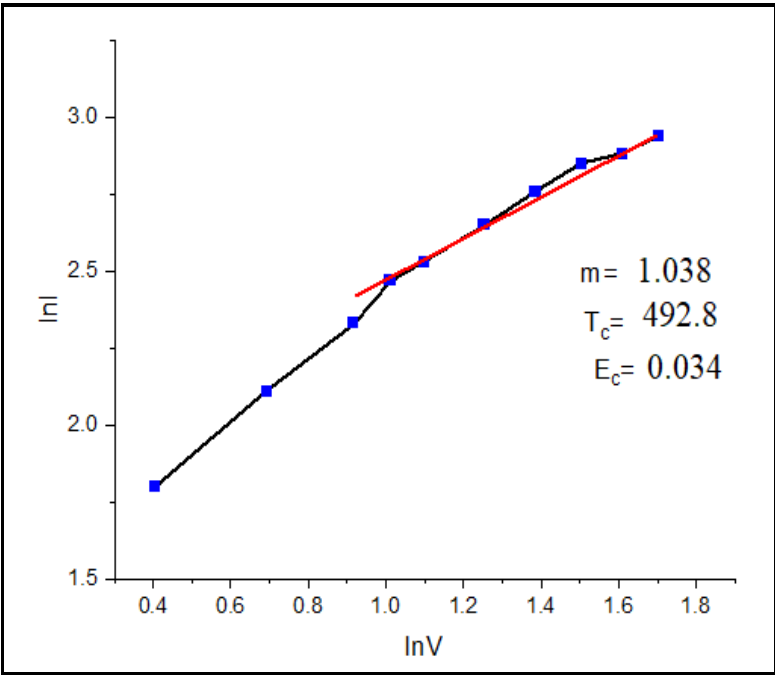
Where N_c is the effective density of states, μ is the mobility, ϵ is the product of the permittivity of the vacuum (ϵ_0) and the dielectric constant (ϵ_r), V is the applied voltage, L is the thickness of the active layer, and m is the ratio of the characteristic temperature T_c with absolute temperature T ($m = \frac{T_c}{T}$).

From Eqn. 4.12, it can be said that the space charge limited current exhibits the power-law dependence in between current voltage,

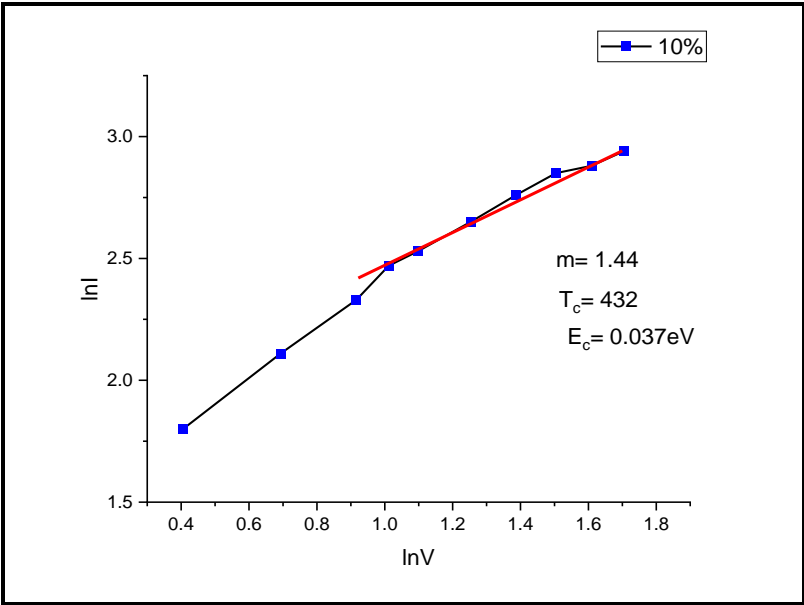
$$I \approx V^{m+1} \quad (4.13)$$

Using this equation, we have estimated the trap energy of the herbal diode from $\ln I$ vs. $\ln V$ plot. The $\ln I - \ln V$ plot is shown in Fig. 4.10.

We can suppose that Eqn. 4.5 represents the diode's temperature-dependent current equation. The exponents can be estimated by the plot of $\ln I_0$ vs. $1/T$ for different voltage such as 2V, 4V, 6V respectively. In low temperature regions, the slope is different from high temperature regions. The curve is fitted in a linear fashion. Due to specific restrictions in our experimental facilities, we have left the low temperature zone, even though it is crucial for the computation of the defect potential barrier. Which may be studied in future.



(a)



(b)

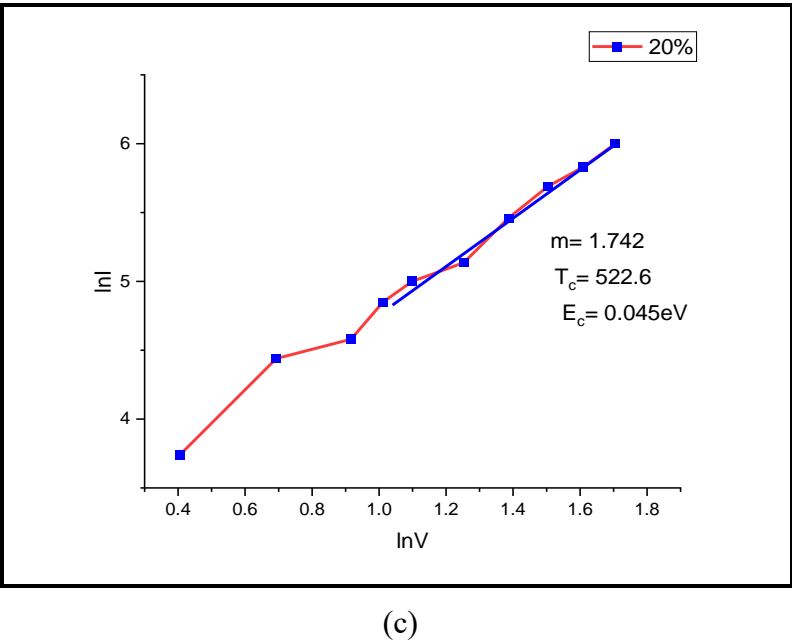


Fig. 4.10 (a), (b), (c) are curves for estimation of trap energy (E_c) of 5%, 10% and 20% Turmeric dye concentration cells respectively

The extracted values are shown in Table 4.2 and 4.3

Table 4.2 Values of barrier height (ϕ_b) and series resistance (R_s)

Dyes and Electrode	Ideality factor (n)	Barrier height, ϕ_b (eV)	Series resistance R_s (K Ω)
Cu/5% Turmeric/Al	42.19	0.39	13.738
Cu/10% Turmeric /Al	38.78	0.43	6.236
Cu/20% Turmeric/Al	32.00	0.50	0.360

Table 4. 3 Values of trap energy (E_c) of different Cells

Dyes	m	T _c (K)	E _c (eV)
ITO/5% Turmeric dye/Al	1.038	392.4	0.034
ITO/10% Turmeric dye/Al	1.440	432.0	0.037
ITO/20% Turmeric dye/Al	1.742	522.6	0.045

The electron concentration is largely independent on temperature, activation energy, and could be related to mobility in low temperature range.

Low band gap is present in higher concentration of Turmeric dye. The actual cause is still a mystery. However, we can expect that higher dye concentration will result in reduction in the trap energy of the Gaussian density of states [15, 16]. Here, we assume that Turmeric dye is a semiconducting substance, and Eqn. 4.14 provides the band gap relations with free charge of the substance. The band gap is written in the following form,

$$E_g = qV_{jc} + \left(\frac{\sigma_n^2}{2} + \frac{\sigma_p^2}{2}\right) + KT \ln \left(\frac{N_n N_p}{np}\right) \tag{4.14}$$

where E_g is the cell's band gap, V_{jc} is the junction potential in volts, q is the elementary charge, N_n and N_p are the effective conduction band and valance band density states, and n and p are the free electron and hole concentrations. We can suppose that when the dye concentration increases the cell's free electron and whole concentration will also increase.

4.4 Conclusions

In the above discussion, we have observed the semiconducting behaviour of the Turmeric dye and quantified the band gap using the measurement of I-T characteristics for varying dye concentrations. From the experiment it is also observed that the band gap changes with the variation of concentration of the dye. The variation of band gap with dye concentration reveals that trap energy level also changes with the dye concentration. The device works as a Cu/Turmeric/Al diode and we have measured different diode parameters. Comparing with

different dye concentration, we have found that the ideality factor of diode is low for higher dye concentration. We have also observed that series resistance of the diodes varies with the dye concentration. Series resistance is low for higher concentration of diodes.

4.5 References

1. K. E. Jasim et al., Thermal Performance Analysis of Solar Dryer Integrated with Heat Energy Storage System and a Low-Cost Parabolic Solar Dish Concentrator for Food Preservation, *Journal of Energy and Power Engineering*, 11 409-416 2017
2. S. Shalin, et al., Renewable and Sustainable Energy Reviews: Environmental impact networks of renewable energy power plants, *Renewable and Sustainable Energy Reviews*, 51 1306-1325 2015
3. G Richhariya et al., Natural dyes for dye sensitized solar cell, *Renewable and Sustainable Energy Reviews*, 69 705-718 2017
4. S. D. Baranovskii et al, "Charge-carrier transport in disordered organic solids", *Physical Review B*, 2000, 62, 7934-7938 S. Maity et al, Temperature dependent dark current-voltage study of thionine dye doped solidstate photo electrochemical cell (PEC), *Journal of optoelectronics*, 15 1417-1422 2013
5. H. li et al, A label-free fiber optic SPR biosensor for specific detection of C-reactive protein *Scientific Reports*, 10 2017
6. A. Halder et al, Effect of Back electrode on photovoltaic properties on crystal violet dye basedsolid state thin film, *Ionics*, 14 (3) 263 2008
7. A. Halder et al, Effect of plasticizer on safranin-T-dye-based solid-state photo electrochemical cell *Ionics*, 14 (5) 427 2008
8. S. Maity et al, Effect of plasticizer on safranin-T-dye-based solid-state photo electrochemical cell *Ionics*, 14 (6) 549 2008
9. A. Halder et al, Electrical and photovoltaic characterisations of methyl red dye doped solid-state photoelectrochemical cell *Ionics*, 15 (1) 79 2009
10. A. Rose, "Space-Charge-Limited Currents in Solids", *Physical Review*, 1955, 97, 1538–1544

11. S. K. Dey et al, Transient current study in safranine-T dye based organic photo-electrochemical cell using exponentially distributed trap assisted charge transport model, J. Mat. Sci., 38 93 2011
12. M.A. Lampert et al, volume – controlled current injection in insulators: Rep, Prog. Phys 27 329 2011
13. S. Antohe et al, The Effect of The Electron Irradiation On The Structural And Electrical Properties Of A^{II} - B^{VI} Thin Polycrystalline Films J. Optoelectronic. Adv. Mater 5(4) 801 2003
14. A. Salleo et al, “Organic Electronics”, 2013, Wiley-VCH Verlag GmbH & Co. KGaA, Weinheim, Germany
15. P. McEuen et al, Single-walled carbon nanotubes electronics, IEEE Transactions on Nanotechnology, (2002), 1(1) : 78-85
16. T. Belin et al, Characterization method of carbon nanotubes: a review, Materials Science and Engineering B, (2005), 119 : 105-118

Chapter 5

Effect of ZnO, TiO₂ nanoparticle on solid state Turmeric dye thin film

5.1 Introduction

5.2 Experimental details

5.2.1 Sample preparation

5.2.2 Measurements

5.2.3 Results and Discussions

5.3 Conclusion

5.4 References

5.1 Introduction

In the previous chapter, we have discussed the Turmeric dye-based devices and its performance with different dye concentration. In this chapter, we report the performances of the Turmeric dye-based herbal device by incorporating NP. Generally, the typical conductivity of the herbal dye is quite low. Different NP like ZnO, TiO₂ are being incorporated with dye layer in different ways to improve the device conductivity. Though the exact role of the nano particles is not clear but it is reported that due to addition of the NP, dissociation energy, and the charge transport parameter of Turmeric dye-based device changes. Charge injection and the recombination within the bulk layer reduces. In this chapter, our aim is also to investigate the role of different NP on the charge transport mechanism of Turmeric dye-based device. Traps are also following the exponential and Gaussian distribution. There are also different types of transport model available considering these types of traps. We assume that the charges are being trapped at the trap centers and get immobilized. Traps are considered as potential well and trapping and de-trapping of charge carriers are the major factor to control the charge transport mechanism during transport. Due to traps some charges are being accumulated as the space charge within the devices. In this chapter we have measured trap energy, barrier height and series resistance of the system.

5.2 Experimental details

5.2.1 Sample preparation

In review section (Section 3.2) we have reviewed briefly on Turmeric dye. Here we have prepared the Turmeric dye cells. Three thin films have been prepared for comparing the performance of Turmeric diodes with and without NP. To see the effect of nano particles two different nano particles, namely TiO₂ and ZnO, are incorporated to the Turmeric dye-based diode. These two diodes are termed as ITO/Turmeric+TiO₂/Cu diode and ITO/Turmeric+ZnO/Cu diode. Here the structures of the TiO₂ and ZnO nano particles brought from Sigma-Aldrich, Germany are shown in Fig. 5.1 (a) and Fig. 5.1 (b) respectively. In order to make the Turmeric solution, 30 ml of distilled water were first added to a clean beaker. 5g of the highly viscous Poly Vinyl Alcohol (PVA) is added to the water and swirled with a magnetic stirrer at 80°C for 30 minutes. The dye solution is applied to the electrodes using PVA. 2 milligrammes of Turmeric colour is added to the PVA solution and well mixed again

for an additional 10 minutes. Next, this solution is divided into three equal portions and placed in the test tubes before being cleaned. There is one test tube set aside. This Turmeric solution does not contain any NP. To make Turmeric dye with TiO_2 nanoparticle solution and Turmeric dye with ZnO nanoparticle solution, 2 mg of TiO_2 nanoparticle and 2 mg of ZnO nanoparticle are added individually to the other two test tubes. The prepared Turmeric solution is spin-coated onto an ITO-coated glass plate that has already been cleaned to prepare the cell. The spin coater's speed can be adjusted to manage the active layer's thickness. Similarly, the same solution is spin-coated on a Cu plate. The Turmeric diode (D1) is then formed by sandwiching both of these electrodes together. The cell is vacuumed for 12 hours to dry. Similarly, Turmeric solution with TiO_2 and ZnO NP are spin-coated separately to generate ITO/Turmeric+ TiO_2 /Cu diode 2 (D2) and ITO/Turmeric+ ZnO /Cu diode 3 (D3). These produced diodes are dried in a vacuum for 12 hours. These diodes are then characterized, and the results are explored further below. The molecular structure of curcumin is shown in Fig. 5.1 (c), and the basic Turmeric dye-based herbal Schottky diode is shown in Fig. 5.1 (d).

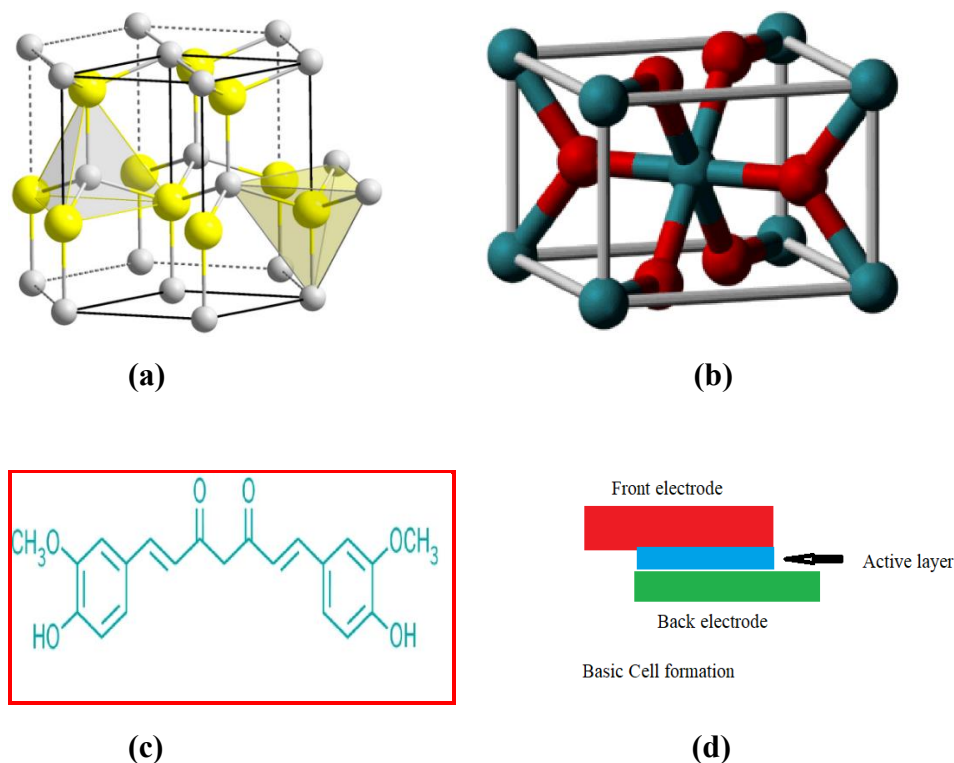


Fig. 5.1 (a) Molecular structure of ZnO, (b) Molecular structure of TiO_2 (c) Molecular structure of Curcumin (d) Basic structure of Turmeric dye-based diode

SEM images play a crucial role in revealing the film's shape. Discovering the NP' orientation within the active substance is also helpful. In this study, SEM images of the Turmeric+TiO₂ and Turmeric+ZnO diode is displayed in Fig. 5.2 were acquired. On a JEOL field emission scanning electron microscope, SEM analysis is carried out. The Turmeric+TiO₂ cell is depicted in Fig. 5.2(d), which also illustrates the size of the TiO₂ NP. The Turmeric+ZnO cell in Fig. 5.2(e) also depicts the size of the ZnO.

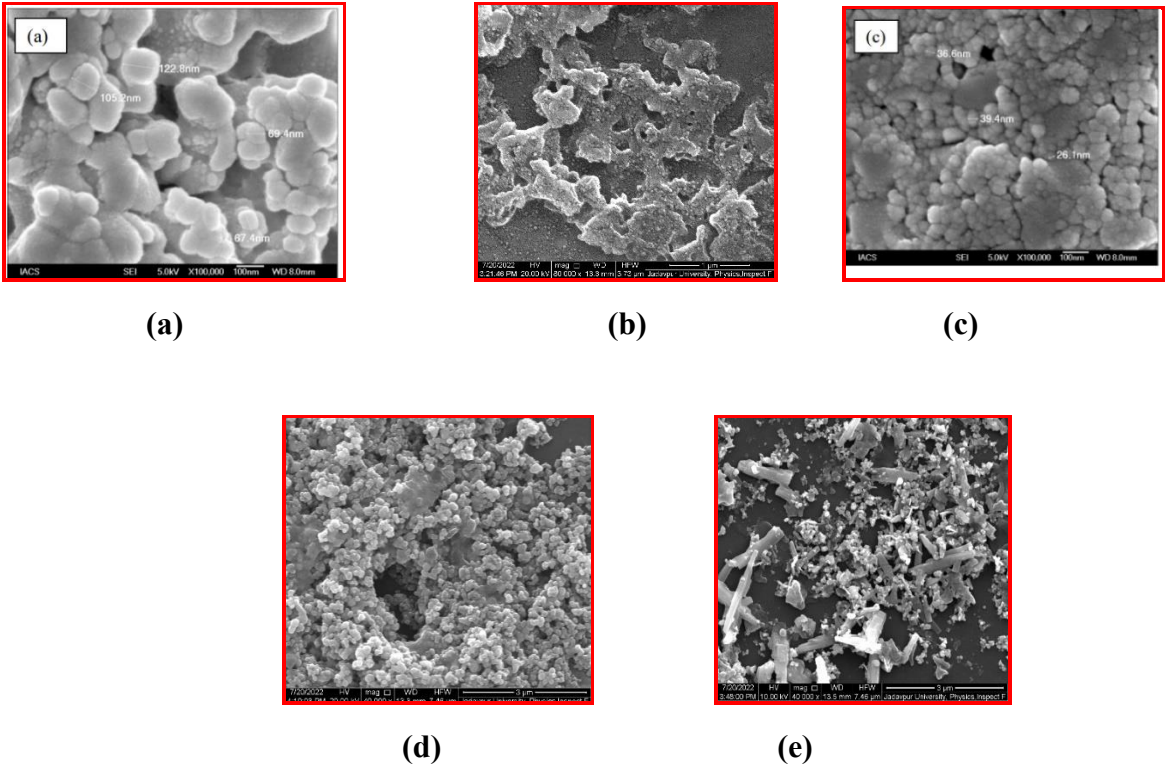


Fig. 5.2 (a) SEM image of TiO₂ (b) SEM image of Turmeric (c) SEM image of ZnO (d) SEM image of Turmeric+ TiO₂ (e) SEM image of Turmeric+ ZnO

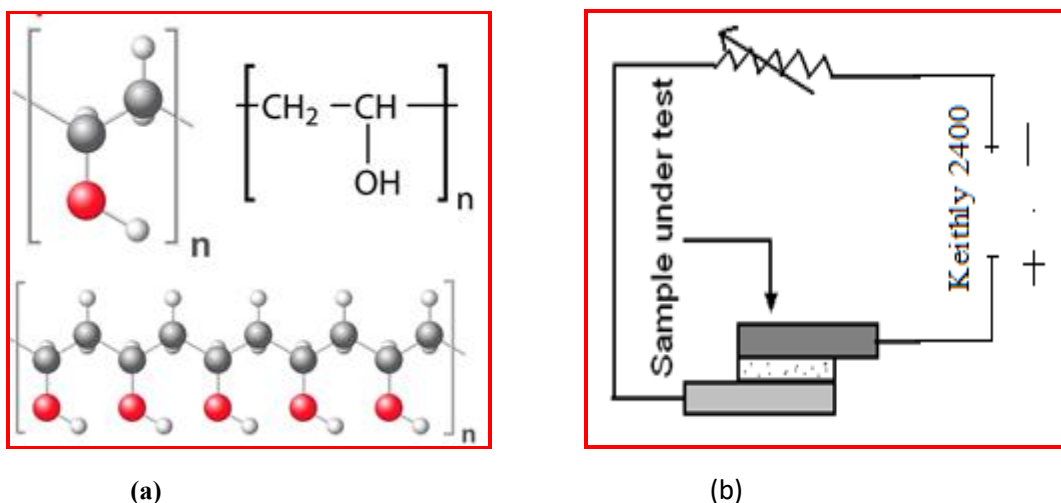


Fig. 5.3 (a) Structure of PVA (b) The circuit diagram of the reverse bias connection of the diode to the Keithley 2400

NP. Due to the presence of PVA, which causes the NP to coagulate, it can be seen from Fig. 5.2 (d) and (e) that there is a tendency for the NP to coagulate. The PVA concentration, which limits the passage of charges, should therefore be employed as little as feasible.

Now three diodes are ready to measure I-V and I-T characteristics. The PVA structure and the circuit diagram is given in Fig. 5.3.

5.2.2 Measurement

Keithley's 2400 source measuring equipment is carried out the I-V measurements. A digital voltmeter, multimeter, and dc supply can all be used to make the same measurement. In our lab, we designed a heater with a temperature control circuit. With that heater and a Keithley 2400 source measure unit are used to test the I-T characteristic. The experiment is conducted between 306-348 K in temperature. A K-type thermocouple (Cromel Allamel) was used to measure temperature with an accuracy of 0.15 K.

5.2.3 Result and Discussion

The dependence of electroconductivity of the semiconductor on temperature is expressed by Van't Hoff formula [1-3]

$$\sigma = A e^{\frac{-U}{2KT}} \quad (5.1)$$

where U is the dissociation energy of the electron (or hole). According to this formula, between $\log \sigma$ vs $\frac{1}{KT}$ plot must hold linear dependence. We can estimate the value of U by calculating the angular coefficient of the straight line. If adding more impurity levels, a change in the constant U should be anticipated.

In this chapter, we have also estimated current by adjusting the device's voltage. Cu and ITO-coated glass are coupled with the positive and negative terminals respectively for forward bias. Both devices' I-V curves are of a non-linear type. For the TiO_2 PVA Turmeric dye-based devices in Fig. 5.6, the current is high. It is possible to say that the thermionic emission (TE) theory could be fitted to the device's I-V. According to the TE theory [4-9] the forward bias I-V characteristics of a diode can be expressed as

$$I = I_0 [e^{\frac{qV}{\eta KT}} - 1] \quad (5.2)$$

where I_0 is the reverse saturation current which is described as,

$$I_0 = AA^* e^{\frac{-q\Phi_b}{KT}} \quad (5.3)$$

Here A is contact area, A^* is the Richardson constant, T is the absolute temperature and Φ_b is barrier height.

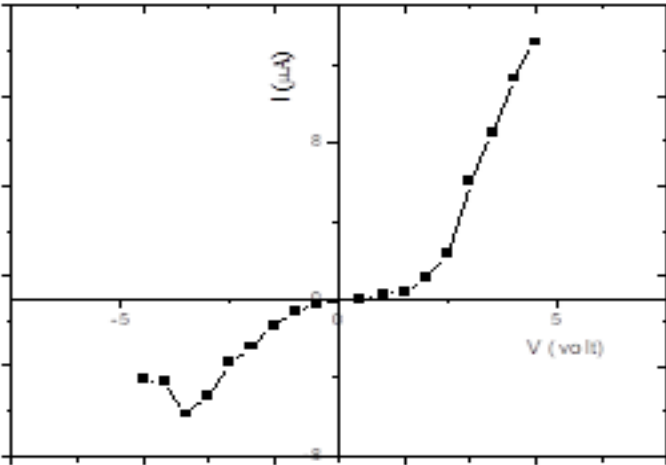


Fig. 5.4 Forward and reverse bias I-V curve of Turmeric diode

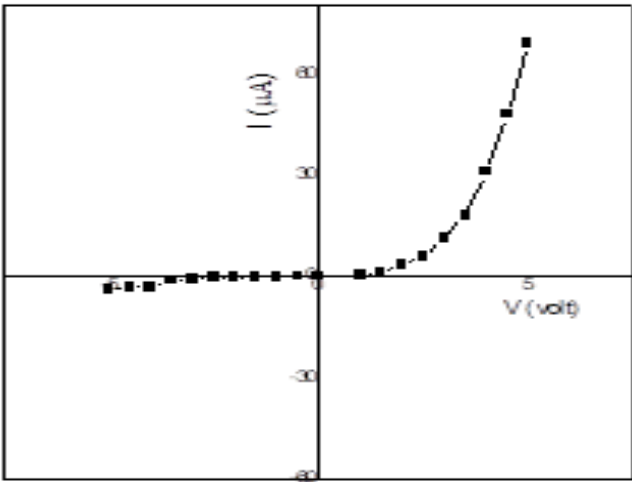


Fig. 5.5 Forward and reverse bias I-V curve Turmeric with TiO₂ diode

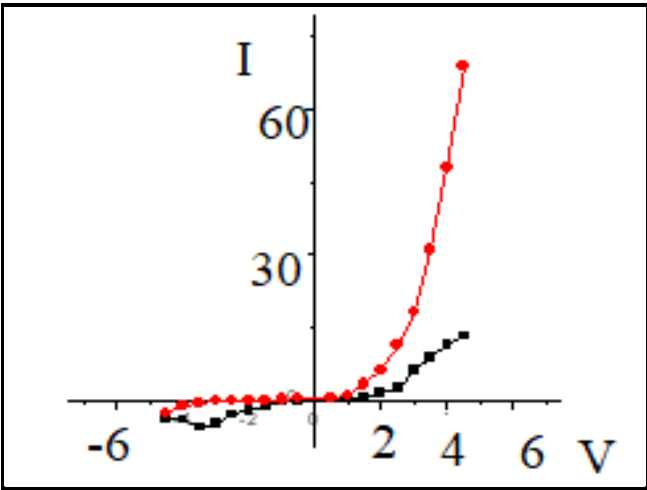


Fig.5.6 Comparison curve of Turmeric diode with and without TiO₂

Table 5.1 Values of U (dissociation energy) of Turmeric dye with and without TiO₂ nanoparticles

Type of films	Values of U (eV)
ITO/PVATTurmeric/Cu	0.55
ITO/TiO ₂ +PVA Turmeric/Cu	0.40

Here the covalent bond breakdown could be the reason for the production of Turmeric dye carriers, which calls for the input of energy equal to U. So, it is feasible to assess U by looking at the carrier's temperature fluctuation. A study of the temperature change of reverse saturation current, which is the current flowing through the diode under reverse bias conditions equation is given bellow [10,11].

$$I_0 = C \exp \left(- \frac{U}{2kT} \right)$$

(5.4)

Where I_0 is reverse saturation current, C is constant which balances the units of both side, U is dissociation energy, and T is Temperature in K. It is seen from Eqn. 5.4 that the saturation current depends on $U/2kT$ exponentially. Taking logarithms on both sides of Eqn. 5.4 we get

$$\ln I_0 = \ln C - U/2kT \quad (5.5)$$

According to Eqn. 5.5, the junction temperature is the single factor affecting the reverse saturation current I_0 in semiconductor diodes. The temperature has an exponential effect on it. A straight line with a negative slope have been found and a value of $U/2k$ is produced by plotting $\ln I_0$ vs. $1/T$. The slope (m) of the straight line can be used to compute the value of U . Thus

$$U = 2m k \quad (5.6)$$

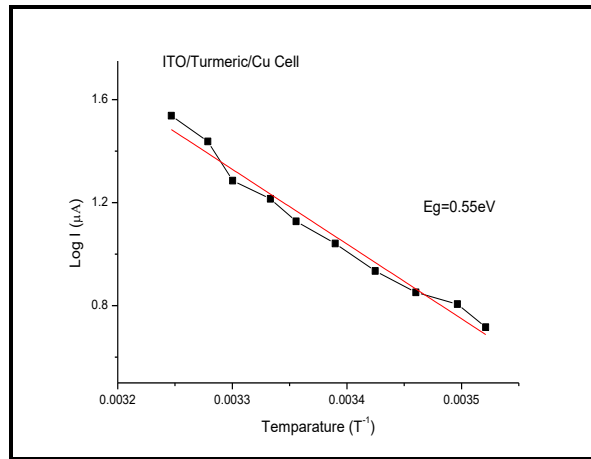


Fig. 5.7 log I-1/T curve of ITO/ Turmeric /Cu cell

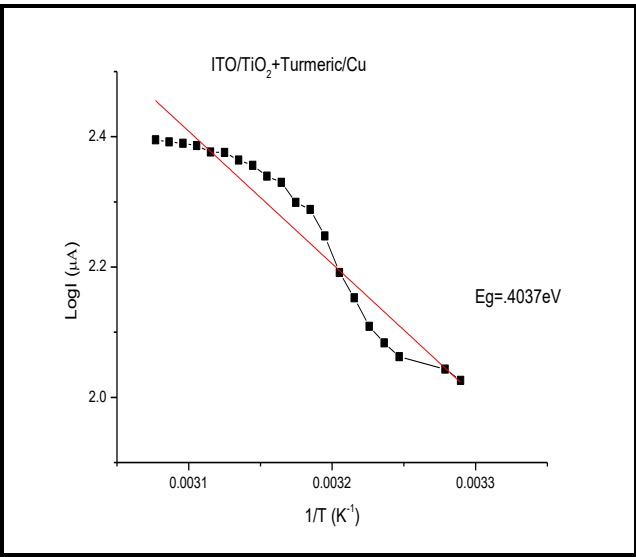


Fig. 5.8 log I-1/T curve of ITO/TiO₂ + Turmeric /Cu

I-T data is collected utilizing the thermal bath while keeping the reverse bias voltage constant across the device. The data from Fig. 5.8, $\log I_0 - 1/T$ plot are shown here. They are using the diode's equation for temperature-dependent current. Eqn. 5.5. The exponents for various voltages of 2V, 4V, and 6V can be determined using Eqn. 5.6, accordingly. In the low-temperature zone compared to the high-temperature region, the slope of curves varies. Thus, linear fitting has been performed. Due to some restrictions in our experimental facilities, we have left the low-temperature region even though it is crucial for the computation of the defect potential barrier. The electron concentration is generally temperature independent in the low temperature region. However, this section is outside the scope of the current discussion. It is demonstrated that the dissociation energies of two thin films differ. Dissociation energy values are 0.55 eV and 0.40 eV without and with a thin layer of TiO₂ Turmeric dye, respectively shown in Table 5.1. According to our earlier research, the ITO/TiO₂ Turmeric PVA/Cu structure develops a better electroconductive device than Cu/Turmeric/Al. Impurity or flaws in film production may result differently. The dissociation energy of the thin layer of TiO₂ and Turmeric dye is low. The precise reason is yet unknown. The PVA Turmeric thin film should, however, have a lower free charge carrier density than the TiO₂ layer. As a result, the addition of TiO₂ and Turmeric dye based cell reduces the density of the Gaussian state [12,13]. Here, we suppose that Turmeric dye is a semiconducting substance, and Eqn. 5.7 provides the dissociation energy relations of Turmeric dye with free charge.

$$U = q V_{oc} + \left(\frac{\sigma_n^2}{2} + \frac{\sigma_p^2}{2} \right) + K T \ln \left(\frac{N_p N_n}{np} \right) \quad (5.7)$$

Where U is the cell's dissociation energy, V_{oc} is the open circuit voltage, q is the elementary charge, n , p is the width of the acceptor and donor Gaussian density states, N_n and N_p are the effective conduction band and valance band density states, and n and p are the concentrations of free electrons and holes. It might be claimed that the incorporation of TiO_2 with Turmeric dye has reduced the width of the acceptor and donor's Gaussian density states.

We used the Shockley equation provided above, Eqn. 5.1 and Eqn. 5.2, to analyze the dark I-V characteristics in order to measure the series resistance, barrier height, and trap energy of the three diodes. In Fig. 5.9, curves are displayed.

The deviation of the curve occurred mainly due to the presence of high series resistance (R_s) of the thin films. We have also measured the R_s and Φ_b of the device by using the Cheng Cheung equation [14,15] given below,

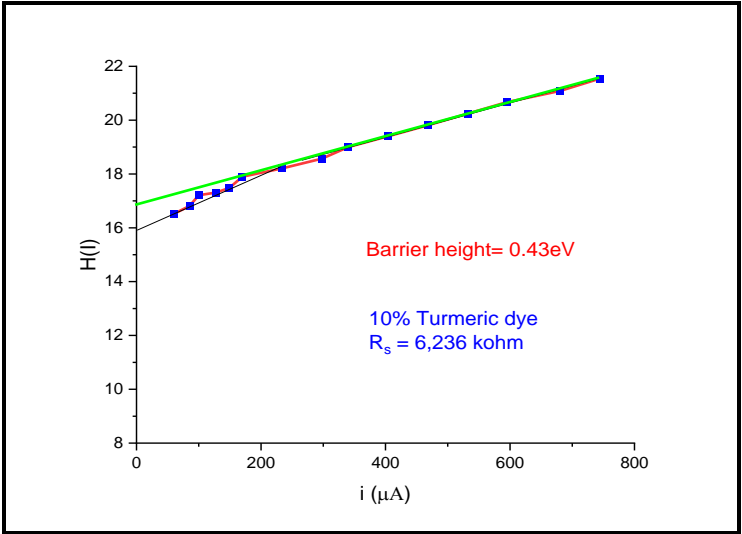
$$\frac{dV}{d \ln I} = \frac{nKT}{q} + IR_s \quad (5.8)$$

$$H(I) = n\phi_b + IR_s \quad (5.9)$$

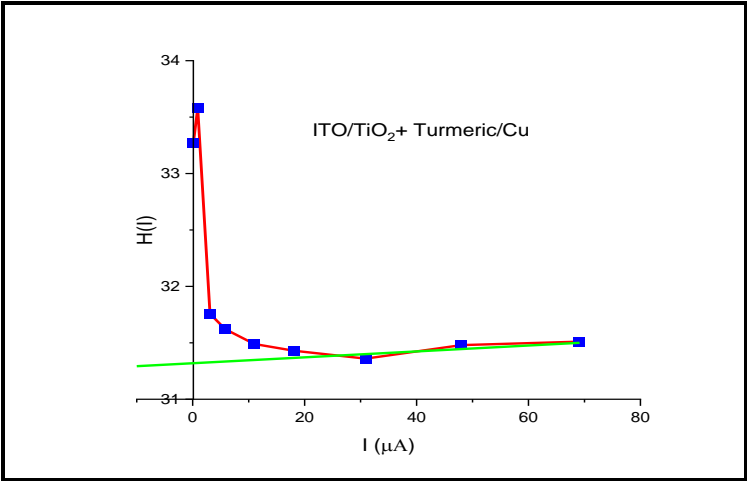
Where,

$$H(I) = V - \left(\frac{nKT}{q} \right) \ln \frac{I}{A A^* T^2} \quad (5.10)$$

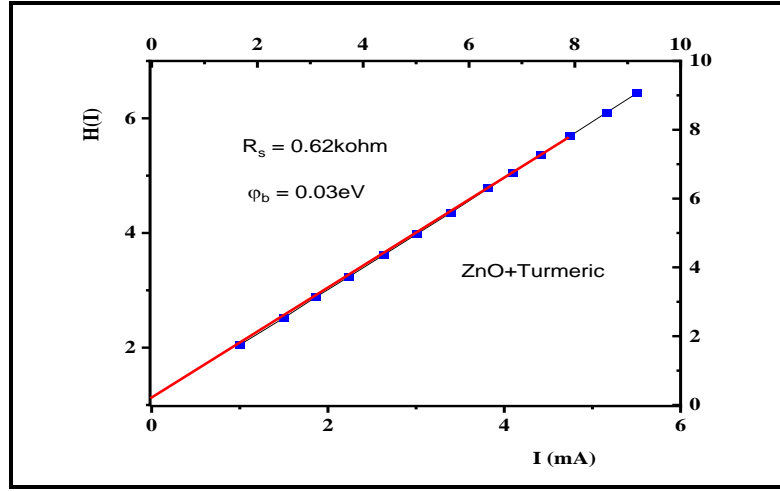
From Eqn. 5.8, we have measured the device R_s . To extract the device R_s , we have plotted $H(I)$ Vs. I curve shown in Fig. 5.9.



(a)



(b)



(c)

Fig. 5.9 (a), (b) and (c) Curves for estimation of series resistance, barrier height and ideality factor of Turmeric dye- based diode, with TiO_2 , and ZnO nanoparticles respectively

The $\frac{dV}{d \ln I}$ vs. I plot gives a straight line with an intercept of $\frac{nKT}{q}$. The slope of the curve yields the value of R_s from the intercept after we have retrieved the value of ϕ_b . Additionally, we have estimated the value of R_s using Eqn. 5.10. We have plotted the $H(I)$ vs. I curve displayed in Fig. 5.9 in accordance with the equation. From this curve's slope, we have investigated the value of R_s , and the intercept yields the barrier height (ϕ_b) value. The extracted values of R_s of the Turmeric dye-based diode by using $\frac{dV}{d \ln I}$ vs. I and $H(I)$ vs. I plot shows consistency with each other. We have measured the device's trapped energy as part of our investigation. We have regarded the distribution of traps to be exponential in order to quantify the trapped energy, and using this distribution, the concentration of trap energy may be determined by [15],

$$n_t = H_n \exp\left(\frac{F_n}{KT_c}\right) \quad (5.11)$$

Where H_n is the trap density, F_n is the electron Fermi level, K is the Boltzmann constant, and T_c is the characteristic temperature which is given by,

$$T_c = \frac{E_c}{K} \quad (5.12)$$

Where E_c is the characteristic trap energy.

Now by this considering this exponential trap distribution, we have estimated the E_c from the space charge limited current given by,

$$I = AN_c \mu q^{1-m} \left(\frac{m\varepsilon}{H_n(m+1)} \right)^m \left(\frac{2m+1}{m+1} \right)^{m+1} \left(\frac{V^{m+1}}{L^{2m+1}} \right) \quad (5.13)$$

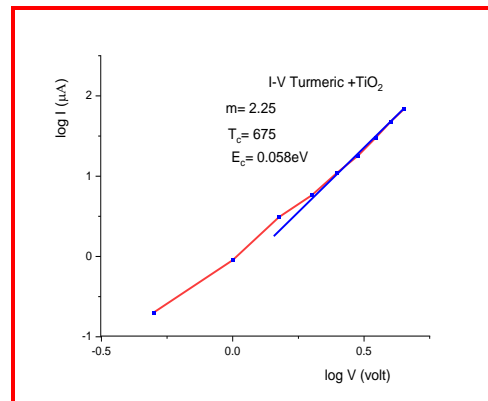
Where N_c is the effective density of states, m is the ratio of the characteristic temperature T_c to absolute temperature, V is the applied voltage, L is the thickness of the active layer, and is the product of the permittivity of the vacuum (ε_0) and the dielectric constant (ε_r).

Temperature $T \left(m = \frac{T_c}{T} \right)$.

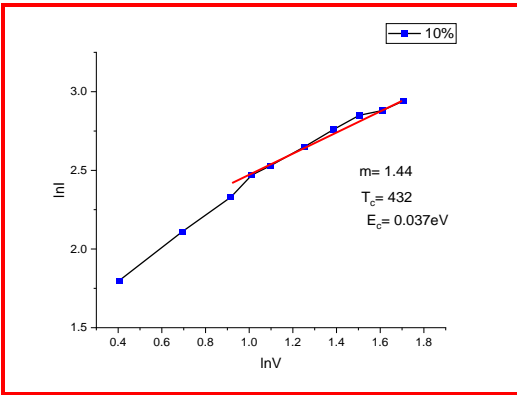
According to Eqn. 5.13, the space charge limited current displays a power-law dependency between current voltage and current,

$$I \approx V^{m+1} \quad (5.14)$$

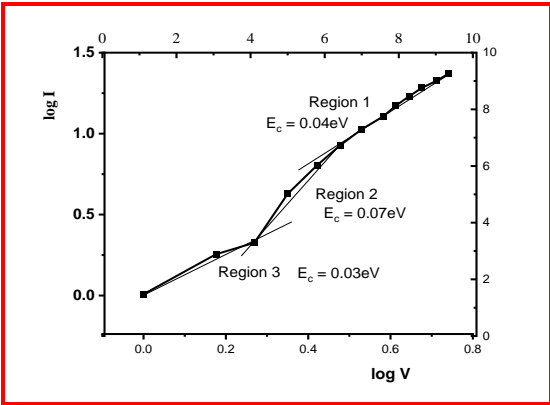
We have estimated the Turmeric diode's trap energy using the Eqn. 5.14 and from $\ln I$ vs. $\ln V$ shown in Fig. 5.10. Table 5.2 displays the estimated values of the charge transfer parameter of the Turmeric dye based diode with and without NP.



(a)



(b)



(c)

Fig. 5.10 (a), (b) and (c) Curves for estimation of trap energy of Turmeric dye- based diode, Turmeric diode with TiO_2 , and ZnO nanoparticles respectively

Table 5.2 Values of barrier height (ϕ_b), series resistance (R_s) and trap energy (E_c) of different Cells

Name of the diode	Trap energy (E_c) eV	Series resistance (R_s) K Ω	Barrier height(Φ_b) eV
ITO/Turmeric+ ZnO /Cu	0.046	0.62	0.03
ITO/Turmeric+ TiO_2 /Cu	0.059	0.276	0.78

We have compared two cells of the Turmeric dye. ITO/10% Turmeric dye/Cu diode and ITO/ TiO_2 + Turmeric/Cu diode are two examples. For the Turmeric diode added with TiO_2 , series resistance, trap energy value is lower, and barrier height is higher.

5.3 Conclusions

In this chapter, we have analysed the semiconducting properties of PVA Turmeric composite-thin film in presence of NP. A challenging method is the charge injection mechanism from metal into disordered Turmeric dye. However, we have shown that TiO₂ PVA Turmeric composite thin films exhibit more charge conduction than PVA Turmeric composite films alone. TiO₂ is used as a charge transfer layer. We have taken three diodes. They are ITO/PVA Turmeric/Cu, ITO/PVATurmeric+TiO₂/Cu and ITO/PVATurmeric+ZnO/Cu. We have observed the I-T characteristics of the diode. We have found current increases with temperature which is a characteristic of semiconductors. We have also estimated dissociation energy. TiO₂ inclusion reduces the dissociation energy. Change in trap level energy states can be seen in the variation of dissociation energy with NP inclusion. A lower series resistance indicates a higher charge conduction in the device. Increases in the barrier height and trap energy of the TiO₂ added Turmeric dye-based device indicate more charges are trapped in the dye layer.

5.4 References

1. K. E. Jasim et al, Curcumin Dye-sensitized Solar Cell, Journal of Energy and Power Engineering 11 409-416 (2017)
2. S. Shalini et al, Review on natural dye sensitized solar cells: Operation, materials and methods, Renewable and Sustainable Energy Reviews 51 1306-1325 (2015)
3. G.Richhariya et al, Natural dyes for dye sensitized solar cell: A review, Renewable and Sustainable Energy, 69 705-718 (2017)
4. S. G. Torzo et al, Experiment on the physics of the pn junction, American Journal of Physics, 62 66-70 (1994)
5. S. Maity et al, Temperature-dependent dark current-voltage study of thionin dye doped solid state photo electrochemical cell (PEC), Journal of optoelectronics 15 12 1417-1422 (2013)
6. H. li et al, Temperature-dependent Schottky barrier in high-performance organic solar cells, Scientific Reports 107-40134 (2017)
7. A. Halde et al, Effect of C₆₀ on methyl red and crystal violet dye-doped, Ionics, 14 263-267 (2008)

8. A. Halde et al, Effect of back electrode on photovoltaic properties of crystal-violet-dye-doped solid-state thin film, *Ionics*, 14 5 427- 432 (2008)
9. S. Maity et al, Effect of plasticizer on safranin-T-dye-based solid-state photo electrochemical cell, *Ionics* 14 6 549-554 (2008)
10. A. Halde et al, Electrical and photovoltaic characterisations of methyl red dye doped solid-state photoelectrochemical cell, *Ionics*, 15 1 79-83 (2009)
11. S. K. Dey et al, A dye/polymer based solid state thin film photoelectrochemical cell used for light detection, *Syn. Met.*, 118 19-23 (2001)
12. S. K. Dey et al, Safranin-T dye doped solid state polymer photo electro chemical cell, *Sci.*, 38 1 93-99 (2003)
13. M.A. Lampert. controlled current injection in insulators, *Prog. Phys* 27- 329 (1964)
14. S. Antohe et al, The effect of the electron irradiation on the structural and electrical properties of A II-B VI thin polycrystalline, *J. Optoelectron. Adv. Mat.* 5 4 801-816 (2003)
15. S. Antohe et al, Electrical properties of electron irradiated thin polycrystalline CdSe layers, *J. of Appl. Phys.* 90 5928- 5932 (2001)

Chapter 6

Study on the Conductivity of a Sunset Yellow and Phenosafranine dye-Based Diode in Presence of TiO₂ and ZnO nanoparticles

6.1 Introduction

6.2 Selection of dye

6.3 Experimental details

6.3.1 Sample preparation

6.3.1.1 Sunset Yellow Diode

6.3.1.2 Measurement on SY natural dye-based diode

6.3.1.3 Material Characterization

6.3.1.4 Results and Discussion

6.3.2 PSF Diode

6.3.2.1 Measurements on PSF diode

6.3.2.2 Results and Discussions of PSF diode

6.4 Conclusion

6.5 Reference

6.1 Introduction

In the last three chapters, we have discussed the conductivity and charge transport mechanism of Turmeric dye-based electronic devices. In this current chapter the AC and DC conductivity and charge transport processes of other two natural organic dye called Sunset Yellow (SY) dye and Phenosafranin are discussed here. The SY dye is a safe, non-toxic food coloring that has no negative effect on the environment [1-3]. Compared to other types used dyes, this one has a cheaper production cost since it is simple to extract. We have used a sandwich arrangement in which these dyes were sandwiched in between an indium-tin oxide-coated glass (ITO) front electrode and a copper plate (Cu) as back electrode.

The I-V properties of ITO/PSF/Al organic device have also been examined. Devices have also been prepared by incorporating the ZnO and TiO₂ nanoparticle. It has been found that adding of NP of TiO₂ and ZnO can greatly reduce the R_s that affect device performance. For PSF only, PSF+ZnO, and PSF+TiO₂, the retrieved values of R_s are around 250.8 K, 108.0 K, and 98.4 K, respectively. Additionally, it has been noted that addition of NP lowers the trap energy. For PSF only, PSF added ZnO, and PSF added TiO₂, the estimated values of the trap energy are 0.090 eV, 0.078 eV, and 0.072 eV, respectively. We have also estimated series resistance and compared for three cells.

6.2 Selection of the dyes

SY dye is a powder that is red in color, but when it is dissolved in a solvent (such DI water or ethanol), it takes on an orange hue color. Fig. 6.1 shows the SY dye's chemical structure. SY dye, sometimes referred to as orange yellow Sunset or C.I. 15985, is generated from petroleum and is distinguished by a chromophoric azo group $-N=N-$, in which the nitrogen atoms are joined to an sp^2 -hybridized carbon atom [4-7]. While the second carbon atom next to the azo group may likewise be a component of an analyzable aliphatic derivative, at least one of these carbon atoms is a member of an aromatic carbocycle or heterocycle [8,9]. Disodium 6-hydroxy-5-[(4-sulfophenyl) azo]-2-naphthalenesulfonate ($C_{16}H_{10}N_2Na_2O_7S$) is the IUPAC designation for SY dye. Typically, the SY colour is found in confections, pastries, snacks, sauces, and preserved fruits as well as in cosmetics and medications. Sunset yellow is used in foods, cosmetics, and drugs. Sunset yellow FCF is used as an orange or yellow-orange dye. However, we have not found any literature about its conductivity.

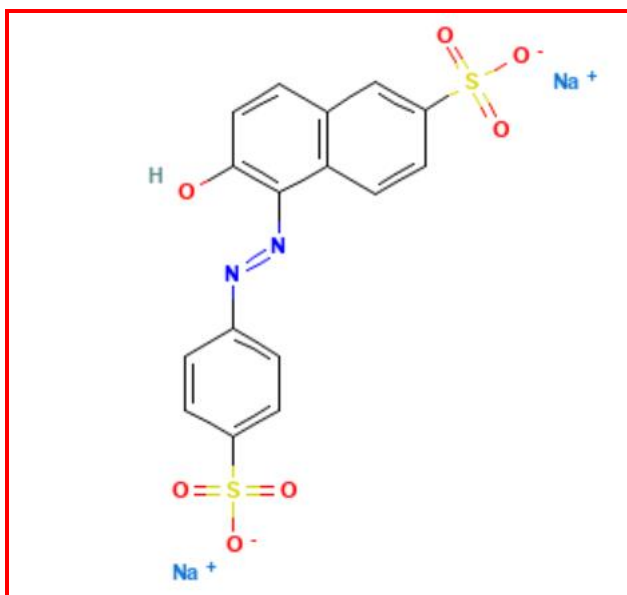
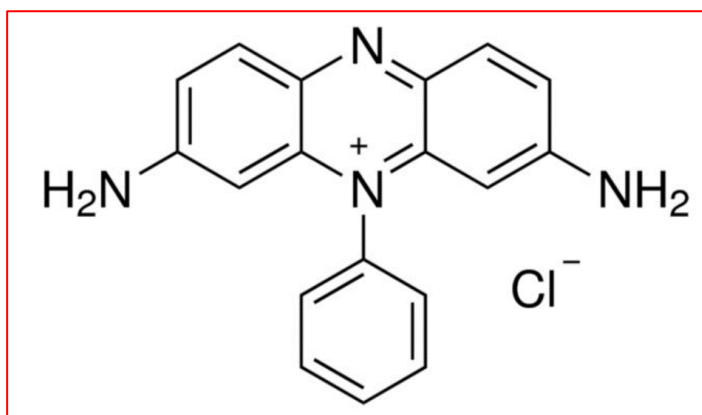
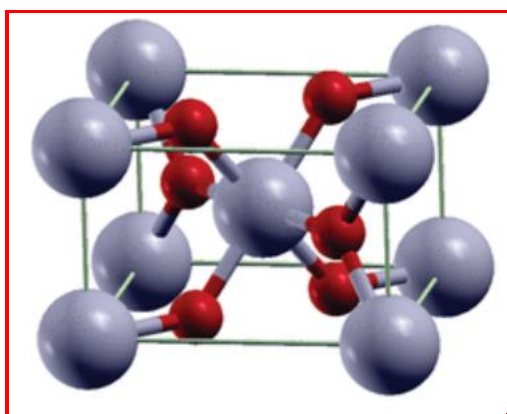


Fig. 6.1 Chemical structure of sunset yellow dye

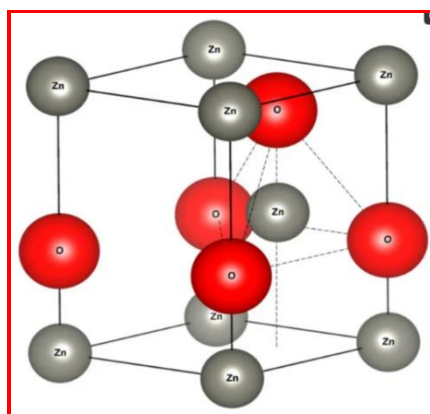
Fig. 6.2 depicts the structure of PSF (3,7-diamino-5-phenylphenazinium chloride). In the phenazinium group of chemicals, PSF is one of the most significant cationic dyes having a planar conjugated stiff structure, as was previously stated. Phenazinium dyes (available from Sigma-Aldrich in Germany) offer a wide range of uses in semiconductors, energy sensitizers, exploring micro heterogeneous environments, and several biological photochemical applications [10–13]. In Fig. 6.2(b) and 6.2(c) the architectures of TiO₂ and ZnO NP (Sigma-Aldrich, Germany) are depicted. The front electrode for the organic device was made of Indium Tin Oxide (ITO) coated glass, and the rear electrode is made of aluminum.



(a)



(b)



(c)

Fig. 6.2 Structure of (a) PSF dye, (b) TiO_2 nanoparticle, and (c) ZnO nanoparticles

6.3 Experimental details

6.3.1 Sample preparation

6.3.1.1 Sunset Yellow Diode

ITO-coated glass and Cu plate are first swabbed with two pieces each under a diluted detergent (such as Deconex or FPD detergent, Alconox). Following a 10-minute soak in the detergent at 60°C , they are rinsed with distilled water. The electrodes are then placed in a nitrogen atmosphere to dry after being sonicated for 10 minutes with DI water, 2-propanol, and acetone, respectively. The sample is treated to UV ozone for 10 minutes prior to spin coating. We have measured 2 mg of SY dye using a DHONA100DS, and we have dissolved it in 0.5 ml of deionized water using an ultrasonicator for 30 minutes at room temperature. Then, using a desiccator, the samples are kept in a vacuum. We have spin-coated the prepared samples separately on the previously cleaned ITO glass slides at 2000 r.p.m. In semi-dried state, we place the previously cleaned Cu plate on the sample as a back electrode and then heated the sample with a regulated hotplate at 60°C for 1 h. The schematic diagram of the cell is given in Fig. 6.3.

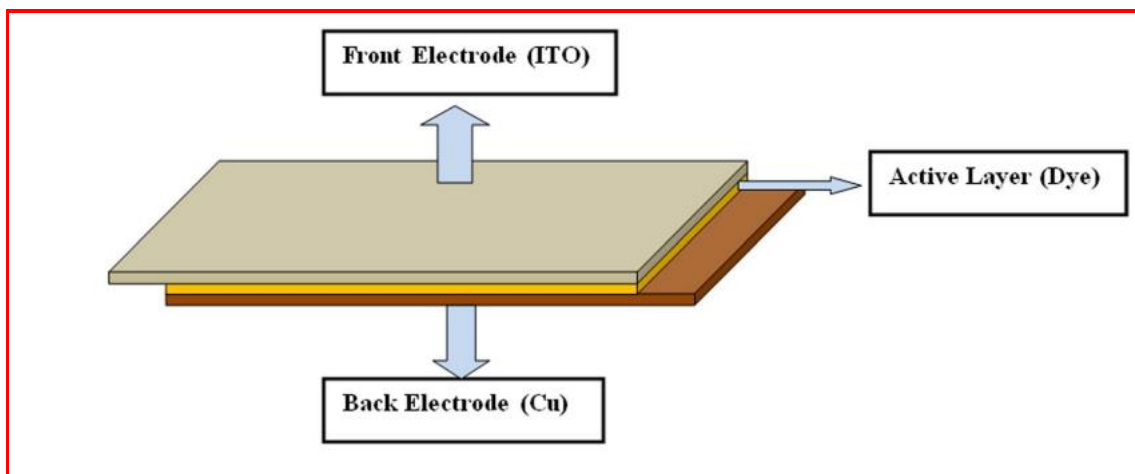


Fig. 6.3 Schematic diagram of the cell

6.3.1.2 Measurement on SY natural dye-based diode

6.3.1.3 Material Characterization

Absorption Spectroscopy of SY Dye

The UV-VIS absorption spectra for the natural dye are shown in Fig. 6.9(a) as a function of wavelength. Absorption spectra were collected in the 200-800 nm wavelength range. The SY dye exhibits a distinct absorption peak at 483 nm. This maximal absorption can be attributed to xanthophyll, flavone, carotene, and rehein molecules [14-18]. The Tauc plot, illustrated in Fig. 6.4 (b), was utilized to determine the bandgap of this dye. The nature and value of the optical bandgap are determined by the fundamental absorption, which corresponds to electron excitation from the valance band to the conduction band. Eqn. 6.1 shows the relationship between the absorption coefficient (α) and the incident photon energy ($h\nu$).

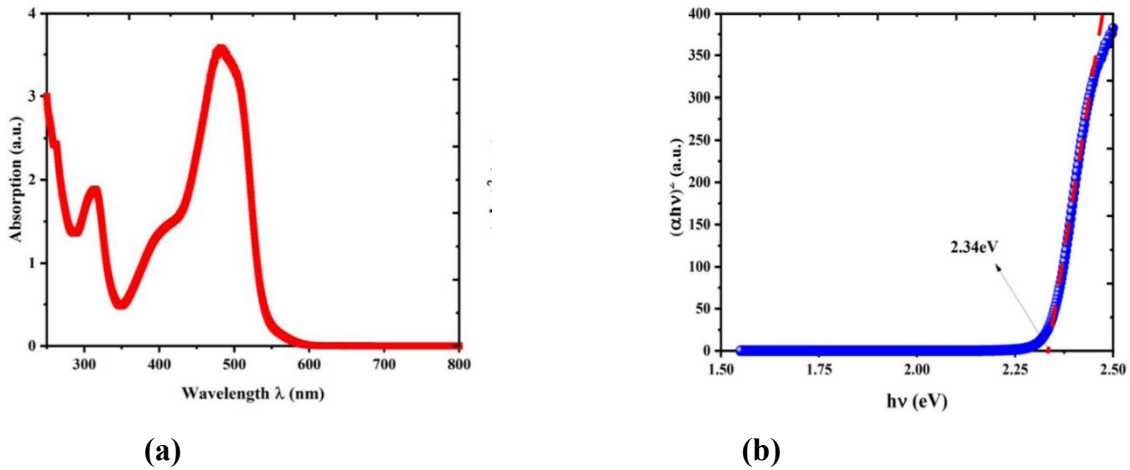


Fig. 6.4 (a) Absorption spectroscopy of SY dye. (b) Tauc plot of SY dye

$$(\alpha hv)^{\frac{1}{n}} = A[hv - E_g] \quad (6.1)$$

where A is a constant, E_g is the bandgap of the material, and n is an exponent depending on the type of transition. For direct allowed transition $n=1/2$, for indirectly allowed transition $n=2$, and for directly forbidden transition $n=3/2$. The graphs were drawn between $h\nu$ and $(\alpha h\nu)^2$ as shown in Fig. 6.4(b), and the corresponding bandgaps were obtained by extrapolating the straight portion of the graph on the $h\nu$ axis at $\alpha=0$ and have the value 2.34 eV.

XRD Analysis

A Bruker D8 SWAX diffractometer is used to get the x-ray diffraction (XRD) pattern for the powdered SY dye. Cu-K α radiation of wavelength 1.5404 Å at 35 keV and 35 mA x-ray with a 300 ms delay and rotation between the 10° to 80° angle were used. In Fig. 6.5, the diffraction pattern is shown. Considering that there are numerous diffraction peaks present with different strengths, it was assumed that the SY powder is polycrystalline. Sharp XRD peaks suggest that the SY dye has good crystallinity [19-23].

6.3.1.4 Results and Discussion

DC Conductivity Measurement of SY diode

The DC conductivity is estimated using Eqn. 6.2 given below.

$$\sigma_{DC} = \frac{Id}{VA} \quad (6.2)$$

where d is the thickness of the thin film, I is the current through the sample, A is the effective area, and V is the applied bias voltage. The variation of σ_{DC} with a temperature range of 303 K to 373 K of SY dye is shown in Fig. 6.4(a) at 4 V bias voltage. In this study, a correlation between temperature increase and a rise in DC conductivity was found. This is due to the greater mobility of free charges at higher temperatures, such as polarons and free ions, and it is an excellent fit to the Arrhenius exponential law equation [24-27]. The -electron mobility and semiconductor behavior of SY dye cause the transfer of -electrons [28]. Fig. 6.4(b) depicts the Arrhenius plot of the SY dye.

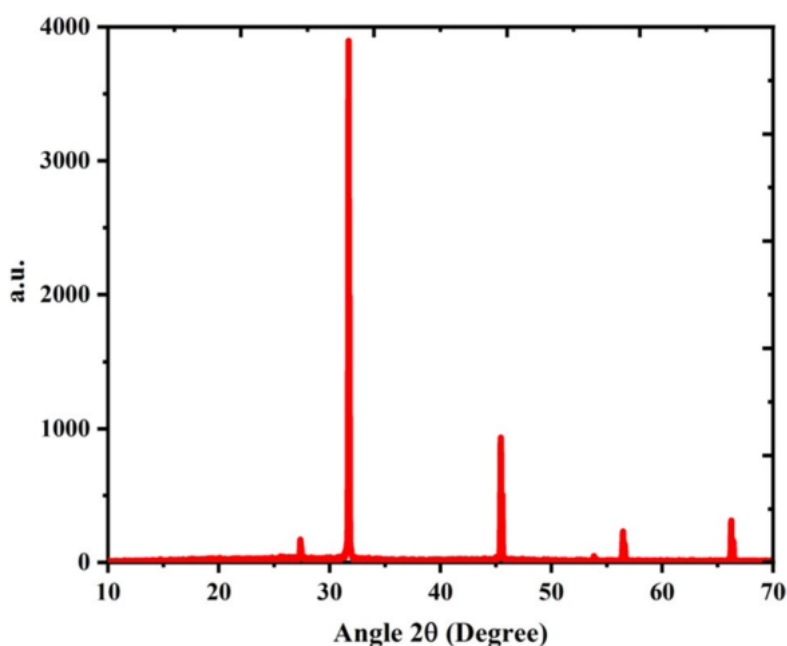


Fig. 6.5 The x-ray pattern of the SY dye in powder form

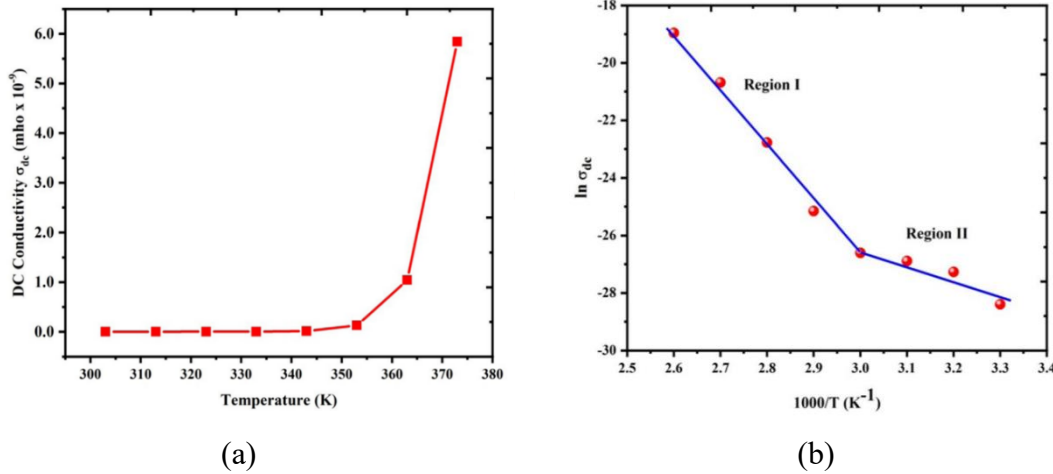


Fig. 6.6 (a) DC conductivity plot of SY natural organic dye with temperature. (b) A semi-logarithmic plot of the temperature dependence of the DC electrical conductivity of SY natural organic compound. The solid lines represent the best linear fits to the data

The DC conduction mechanism has been analyzed using the well-known Arrhenius equation shown below [29],

$$\sigma = \sigma_{01} e^{\frac{-\Delta E_1}{TK_B}} + \sigma_{02} e^{\frac{-\Delta E_2}{TK_B}} \quad (6.3)$$

where T is the absolute temperature, k_B is the Boltzmann constant, σ_{01} and σ_{02} are the high-temperature limits of conductivity from regions I and II, as shown in Fig. 6.6, including the charge carrier mobility and density of states, and ΔE_1 and ΔE_2 are the DC activation energy (in keV) in region I and region II, respectively. We can infer from the Arrhenius figure that there are two conduction mechanisms operating within the investigated temperature range. The least amount of energy needed to go beyond the potential barrier is represented by the activation energy of the conductivity that is temperature-dependent. It is implied that there are two different types of conduction mechanisms since the two zones of the Arrhenius plot indicate the various activation energies, one for the higher temperature and the other for the lower temperature. From the slope and the intercept of the Arrhenius plot, we have the values of ΔE_1 and σ_{01} for region I are 0.683 eV and $6.18 \times 10^{-8} (\Omega - m)^{-1}$, respectively, and the values of ΔE_2 and σ_{02} for region II are 0.466 eV and $1.01 \times 10^{-8} (\Omega - m)^{-1}$, respectively. This finding demonstrates that the SY dye's DC conductivity is dependent on the temperature.

6.3.2 PSF Diode

In order to prepare, we have made a Poly Vinyl Alcohol (PVA) solution by combining 4 mg of PVA with 20 ml of distilled water, stirring the mixture for 30 minutes at 80°C using a magnetic stirrer. The PVA solution is then thoroughly frenzied for an additional 30 minutes while 2 mg of PSF dye is added. The PSF dye solution is then divided into three portions and stored in three test tubes that have already been cleaned. Now, separate mixtures of 2 mg each of ZnO and TiO₂ NP are added to the two test tubes. The remaining test tubes are left alone. So, we have three test tubes one is with only PSF solution, 2nd test tube is PSF with ZnO nanoparticle solution and 3rd test tube is PSF with TiO₂ nanoparticle solution. The PSF dye solution is spin-coated on an ITO-coated glass at a speed of 1500 rpm and then dried at a speed of 2500 rpm. In a similar manner, the same solution is spin-coated on the Al electrode. These two electrodes are sandwiched together to form a PSF dye-based organic device. Similarly, the solution of PSF with TiO₂ and PSF with ZnO is spin-coated on ITO and Al electrodes and prepared two other organic devices. One is a PSF dye-based organic device in presence of ZnO NP and another is a PSF dye-based organic device in presence of TiO₂ NP. After preparing these three devices they are kept under a vacuum for 12 h.

6.3.2.1 Measurements on PSF diode

After thorough drying, these cells are examined. PSF dye with ZnO and PSF dye with TiO₂ organic devices are imaged using scanning electron microscopy (SEM) in a JEOL field emission scanning electron microscope (JSM-6700F) that is running at a 5 kV accelerating voltage. In order to assess steady-state I-V characteristics, a Keithley 2400 source measuring unit is used. With a delay of 1000 ms, the applied voltage has been changed from 0 to 5 V in steps of 0.5 ms. The experiment is conducted at 26°C, the average room temperature. Al electrode is connected to the negative terminal, and ITO electrode is attached to the positive terminal of the supply voltage.

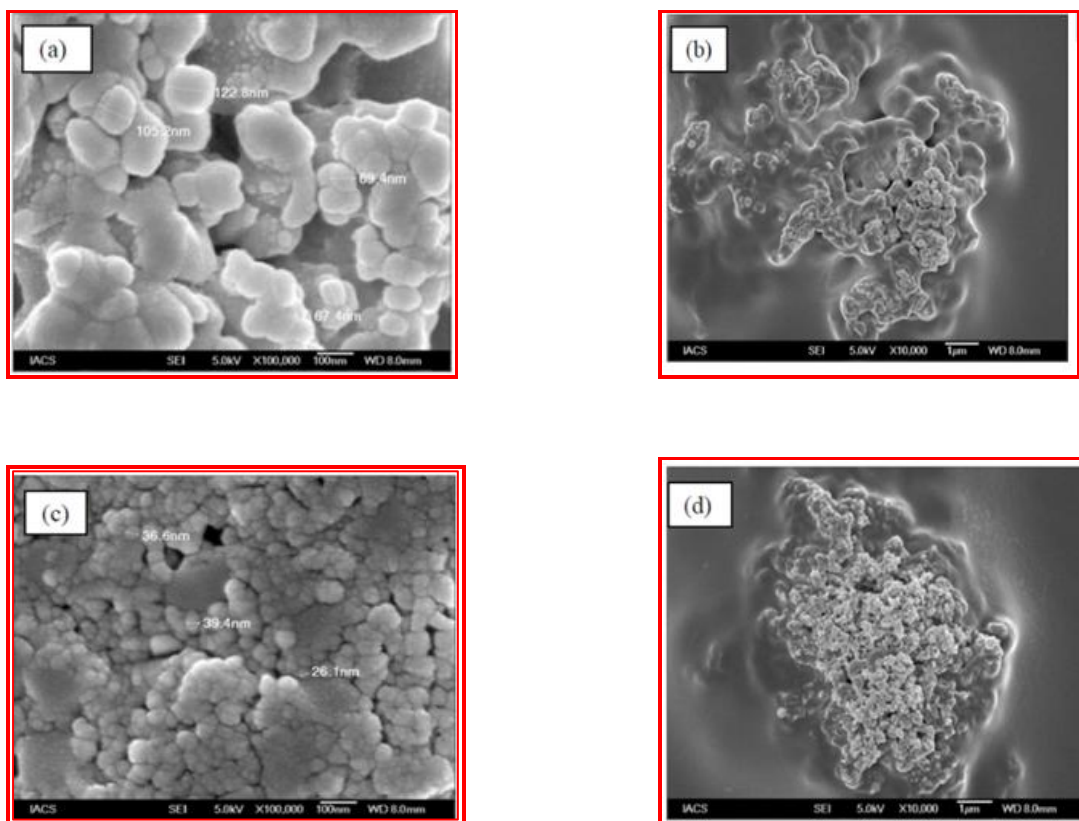


Fig. 6.7 SEM images of (a), (b) PSF + TiO₂ cell and (c), (d) of PSF + ZnO Cell with higher and lower magnifications respectively

SEM images for ITO/PSF + TiO₂/Al and ITO/PSF + ZnO/Al are acquired by using JEOL scanning electron microscope model JMS 6360. The PSF + TiO₂ and PSF + ZnO cells in Fig. 6.7 (a) and (c) demonstrate the sizes of TiO₂ and ZnO NP. Additionally, it can be shown from Fig. 6.7(b) and 6.4(d) that the congelation of NP brought on by PVA inhibits the mobility of charged particles.

6.3.2.2 Results and Discussions of PSF diode

Estimation of R_s

The ITO/PSF/Al organic device's dark I-V characteristic depicts an exponential increase in current with voltage; however, the current is boosted by adding NP of TiO₂ and ZnO to that system, as illustrated in Fig. 6.8.

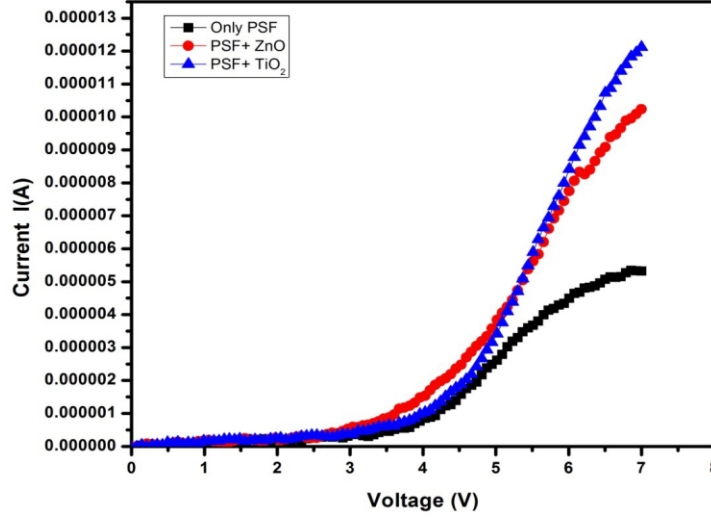


Fig. 6.8 Forward dark I-V characteristics of ITO/PSF/Al, ITO/PSF+TiO₂/Al, ITO/PSF+ZnO/Al

It is evident from the dark I-V characteristics that the current value for each of these systems is extremely low, in the microampere range. There are many causes for this low current, and among them, the impact of R_s is one of the primary ones. The determination of R_s is therefore crucial in order to comprehend the device performance. These three devices' dark I-V characteristics have been examined using the following equation [30],

$$I = I_0 \left[e^{\frac{qV}{\eta KT}} - 1 \right] \quad (6.4)$$

Where I_0 is the reverse saturation current which is given by,

$$I_0 = AA^* e^{\frac{-q\phi_B}{KT}} \quad (6.5)$$

Where q is the electronic charge, K is the Boltzmann constant, T is the temperature, V is the applied voltage η , is the ideality factor, I_0 is the reverse saturation current. We already know that the slope of the linear section of the $\ln I$ - V plot may be used to determine the ideality factor, which indicates how closely a device complies with the diode equation or the thermonuclear emission process.

$$\eta = \frac{q}{kT} \frac{dV}{d \ln I}$$

(6.6)

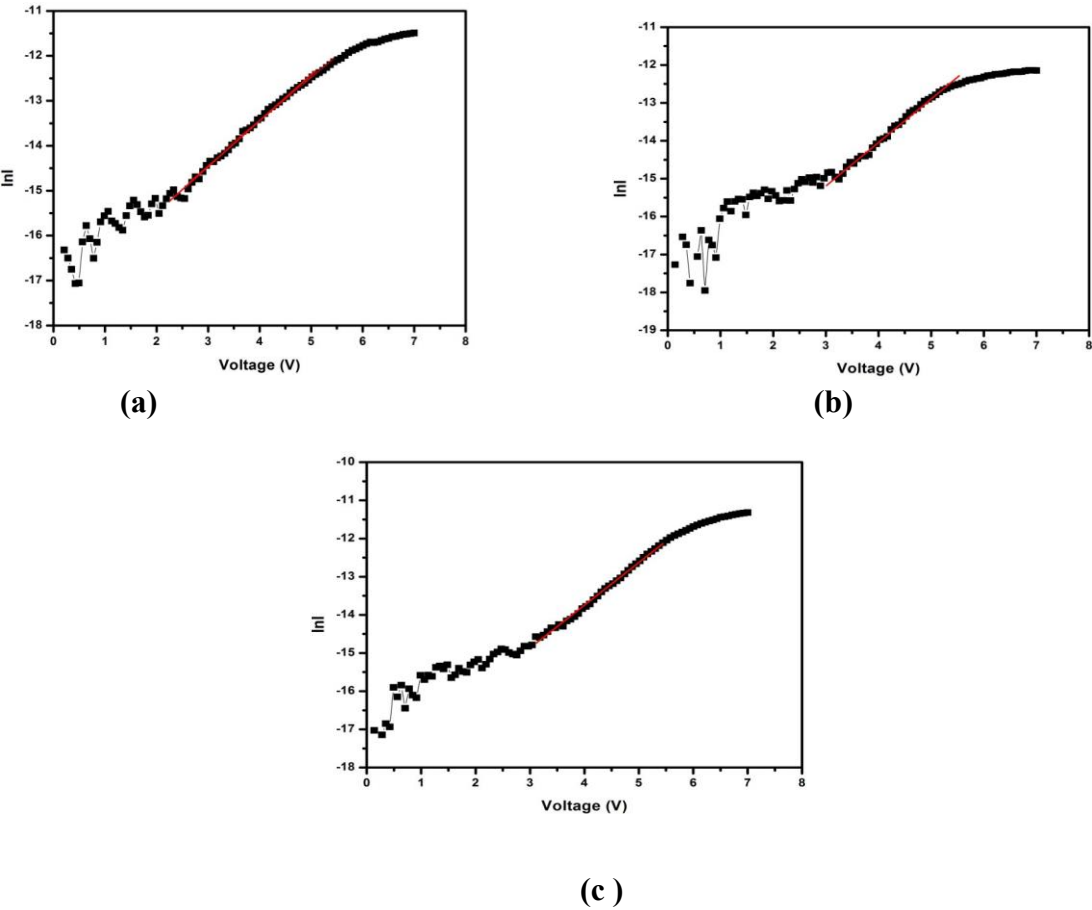


Fig. 6.9 lnI vs V characteristics of ITO/PSF/Al diode (a) for without nanoparticle, (b) for ZnO, (c) for TiO₂ nanoparticle

Table 6.1 The extracted value of η from lnI vs V plot for these three different cells without and with TiO₂ and ZnO nanoparticles

Sample	Value of ideality factor (η)
Only PSF	38.17
PSF+ ZnO	37.50
PSF+TiO ₂	34.59

To estimate the value of R_s the data have been fitted by the Cheung Cheung method [31-34]. This method by considering R_s the I-V equation can be written as

$$I = I_0 e^{\frac{q(V-IR_s)}{\eta KT}}$$

(6.7)

the η and R_s are obtained by using the following equations given below.

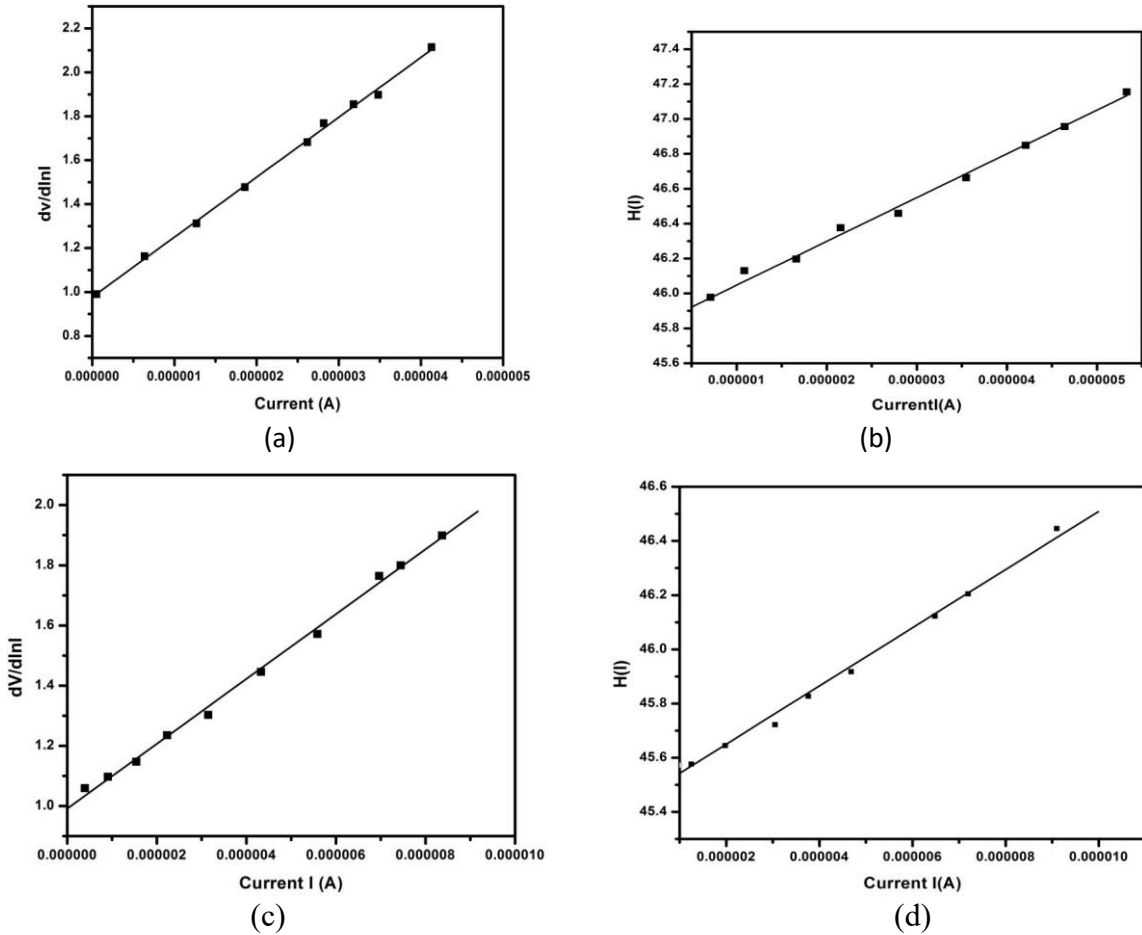
$$\frac{dV}{d \ln I} = \frac{\eta KT}{q} + IR_s \quad (6.8)$$

$$H(I) = n\phi_b + IR_s \quad (6.9)$$

Where,

$$H(I) = V - \left(\frac{\eta KT}{q} \right) \ln \frac{I}{AA^*T^2} \quad (6.10)$$

The plot of $dV/d \ln I$ vs I and $H(I)$ vs I is shown in Fig 6.10. From this figure it is seen that the slope of the curve gives the value of the R_s and the y-axis intercept gives the value of η from $dV/d \ln I$ vs I Plot and from $H(I)$ vs I plot intercept gives the barrier height (Φ_b) and slope of the curve gives the value of R_s .



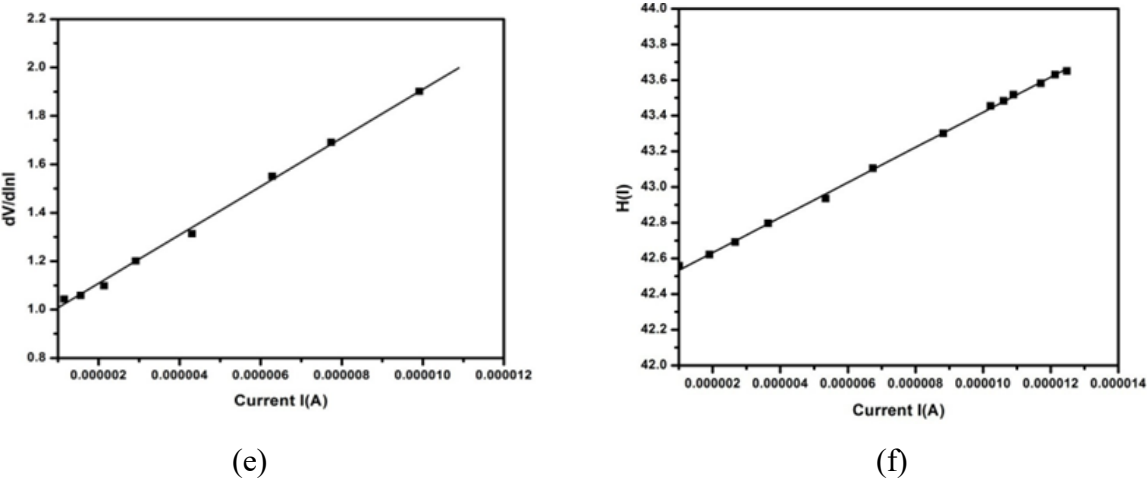


Fig. 6.10 $dV/d\ln I$ - current (I) and $H(I)$ – current (I) plot; (a) & (b): for without nanoparticle, (c) & (d): for ZnO, (e) & (f): for TiO₂ nanoparticles

Table 6.2 The extracted value of η and R_s for three different cells without and with TiO₂ and ZnO nanoparticles

Sample	Value of η	R_s from $dV/d\ln I$ plot ($K\Omega$)	R_s from $H(I)$ vs I plot ($K\Omega$)
PSF	37.47	272.70	250.80
PSF+ ZnO	36.90	112.10	108.30
PSF+TiO ₂	34.80	100.10	98.30

Estimation of trap energy (E_c)

The connection between organic molecules is exceedingly weak because organic semiconductors are disordered in nature. This weak contact, along with structural imperfections in the organic material, creates extra energy states known as traps in the energy region between the highest occupied molecular orbital (HOMO) and the lowest unoccupied molecular orbital (LUMO). Any biological device's trap distribution can be explained by a Gaussian distribution or an exponential distribution. As a result, during conduction, free charge carriers are imprisoned by localized energy states, preventing them from participating in the charge transport process. By assuming the trap energy distribution as exponential, the trap energy concentration may be expressed as

$$n_t = H_n \exp\left(\frac{F_n}{KT_c}\right) \quad (6.11)$$

Where H_n is the trap density, F_n is the electron Fermi level, K is the Boltzmann constant, and T_c is the characteristic temperature which is given by,

$$T_c = \frac{E_c}{K} \quad (6.12)$$

Where E_c is the characteristic trap energy.

Now by considering this exponential trap distribution, we have estimated the E_c from the space charge limited current given by,

$$I = AN_c \mu q^{1-m} \left(\frac{m\epsilon}{H_n(m+1)}\right)^m \left(\frac{2m+1}{m+1}\right)^{m+1} \left(\frac{V^{m+1}}{L^{2m+1}}\right) \quad (6.13)$$

Where N_c is the effective density of states, μ is the mobility, ϵ is the product of the vacuum permittivity (ϵ_0) and the dielectric constant (ϵ_r), V is the applied voltage, L is the active layer thickness, and m is the ratio of T_c to absolute temperature. $T \left(m = \frac{T_c}{T}\right)$.

From Eqn. 6.10, it can be said that the space charge limited current exhibits the power-law dependence in between current voltage,

$$I \approx V^{m+1} \quad (6.14)$$

This equation is used to investigate the trapped energy of the phenosafranin diode from the $\ln I$ vs. $\ln V$ graph. The $\ln I$ vs. $\ln V$ figure is shown in Fig. 6.11. When m is less than one, there is a transition voltage in region-1 below which conduction is injection limited and Ohmic. When a voltage is given to this region, charge carriers are injected from the electrode into the bulk region, and because the organic material is prone to electron traps, the majority of the charge carriers injected from the electrode are trapped.

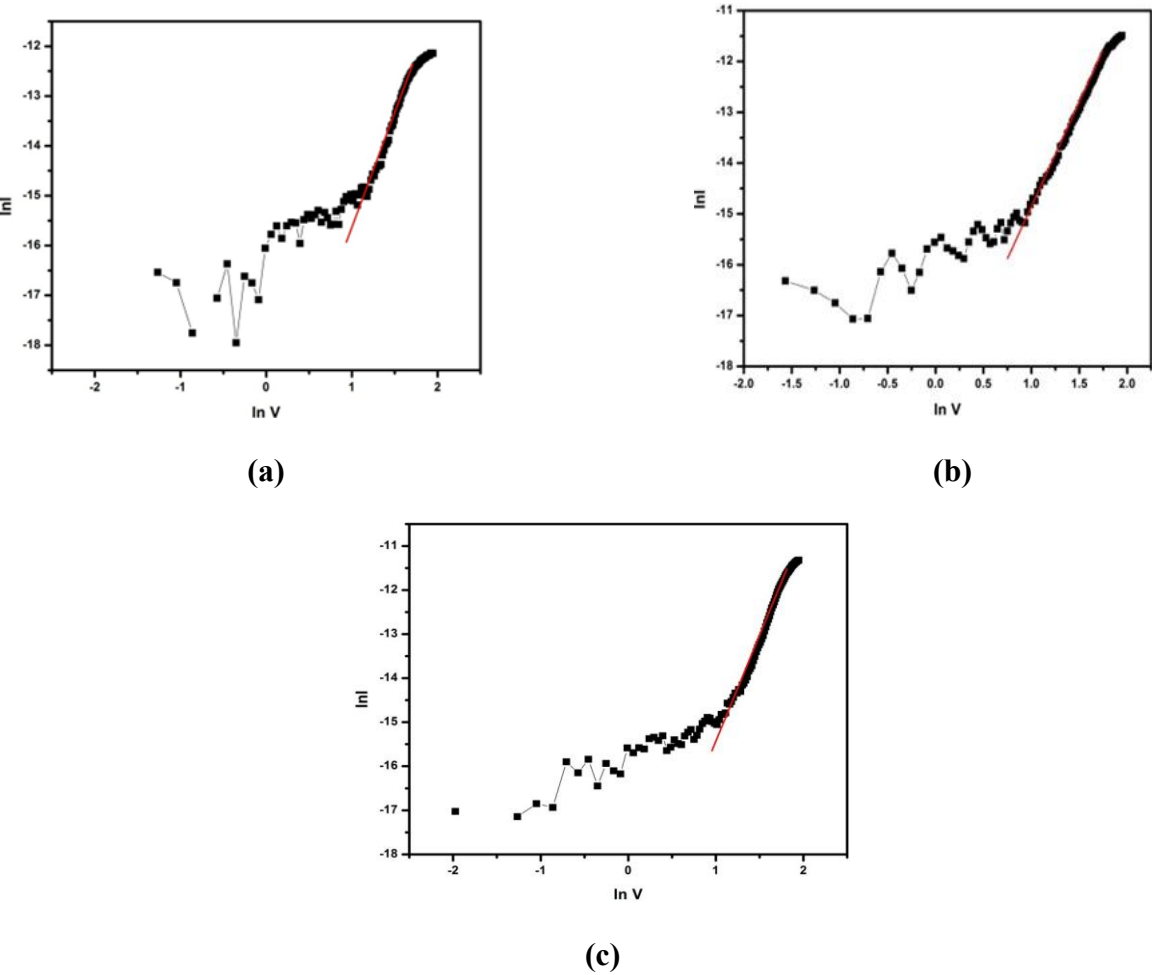


Fig. 6.11 $\ln I$ - $\ln V$ plot (a) for without nanoparticle, (b) for TiO_2 , (c) for ZnO nanoparticle

The outside electrode will only be reached by a very small percentage of charge carriers. Net current of the device is therefore quite modest. At the transition voltage in region 2 when m is greater than 2, the trapped charge carriers between HOMO and LUMO may be released or recombined with the opposing charge carriers, boosting the device's current. The extracted values of m and trap energy for these three different systems are shown in Table 6.3, which is supplied below.

Table 6.3 Extracted values of trap energy for three different system without and with TiO₂ and ZnO nano particles

Sl. no	System	Extracted value of m	Extracted value of E _c in eV
1	Only PSF	3.38	0.090
2	PSF+ ZnO	3.04	0.078
3	PSF+TiO ₂	2.80	0.072

Trap Energy and R_s

It has been shown that the trap energy decreases when NP are added. It has already been discovered that the R_s decreases when NP are present. Now, the experimental findings demonstrate that lowering trap energy reduces series resistance, which is the reason why device conductivity and efficiency increase. R is hence proportionally reliant on E_c. Table 6.4 shows the 33.35% decrease in R_s and E_c when NP are present.

Table 6.4 Estimated reduction percentage (%) of R_s and E_c in presence of TiO₂ and ZnO nanoparticles

NP used	Reduction percentage (%) of series resistance R _s using NP	Reduction percentage (%) of trap energy E _c using NP
PSF+ ZnO	58.82	13.33
PSF+ TiO ₂	63.29	20

The results demonstrate that traps present in the organic materials introduce extra localized energy states at the interface when a metal is in contact with an organic dye. These localized energy levels contribute new energy states to the band structure. On the other hand, traps that are added at the interface can be seen as structural defects. As a result of this process, both the surface potential and series resistance considerably rise. However, the addition of NP that act as filler at the interface reduces the density of traps and trap energy. The amount of injected charge carriers increases along with their mobility as trap energy is reduced, which lowers the device series resistance and enhances device performance.

6.4 Conclusion

In this chapter, we have studied characterization of two dyes namely SY and PSF. We have prepared two diodes namely ITO/SY/Al and ITO/PSF/Al. We have measured optical bandgap using UV VIS spectroscopy. At 483 nm, the SY dye exhibits a distinct absorption peak. The absorption spectroscopy result yielded an estimated optical bandgap of 2.34 eV. The results of an X-ray diffraction investigation demonstrate that this dye has good crystallinity. SY dye's DC electrical conductivity shows symmetrical behaviour.

The I-V data of ITO/PSF/Al are also studied in similar way. The thermionic emission theory and the Cheung Cheung function have been used to fit the data. It has been found that addition of TiO₂ and ZnO NP can greatly reduce the R_s and enhance the device performance. Additionally, it has been noted that adding NP lowers the trap energy. Analysis of the experimental data reveals that the consistency of previous observation. In the presence of NP, series resistance lowers along with a reduction in trap energy. These findings will be instructive for further research into the precise semiconducting behavior of natural organic dye-based devices.

6.5 References

1. H. Naarmann et al, The Development of Electrically Conducting Polymers, Adv. Mater. 2 345 (1990).
2. D. Mulati et al, The Absorption Spectra of Natural Dyes and Their Suitability as a Sensitiser in Organic Solar Cell Application, Jagst 14 1 (2012)
3. K.U. Isah et al, Alu, Betalain Pigments as Natural Photosensitizers for Dye-Sensitized Solar Cells: The Effect of Dye PH on the Photoelectric Parameters, Mater. Renew. Sustain. Energy, 4 5 (2015)
4. A.R.H.Martínez et al, Stabilized Conversion Efficiency and Dye-Sensitized Solar Cells from Beta Vulgaris Pigment, Int. J. Mol. Sci., 14 4081 (2013)
5. D. Chen et al, Study on Extraction and Purification Process of Capsicum Red Pigment, Spring Conf. 1, 1450 (2009)
6. K.E. Jasim et al, Curcumin Dye-Sensitized Solar Cell, J. Energy Power Eng., 11 1 (2017)

7. A.S. Polo et al, Blue Sensitizers for Solar Cells: Natural Dyes from Calafate and Jaboticaba, *Energy Mater. Sol. Cells*, 90 1936 (2006)
8. M.Irimia et al. Indigo - A Natural Pigment for High Performance Ambipolar Organic Field Effect Transistors and Circuits, *Adv. Mater.*, 24 375 (2012)
9. E.D. Glowacki et al, Natural and NatureInspired Semiconductors for Organic Electronics, *Org. Semicond. Sensors Bioelectron*, 8118, 81180M (2011)
10. M. Irimia et al., Environmentally Sustainable Organic Field Effect Transistors. *Org. Electron*. 11, 1974 (2010)
11. C.J. Bettinger et al, Organic Thin-Film Transistors Fabricated on Resorbable Biomaterial Substrates, *Adv. Mater*, 22, 651 (2010)
12. M. Irimia et al., Biocompatible and Biodegradable Materials for Organic Field-Efect Transistors, *Adv. Funct. Mater*, 20 4069 (2010)
13. W. R. Klaus et al, General, in *Ullmann's Encyclopedia of Industrial Chemistry* (2012).
14. A. Shinohara et al, Role of Regional Medical Support and Collaboration Center in Regional Medical Care Support Hospitals., 71 (2017)
15. E. Jeong et al, Synthesis, Mutagenicity, and Metabolism of Substituted 4,4'- Amino - alkoxyazobenzene Dyes (Partial Fulflment Requir. Degree Dr. Philos, North Carolina State Univ, (2008)
16. S. Ahamad et al, Organic semiconductors for device applications: current trends and future prospects, *Journal of Polymer Engineering*, 34 279- 338 (2014)
17. K. Kawano et al, Effect of solvent on fabrication of active layers inorganic solar cells based on poly (3-hexylthiophene) and fullerene derivatives, *Energy Mater. Sol. Cells*. 93 514–518 (2009)
18. M. Eslamian et al, Inorganic and Organic Solution- Processed Thin Film Device, *Nano – Micro Letters*. 9 1-23 (2017)
19. K. Feron et al, Organic solar cells: understanding the role of forster resonance energy transfer, *Int. J. Mol. Sci*. 13 17019–17047 (2012)

20. T. L. Benanti et al, Organic solar cells: an overview focussing on active layer morphology, *Photosynth. Res.* 87 (2006) 73–81.
21. S. Chakraborty et al, Effect of COOH-functionalized SWCNT addition on the electrical and photovoltaic characteristics of Malachite Green dye based photovoltaic cells, *Journal of Semiconductors*, 35 124004(1-6) (2014)
22. D. P. Hagberg et al, Tuning the HOMO and LUMO energy levels of organic chromophores for dye sensitized solar cells, *Journal of Organic Chemistry*, 72 (2007) 9550–9556
23. M. Ikram et al, Enhanced performance of P3HT/ (PCBM:ZnO:TiO₂) blend based hybrid organic solar cells, *Materials Research Bulletin*, 75 (2016) 35-40.
24. A.P. Wanninayake et al, Effect of ZnO nanoparticles on the power conversion efficiency of organic photovoltaic devices synthesized with CuO nanoparticles, *AIMS Materials Science.*, 3 927-937 (2016)
25. M. Rani et al, A Comparative Study of Nanostructured TiO₂, ZnO and Bilayer TiO₂/ZnO Dye-Sensitized Solar Cells, *Journal of Electronics Materials*. 44 1151- 1159 (2015)
26. K. S. Khasan et al, I–V characteristics of vanadium- flavonoid complexes based Schottky diodes, *Physica B*. 406 3011-3017 (2011)
27. Z. Ahmad et al, Electrical characteristics of a high rectification ratio organic Schottky diode based on methyl red, *Optoelectronics and Advanced Materials Rapid Communications*. 3 509 – 512 (2009)
28. M. Shah et al, Electrical characterization of the organic semiconductor Ag/CuPc/Au Schottky diode, *Journal of Semiconductors*, 32 044001(1-5) (2011)
29. J.A. Carr et al, On the identification of deeper defect levels in organic photovoltaic devices, *J. Appl. Phys*, 114 (2013) 064509-7
30. S.M. H. Rizvi et al, Investigation of Traps in Thin-Film Organic Semiconductors Using Differential Analysis of Steady-State Current–Voltage Characteristics, *IEEE Transactions on Electron Devices*, 65 (2018) 3430 - 3437.

31. A. Haldar et al, Electrical and photovoltaic characterisations of methyl red dye doped solid-state photoelectrochemical cell, *Ionics*. 15 79–83 (2009)
32. S. Chakraborty et al, Effect of COOH-functionalized SWCNT addition on the electrical and photovoltaic characteristics of Malachite Green dye based photovoltaic cells, *Journal of Semiconductors*, 35 124004 (1-6) (2014)
33. A. Y. Khan et al, Phenazinium dyes safranin O and phenosafranin induce self-structure in single stranded polyadenylic acid: Structural and thermodynamic studies, *Journal of Photochemistry and Photobiology B: Biology*. 132 17-26 (2014)
34. A. K. Jana et al, Solar cells based on dyes, *Journal of Photochemistry and Photobiology A: Chemistry*. 132 1-17 (2000)

Chapter 7

Conclusion and Future Scope of the work

7.1 Summary

7.2 Findings of the work

7.3 Overall conclusion

7.4 Future Scope of the work

7.1 Summary

The objectives of our present thesis are to study on the charge transport properties of organic and herbal dye-based photovoltaic cell in presence of different nano particles. Generally, electronic devices are fabricated with inorganic materials such as silicon and its composites. Such devices may possess high efficiency but there are also certain limitations. These are not nature friendly, and biodegradable. For these reasons organic and herbal dye based electronic devices are currently being research into. The performance of these devices is quite low at present in comparison to their inorganic counterparts. Different researchers are working upon it to enhance the device performance. Addition of guest materials such as TiO_2 , ZnO NP have shown better device efficiency. We have used TiO_2 and ZnO as the NP and studied their effect on these devices. Systematically we have studied with organic and natural dye in its solid state thin film. To ensure the semiconducting property, I-T characteristic, Hall experiments have been done. Different diode parameter such as η , Φ_B , and R_s have been estimated. Devices are prepared by varying concentration of the dye, and also electrode. To enhance the conductivity NP like ZnO , TiO_2 , have been incorporated and all the measurements have been done to see the effect of NP. All the necessary characteristic like XRD, SEM, UV, steady state I-V, I-T characteristic, Hall experiment, Photovoltaic measurement are carried out. Side by side we have observed that there is not much report available on charge transport theory for these systems. We have used exponentially trap assisted charge transport method which are generally being used for different amorphous organic solid. We have found that these theories are applicable in our system. We have also seen the photovoltaic effect of the dyes. But in the present thesis we have not shown these.

We have designed our present work into seven chapters.

In **Chapter 1**, we have discussed the problem of electronic waste in near future and requirement of nonconventional electronic materials. Organic and natural dye- based devices may be used as non-conventional electronic materials. Recently organic dyes and natural dye based photovoltaic devices have emerged as an alternative of the inorganic electronics devices. But these devices suffer from low efficiency and stability. But there is not much study on electronics conductivity of herbal dye. Conductivity of herbal dye is quite low. To overcome this issue new guest materials are being introduced to the medium. Different type of

NP are very promising candidate in this regard. Addition of TiO_2 and ZnO NP increases the conductivity of the device. Keeping all there in mind we have proposed the objective of the work. The outline of the work is also suggested in this chapter.

In **Chapter 2**, we have discussed recent work on nonconventional electronic materials and scrutinized few theoretical models of conductivity of organic dye-based devices. We have discussed the charge transport theories and the Hall Experiment to estimate the charge carrier density. Net flow of current in natural dyes can be attributed as injection-limited current flow and bulk-limited current flow. At voltages below threshold level, current flow is considered as injection-limited current flow and at voltages above threshold voltage, the current flow is considered as bulk-limited current flow. In this regard, we have used space-charge limited current (SCLC) model with exponential trap distribution. We have measured trap energy using SCLC model and correlated it with the threshold voltage of herbal dye device. In this chapter, we have also briefly discussed the thermo- ionic emission theory and magnetic field effect on moving charge for natural dye-based device. We have shown the role of different nano particle on series resistance, barrier height and trap energy of herbal dye based thin film devices. Current voltage characteristics and charge trapping mechanism in herbal dye-based devices also discussed in this chapter. Herbal devices have a higher tendency towards traps. In order to understand the charge transport process, it is very important to have knowledge about traps in these devices. Here we have also discussed the origin of traps and various trap distribution models.

From **Chapter 3 to Chapter 6** we have discussed experimental work to achieve the objective of our work. We have selected Turmeric dye, SY, and PSF. Systematically we have performed experiments on these dyes which have been presented in these chapters.

In **Chapter 3**, we have estimated the charge carrier density of solid state thin film of Turmeric dye. We have also observed the changes of current and voltage of Turmeric dye solid state device. The results are mentioned in this chapter. We have also prepared a Turmeric dye-based diode and extracted reverse saturation current, rectification ratio, ideality factor, series resistance, barrier height, and trap energy. It has been noticed that the diode exhibits a high ideality factor and series resistance. The presence of traps is one of the main reasons for these high values. So, we have also measured the trapped energy of the device considering exponential trap distribution.

In **Chapter 4**, we have studied the effect of dye concentration on the band gap of poly vinyl alcohol Turmeric composite thin film. We have taken three different concentration of Turmeric dye and studied the change of conductivity. By studying the Current-Temperature characteristic of the diode, the band gap has been measured. Here the conduction of ions is slow down by the presence of traps. Particularly we have investigated the change of dye concentration on the trap energy, barrier height and series resistance of these cells. The barrier height is a very important parameter which identifies the concentration of carriers in Turmeric diode. The results are mentioned in this chapter.

In **Chapter 5**, we have studied the effect of ZnO, TiO₂ NP on solid state Turmeric dye thin film. Here we have taken TiO₂, ZnO NP and observed its effect on Turmeric dye-based diode. The conduction process depends entirely on the rate of charge generation and charge separation within the system. Incorporation of guest materials causes a major change to the devices in this regard. The steady state current voltage characteristics has been studied and found that there are three different regions where three different conduction mechanisms occurs. In case of Turmeric diodes. We have estimated and compared the charge transport parameters like barrier height, series resistance and trap energy with or without using nano particles. It is observed that the barrier height and series resistance of the Turmeric diodes decrease by about 30% on addition of TiO₂. Results are discussed in this chapter.

In **Chapter 6**, we have studied the conductivity of Sunset Yellow dye and Phenosafranine dye-based organic diode in presence of TiO₂ and ZnO NP. It is observed that in the presence of NP the trap energy is reduced and the conductivity along with the efficiency of the diode increases. We have also investigated the effect of trap energy on R_s in the presence of TiO₂ and ZnO NP.

In **Chapter 7**, the summary and overall findings of the work are highlighted. This chapter is concluded with an overall conclusion of the work. The future scope of the present work is also mentioned in this chapter.

7.2 Findings of the work

The objective of the thesis is to study on the charge transport properties of organic and herbal dye-based photovoltaic cells in presence of different NP. In the present thesis, we have concentrated to study on the conductivity and charge transport parameters of Turmeric, SY, and Phensafranin dye- based devices. These dyes have shown semiconducting property. But

the typical value of their conductivity is quite low. Our findings show that TiO₂, and ZnO nanoparticle has a strong role in the charge transport mechanism and to enhance the conductivity of the devices. The experimental data for different dyes are presented in different chapters. In this chapter we have summarized our findings to show the salient features of this thesis.

Findings on Estimation of charge carrier density of Turmeric dye film

Table 7.1 Extracted value of Hall coefficient (R_H) from B vs V_H and V_H vs I_H graphs

Thickness of the sample (meter)	R _H from the slope of B vs V _H graph		R _H from the slope of V _H vs I _H graph	
5 × 10 ⁻⁴	Hall current I (mA)	$R_H = \frac{\Delta V_H Z}{\Delta B I}$ (m ³ . Coulomb ⁻¹)	B (Tesla)	$R_H = \frac{\Delta V_H Z}{\Delta I B}$ (m ³ . Coulomb ⁻¹)
	2	37.24 × 10 ⁻⁴	0.050	14.41 × 10 ⁻⁴
	4.03	18.34 × 10 ⁻⁴	0.215	29.20 × 10 ⁻⁴
	6.02	12.25 × 10 ⁻⁴	0.323	27.43 × 10 ⁻⁴

From Table 7.1 we have shown the Hall coefficient of Turmeric dye film for different Hall currents and we have taken the average value of Hall coefficient (R). Its value is 0.0022 m³ Coulomb⁻¹. We have estimated charge carrier density, using average Hall coefficient and its value is 2.8 × 10²³ m⁻³. Hall experiment suggest that Turmeric dye behaves like a n type semiconducters.

Table 7.2 Extracted values of η, φ_b, and R_s and E_c of the Turmeric dye-based herbal diode

Sample	Value of η	Value of φ _b (eV)	R _s from dV/dlnI plot (KΩ)	R _s from H(I) vs I plot (KΩ)	Value of E _c (eV)
ITO/Turmeric/Al	16.73	0.74	3.82	3.81	0.059

Here we have also estimated three charge transport parameters of Turmeric dye-based device. Values of Series Resistance (R_s), Barrier Height (ϕ_b), and Trap energy (E_c) are 3.82 k Ω , 0.74 V, and 0.059 eV respectively. Electrical parameter extracted for Turmeric dye is shown in Table 7.2.

Findings on Effect of dye concentration on the band gap of PVA Turmeric composite film

In Table 7.3 indicate the dark I-V characteristics of Turmeric dye. We have also shown that the series resistance the diodes varies from 13.73 K Ω to 0.36 K Ω due to higher concentration of Turmeric dye.

Table 7.3 Values of Barrier height (ϕ_b) and Series Resistance (R_s) and Trap Energy

Dyes and Electrode	Ideality factor(η)	Barrier height(ϕ_b) In eV	Series resistance R_s (K Ω)	Trap Energy E_c (eV)
Cu/5% Turmeric/Al	42.19	0.39	13.738	0.034
Cu/10% Turmeric /Al	38.78	0.43	6.236	0.037
Cu/20% Turmeric/Al	32	0.50	0.36	0.045

The band gap energy also reduces from 3.36 eV to 2.82 eV with increasing dye concentration from 5% Turmeric dye to 20% Turmeric dye concentration shown in Table 7.4. Reduction in band gap energy helps in better conduction of the nonconventional electronic device.

Table 7.4 Values of η and E_g for different cell

Concentration of Turmeric solution weight ratio (%)	Value of Ideality factor (η)	Value of band gap energy (eV)
5	42.19	3.36
10	38.78	2.91
20	32.00	2.82

Findings on Turmeric dye-based devices in absence and presence of TiO₂, ZnO nanoparticles

Experiment have been done by incorporating TiO₂, ZnO with Turmeric diode. Different diode parameters are extracted from the Table 7.5. Comparing the charge transport parameters, we find that series resistance of Turmeric TiO₂ diode is lower than Turmeric ZnO diode. Lowering of R_s helps in better charge conduction in case of ITO/Turmeric+TiO₂/Cu diode and enhances the overall performance of the device. From the Table 7.5 it can be seen that in the dark I-V characteristics of Turmeric diode, the series resistance reduces from 6.236 (K Ω) to 0.276 (K Ω) in the presence of TiO₂. Decrease in series resistance indicates that the conductivity of the diode will increase. Decrease in dissociation energy indicates that the separation of LUMO and HOMO will decrease. This will enhance the conductivity of the diode.

Table 7.5 Charge transport parameters of three Diodes

Name of the diode Using Turmeric dye	Trap energy (E_c) eV	Series resistance (R_s) k Ω	Barrier height(Φ_b) eV
ITO/Turmeric+ZnO/Cu	0.046	0.62	0.03
ITO/Turmeric+TiO ₂ /Cu	0.059	0.276	0.78
ITO/10% Turmeric /Cu	0.43	6.23	0.62

From the Table 7.6, it is seen that dissociation energy of TiO₂ added Turmeric dye- based diode is lower than Turmeric dye based diode.

Table 7.6 Values of U (dissociation energy)

Type of films	Values of U (eV)
ITO/PVA Turmeric/Cu	0.55
ITO/TiO ₂ +PVA Turmeric/Cu	0.40

Findings on PSF dye-based devices in absence and presence of TiO₂, ZnO nanoparticles

Different electrical parameters for PSF dye are shown in Table 7.7 and 7.8.

Table 7.7 η and R_s extracted for three different cells without and with TiO_2 and ZnO nanoparticles

Sample	Value of η	R_s from $dV/d\ln I$ plot ($k\Omega$)	R_s from $H(I)$ vs I plot ($k\Omega$)
PSF	37.47	272.70	250.80
PSF+ ZnO	36.90	112.10	108.30
PSF+ TiO_2	34.80	100.10	98.30

From Table 7.7, it can be seen that series resistance is less in case of PSF+ TiO_2 diode and more for PSF diode without any nanoparticle.

Table 7.8 Extracted values of trap energy for three different system without and with TiO_2 and ZnO nanoparticles

System	Extracted value of m	Extracted value of E_c in eV
Only PSF	3.38	0.090
PSF+ ZnO	3.04	0.078
PSF+ TiO_2	2.80	0.072

From Table 7.8, it is seen that trap energy reduces for using NP. We have used TiO_2 , ZnO NP. Trap energy is less for TiO_2 +PFS diode.

Table 7.9 Estimated reduction percentage (%) of R_s and E_c in presence of TiO_2 and ZnO nanoparticles

NP used	Reduction percentage (%) of series resistance R_s using NP	Reduction percentage (%) of trap energy E_c using NP
PSF+ ZnO	58.82	13.33
PSF+ TiO_2	63.29	20

From Table 7.9, it is seen that series resistance reduces for using NP. Reduction percentage of series resistance is 13.33 for PSF+ ZnO diode and 20 for PSF+ TiO_2 diode.

7.3 Conclusion

In this entire work we have studied the charge transport properties of organic and herbal dye-based photovoltaic cell in presence of different nano-particles and found the semiconducting property of herbal dye-based devices. The natural dyes show semiconducting property which has been observed from Hall Experiment, I-V, I-T data. The value of conductivity is quite low. The device performance changes significantly when we have incorporated the NP. The nano-composite formation between the dye and NP assists the charge transfer process. Grossly we have found that in presence of ZnO, and TiO₂ the R_s reduces and conductivity increases. We have also given explanation how the R_s reduces, conductivity increases in presence of ZnO, and TiO₂ NP.

7.4 Future scope of the work

One of our approaches was to study the biodegradable electronic devices. The present thesis is informative as far as the nonconventional electronic material is concerned. For that we have used natural dyes as the semiconducting materials. But we have used ITO coated glass plate, Al plate, Cu plate as counter electrodes which are not biodegradable. In light of the future development of implantable and biocompatible electronics, ITO and Al coated glass substrates must be replaced with organic counterparts. Starch, composed of complex carbohydrates, can be proposed as a suitable candidate for biodegradable, recyclable electronic device fabrication. Owing to its tunable solubility, starch can also serve as a transient electronic substrate, potentially adding value to electronic waste disposal. A transient starch substrate can be utilized for the deposition of organic, biocompatible electrodes. By engineering the surface roughness of the substrate, conductivity comparable to glass-ITO can be achieved.

But there are certain problems that still need to be addressed in this regard. The distribution and density of trap states are different from one device to another. Also, the performance of these devices with shallow and deep traps are quite different. These aspects need to be studied in the future to get a deeper view on the charge transport mechanism of these devices and also to select the suitable guest materials to get better performance.

List of Publications

1. Effect of dye concentration on the band gap of PVA turmeric composite film, S. Bhunia, Pallab Kr Das, N.B. Manik, Journal of Indian Chemical Society, CSD- 2019 Special Issue, 97 2937-2942 2020
2. Estimation of charge carrier density of turmeric dye in presence of Polyvinyl Alcohol (PVA) and its electrical characterization as herbal diode, S. Bhunia, Pallab Kr Das, S. Rakshit, N.B. Manik, Journal of Scientific Research 14(1) 11-25 2022
3. Effect of Titanium Dioxide on Solid State Turmeric Dye Thin Film, S. Bhunia, Pallab Kr Das, N.B. Manik, Journal of Indian Chemical Society, 97 2943-2947 2020
4. Effect of trap energy on series resistance of Phenosafranine dye based organic diode in presence of TiO_2 and ZnO NP, Pallab Kr Das, S. Bhunia, N.B. Manik, Advance Materials Research, 1159 112-123 2020
5. Study on the Conductivity of a Sunset Yellow Dye- Based natural Organic Device, Arnab Kanti Karan, Swapan Bhunia, N. B. Manik, Journal of Electronic Materials, 11664-022-09954-4 2022

Book Chapter:

Effect of dye concentration on series resistance of Thionin Dye –Based organic Diode, Pallab Kr Das, S. Bhunia, N.B. Manik, Publishers, Mathematics Applied to Engineering Action, 119-131 2020

Manuscript Communicated: -

Effect of Zinc Oxide on Turmeric dye based Solid State Thin Film, S. Bhunia, Pallab Kr Das, N.B. Manik, Journal of Physical Science

Presentation at International/National conferences/seminars

1. Dependence of trap energy on the incident intensity of light of methylene blue (MB) dye based photovoltaic devices, S. Bhunia, A. Halder, R. Islam, N.B. Manik, Poster Presentation at Condensed Matter Days-2017, Department of Physics Tezpur University, Napaam, Tezpur- 784028, 2017
2. Study on turmeric dye based electronic herbal diode, S. Bhunia, Pallab Kr Das, N.B. Manik, Condensed Matter Days-2018, Poster Presentation, Department of Physics Burdwan University, Rajbati, Burdwan, 731124, 2018
3. Effect of dye concentration on the band gap of PVA turmeric composite film, poster presentation, S. Bhunia, Pallab Kr Das, N.B. Manik, Emerging Frontiers in material Science, 2019
4. Measurement of Hall Co-efficient of turmeric dye film, Swapan Bhunia, Oral presentation, Physics at Surfaces and Interfaces of Soft materials (PSISM 2019), Condensed Matter Physics Research Centre, JU, 2019

Workshop Attendant

1. One day seminar on recent Trend in Physics (RTFRP) Department of Physics, Jadavpur University. RTFRP-2018